TRANSPORTATION RESEARCH RECORD 651

Concrete, Aggregates, Marking Materials, Corrosion, and Joint Seals

TRANSPORTATION RESEARCH BOARD

COMMISSION ON SOCIOTECHNICAL SYSTEMS
NATIONAL RESEARCH COUNCIL

NATIONAL ACADEMY OF SCIENCES
WASHINGTON, D.C. 1977

Transportation Research Record 651
Price $4.00
Edited for TRB by Frances R. Zwanzig

subject areas
03 rail transport
27 bridge design
32 cement and concrete
34 general materials
35 mineral aggregates

Transportation Research Board publications are available by ordering directly from the board. They may also be obtained on a regular basis through organizational or individual supporting membership in the board; members or library subscribers are eligible for substantial discounts. For further information, write to the Transportation Research Board, National Academy of Sciences, 2101 Constitution Avenue, N.W., Washington, D.C. 20418.

Library of Congress Cataloging in Publication Data
National Research Council. Transportation Research Board.
Concrete, aggregates, marking materials, corrosion, and joint seals.

(Transportation research record; 651)
1. Concrete—Congresses. 2. Aggregates (Building materials)—Congresses. 3. Road markings—Congresses. 4. Motor vehicles—Corrosion—Congresses. 5. Bridges—Floors—Joints—Congresses. I. Title. II. Series.
TE7.H5 no. 651 [TE200] 380.5'08s [625.7]
ISBN 0-309-02680-6 78-13539

Sponsorship of the Papers in This Transportation Research Record

GROUP 2—DESIGN AND CONSTRUCTION OF TRANSPORTATION FACILITIES
Eldon J. Yoder, Purdue University, chairman

Concrete Section
Carl F. Crumpton, Kansas Department of Transportation, chairman

Committee on Performance of Concrete—Physical Aspects
David Stark, Portland Cement Association, chairman
Philip D. Cady, Pennsylvania State University, secretary
Frederick Roger Allen, W. P. Chamberlin, Kenneth C. Clear, Herbert K. Cook, Clarence E. DeYoung, Wade L. Gramling, David R. Lankard, Kenneth R. Lauer, Bryant Mather, Joseph E. Ross, Charles F. Scholer, W. M. Stingley, V. R. Sturrup, Harold Edward Vivian, Jukka E. Vuorinen, Richard D. Walker, E. A. Whitehurst

Construction Section
David S. Gedney, Federal Highway Administration, chairman

Committee on Construction of Bridges and Structures
Marvin H. Hilton, Virginia Highway and Transportation Research Council, chairman
Robert M. Barnoff, Harry E. Brown, Dale F. Downing, Howard L. Furr, George A. Harper, Richard Heinen, Wayne Henneberger, J. C. McGrew, G. I. Sawyer, W. H. Shaw, Sydney W. Smith, James T. Triplett, J. R. Wilder, Thomas G. Williamson, Kenneth C. Wilson

General Materials Section
Roger V. LeClerc, Washington State Department of Highways, chairman

Committee on Mineral Aggregates
T. C. Paul Teng, Mississippi State Highway Department, chairman
Frederick Roger Allen, Grant J. Allen, Raymond E. Aufmuth, Gordon W. Beecroft, Richard L. Berger, John C. Cook, J. T. Corkill, Ludmila Dolar-Mantuani, Karl H. Dunn, Richard D. Gaynor, Donn E. Hancher, James C. Hawley, Robert F. Hinshaw, Richard H. Howe, Eugene Y. Huang, William B. Ledbetter, Donald W. Lewis, Charles R. Marek, Marvin L. McCauley, John E. McChord, Jr., Andy Munoz, Jr., N. Thomas Stephens, Hollis N. Walker, Richard D. Walker, Milton H. Wills, Jr.

Committee on Coatings, Signing, and Marking Materials
K. K. Moore, Texas State Department of Highways and Public Transportation, chairman
Harold C. Rhudy, North Carolina Department of Transportation, secretary
Chester J. Andres, Carroll E. Caltrider, Jr., Charles A. Douglas, William E. Douglas, Clarence W. Gault, John S. Humphries, John D. Keane, John C. Moore, E. W. Myers, Philip V. Palmquist, A. J. Permoda, Burton M. Rudy, Lothar S. Sander, F. D. Shepard, Leroy W. Shuger, W. R. Tooke, Jr.

Committee on Sealants and Fillers for Joints and Cracks
Dale E. Peterson, Utah Department of Transportation, chairman
Chris Seibel, Jr., Consulting Engineer, secretary
Grant J. Allen, James E. Bryden, William T. Burt III, John P. Cook, Daniel E. Czernik, Gary L. Fordyce, Frank D. Gaus, C. W. Heckathorn, Richard C. Ingberg, Phillip L. Melville, Issam Minkarah, Leonard T. Norling, Thomas J. Pasko, Jr., William G. Prince, Jr., John J. Schmitt, William T. Stapler, Egons Tons, Stewart C. Watson

Committee on Corrosion
Richard F. Stratfull, California Department of Transportation, chairman
Kenneth J. Boedecker, Jr., Robert P. Brown, John F. Cavanaugh, Kenneth C. Clear, Seymour K. Coburn, Israel Cornet, Carl F. Crumpton, William J. Ellis, E. T. Franzen, Harold J. Fromm, William F. Gerhold, John D. Keane, Ray I. Lindberg, Robert A. Manson, A. H. Roebuck, Arnold M. Rosenberg, Joseph E. Ross, F. O. Waters, Frank O. Wood, Leonard E. Wood

William G. Gunderman and Bob H. Welch, Transportation Research Board staff

Sponsorship is indicated by a footnote at the end of each report. The organizational units and officers and members are as of December 31, 1976.

Contents

Gran Method of Endpoint Determination in Chloride Analysis by Potentiometric Titration

Gerardo G. Clemeña, John W. Reynolds, and Randy McCormick, Virginia Highway and Transportation Research Council, Charlottesville

The Gran method of endpoint determination can replace the currently used first-derivative method in the potentiometric titration procedure for the analysis of chloride in hardened concrete. This modification improves the procedure by (a) circumventing the frequently encountered difficulty in endpoint determination that arises from unstable electrode potentials, (b) eliminating the need to spike solutions of low-chloride concrete samples with a known amount of chloride before titration, (c) enabling the titration to be performed more quickly, and (d) improving the overall precision and accuracy.

To repair the damage to bridge decks that results from corrosion of the reinforcing steel, it is necessary to locate the concrete showing the potential for inducing further corrosion as well as the material already exhibiting damage. The location of the potentially corrosive material requires analysis of the chloride (Cl^-) content of concrete samples from the bridge deck. The chemical procedure widely used for these analyses is based on the potentiometric titration technique developed by Berman (1). Briefly, the procedure has three parts:

1. Extraction of the soluble Cl^- from a powdered concrete sample by using 1:16 nitric acid and separation of the extract from the undissolved residue by filtration;
2. Potentiometric titration of the Cl^- with a standard silver nitrate ($AgNO_3$) solution in the presence of a Cl^- or a silver ion-specific electrode; and
3. Determination of the endpoint of the titration by using the first-derivative ($\Delta E/\Delta V$) method, followed by calculation of the Cl^- content.

A frequently encountered difficulty in this procedure involves the determination of the endpoint, particularly for samples that have relatively low Cl^- contents. Because the method is based on the occurrence of a maximum $\Delta E/\Delta V$ at the endpoint, its accuracy and precision are susceptible to the instability in the electrode potential that occurs in the vicinity of the endpoint.

This difficulty can be circumvented by using the Gran method for endpoint determination, which uses the comparatively more stable potential readings beyond the endpoint (2).

GRAN METHOD OF ENDPOINT DETERMINATION

In a dilute solution, the electrode potential is related to the Cl^- concentration by the simplified Nernst equation

$$E = E_0 - (2.3RT/F)\log C_a \quad (1)$$

where

- E = electrode potential,
- E_0 = constant determined by the normal and junction potentials,
- R = universal gas constant,
- T = temperature (°K),
- F = Faraday constant, and
- C_a = Cl^- concentration.

Before the endpoint in a titration is reached, the Cl^- concentration in the sample solution is related to the amount of silver ion (Ag^+) added by

$$C_a = (C_a'V_a - C_tV_t)/(V_a + V_t) \quad (2)$$

where

- C_a' = initial concentration of Cl^- in the sample solution,
- C_t = concentration of Ag^+ in the titrant,
- V_a = initial volume of the sample solution, and
- V_t = volume of titrant added.

Substituting Equation 2 into Equation 1 gives

$$E = E_0 - (2.3RT/F)\log[(C_a'V_a - C_tV_t)/(V_a + V_t)] \quad (3)$$

which relates the electrode potential to the volume of titrant added and can be rearranged to give

$$(V_a + V_t) \times 10^{(E_0-E)\times(F/2.3RT)} = C_a'V_a - C_tV_t \quad (4)$$

This indicates that a plot of $[(V_a + V_t) \times 10^{(E_0 - E) \times (F/2.3RT)}]$ versus V_t should give a straight line whose point of interception with the V_t-axis corresponds to the endpoint. This is so because at the endpoint $C_a = 0$, and therefore, from Equation 2, the left side of Equation 4 becomes zero. A similar analysis can be made after the endpoint is passed, when the continued addition of titrant increases the concentration of Ag^+ in the solution.

Although such linear plots have many advantages, some of which are illustrated later, the method has not become popular because the time required to calculate the complex term on the left side of Equation 4, which is needed for plotting, usually offsets the advantages. Recently, however, the need for this calculation has been obviated because volume-corrected graph paper for obtaining linear plots directly from the potential readings has become commercially available.

In applying the Gran method for determining the endpoint in the titration of concrete-sample solutions with $AgNO_3$, we have chosen to use the potentials beyond the endpoint ($E > 300$ mV for our titration system) rather than the potentials before the endpoint, because the latter are complicated by the formation of Cl^- complexes that make a linear Gran plot nondefinitive.

ADVANTAGES OF USING GRAN METHOD

The unstable potential readings in the vicinity of the endpoint do not present any difficulty when the Gran method is used. Consider the actual potential readings observed during the titration of a concrete-sample solution (Table 1): The fluctuation in each potential reading becomes larger as the titration approaches the endpoint, which was at approximately 3.5 ml 0.01N $AgNO_3$. With those

large fluctuations, it would be difficult to accurately determine the endpoint by the $\Delta E/\Delta V$ method. However, with the Gran method, the determination of the endpoint is relatively easy because it requires plotting only the few potential readings that are greater than 300 mV on Gran-plot paper and extrapolating the straight portion until it intersects the V_t-axis as shown in Figure 1. In this titration, the endpoint was at 3.45 ± 0.02 ml.

Table 1. Electrode potentials observed in actual titration.

0.009 93N $AGNO_3$ (ml)	Potential (mV)	Range (mV)
0.00 ± 0.01	219.1 to 219.2	0.1
0.50	222.2 to 222.3	0.1
1.00	225.7 to 225.8	0.1
1.50	229.8 to 229.9	0.1
2.00	235.2 to 235.4	0.2
2.50	242.4 to 242.6	0.2
3.00	253.8 to 254.4	0.6
3.10	257.1 to 257.7	0.6
3.20	260.9 to 261.5	0.6
3.30	265.1 to 265.5	0.4
3.40	269.8 to 270.6	0.8
3.50	273.5 to 274.3	0.8
3.60	278.3 to 279.2	0.9
3.70	283.2 to 283.8	0.6
3.80	287.5 to 288.1	0.6
3.90	291.5 to 292.1	0.6
4.00	295.5 to 296.1	0.6
4.10	299.0 to 299.4	0.4
4.20	302.1 to 302.5	0.4
4.50	309.9 to 310.1	0.2
5.00	319.2 to 319.3	0.1
5.50	325.9 to 326.0	0.1
6.00	331.4 to 331.5	0.1
6.50	335.8 to 335.9	0.1
7.00	339.5 to 339.6	0.1

Because the analyst needs only 3 or 4 points at most to obtain a definitive linear plot, the titration can be done more quickly, as shown by the improved procedure outlined in Figure 2, than when using the $\Delta E/\Delta V$ method. In using the latter method, for the region from approximately 0.5 ml before the endpoint to 0.5 ml beyond the endpoint, the analyst must observe the rate of change in the potential with every 0.1-ml increment of $AgNO_3$.

In Berman's original potentiometric titration procedure, ambiguities in determining the endpoint in the titration of samples with Cl^- contents lower than 0.01 percent were another problem. Figure 3 shows an example of an ambiguity that involved titration of a 100-ml aliquot containing 2.4090 g of a concrete sample whose Cl^- content was approximately 0.01 percent. As the figure shows, it is not clear where the endpoint is when the $\Delta E/\Delta V$ method is used. To eliminate such ambiguities, Berman has suggested that voltage readings of less than 65 mV below the endpoint when the electrodes are first immersed in a sample solution be taken as an indication that the sample has a low Cl^- content and that the analyst spike the solution with 1 or 2 ml 0.01N NaCl solution before proceeding with the titration (3). This spiking is supposed to shift the endpoint by 1 or 2 ml so that it is easier to determine. As shown in Figure 4, spiking another aliquot of the same sample with 2.00 ml 0.010 08N NaCl did provide improvement; however, the ambiguity in locating the endpoint was still not completely eliminated.

Figure 1. Use of Gran method to determine endpoint in potentiometric titration of acid extract of concrete.

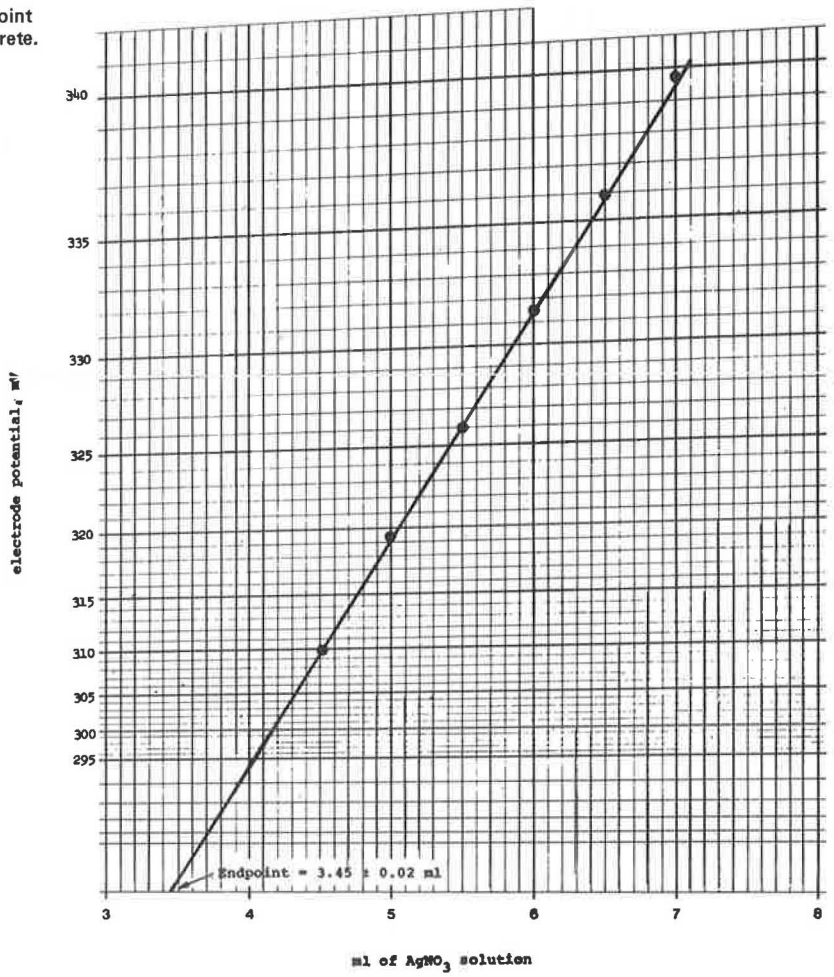

In using the Gran method, the endpoint can be clearly determined with or without spiking, regardless of the Cl^- content of the sample. To illustrate this, the potentials from the titrations shown in Figures 3 and 4 were plotted on Gran-plot paper as shown in Figure 5. The resulting endpoints were 2.58 and 0.63 ml for the spiked and nonspiked solutions respectively. And subtraction of 1.95 ml 0.010 31 N $AgNO_3$ (the equivalence of the 2.00 ml 0.010 08N NaCl added) also gives 0.63 ml as the endpoint for the nonspiked solution.

Figure 2. Procedure for analysis of Cl^- in hardened concrete by improved potentiometric titration procedure.

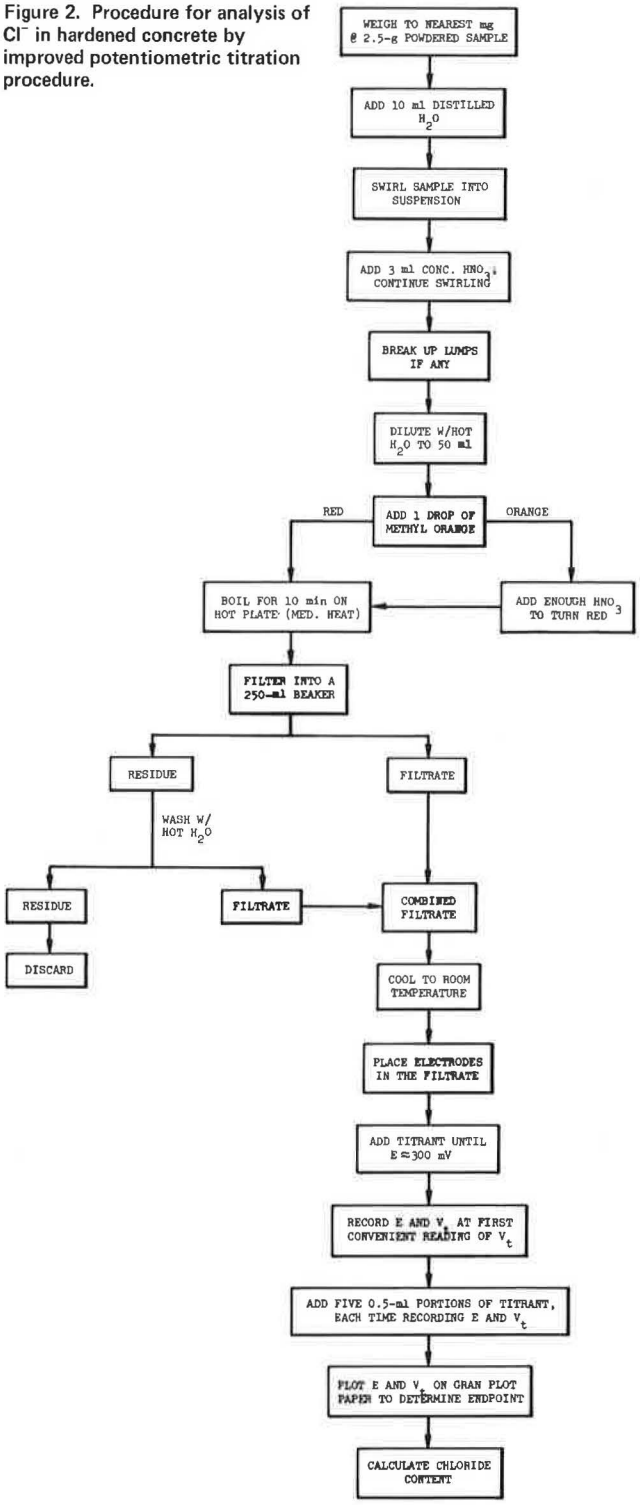

The experiment was repeated with several concrete samples whose Cl^- contents ranged from 0.001 to 0.019 percent. The overall results are shown in Table 2 and indicate that the average absolute difference in the endpoints of the spiked and nonspiked solutions was approximately 0.02 ml. This is about the precision with which one can read the Gran-plot paper, which means that the differences are insignificant.

Figure 3. Titration of low-Cl^- concrete sample (without NaCl spike).

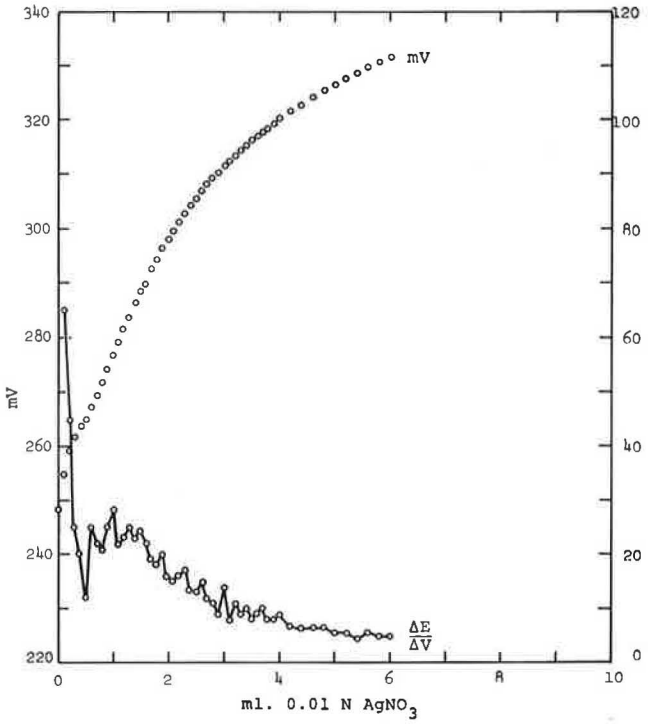

Figure 4. Titration of low-Cl^- concrete sample (spiked with 2.00 ml 0.1N NaCl).

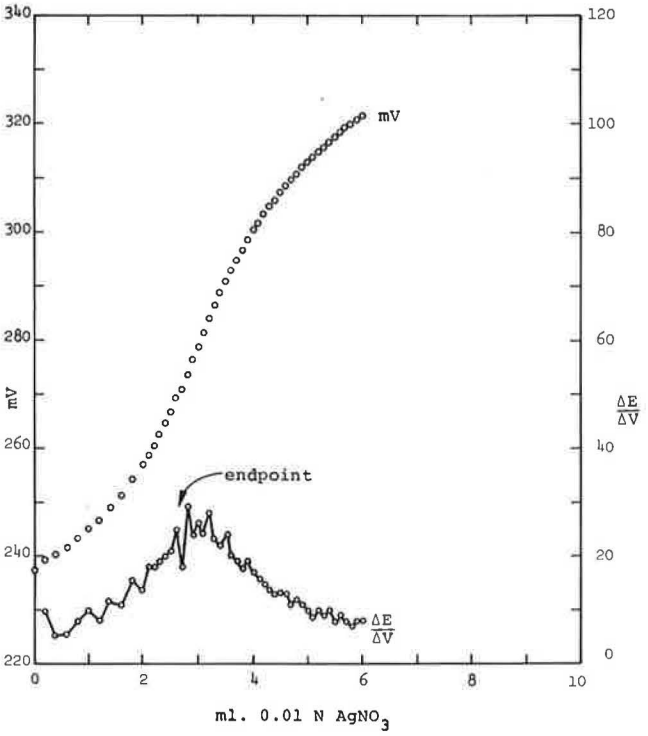

Figure 5. Gran plots of titrations shown in Figures 3 and 4.

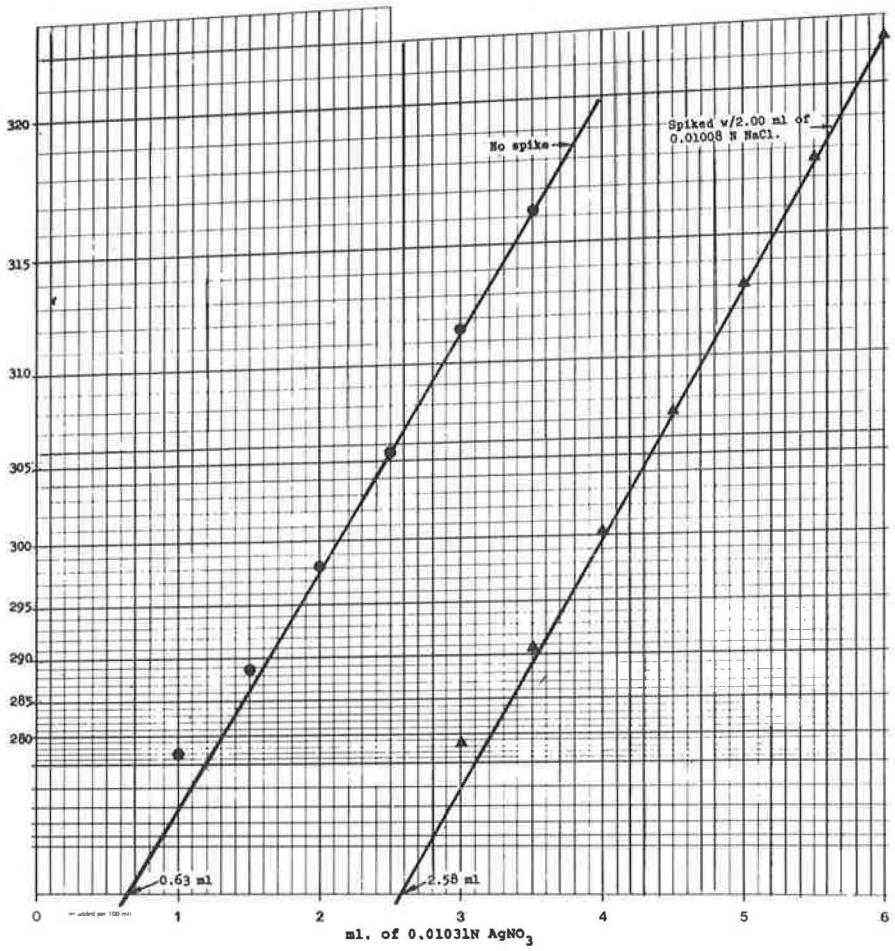

Table 2. Analysis of low-Cl^- concrete samples by using Gran method of potentiometric endpoint determination (with and without added NaCl).

Sample	Mass (g)	NaCl[a] Added (ml)	Total $AgNO_3$[b] Added (ml)	Net $AgNO_3$[c] Needed (ml)	Cl^- (%)
L-1	2.4018	2.00	2.05	0.10	0.0015
		0	0.07	0.07	0.0011
L-3	2.4028	2.00	2.40	0.45	0.0068
		0	0.45	0.45	0.0068
W-3	2.4090	2.00	2.58	0.63	0.0095
		0	0.63	0.63	0.0095
W-4	2.3999	2.00	2.87	0.92	0.0140
		0	0.96	0.96	0.0146
W-5	2.4005	2.00	3.18	1.23	0.0187
		0	1.22	1.22	0.0186

[a] 0.010 08 N.
[b] 0.010 31 N.
[c] Including adjustment for equivalency between NaCl and $AgNO_3$ solutions.

PRECISION AND ACCURACY

The replacement of the $\Delta E/\Delta V$ method by the Gran method should also improve the overall precision and accuracy of the potentiometric titration procedure. This agrees with the results of a theoretical study [Anfalt and Jagner (4)] that compared the various methods of endpoint determination.

Precision

As a test of the overall precision of the improved procedure using the Gran method, two concrete samples were divided into five portions each, and each portion was analyzed for Cl^-. The results shown below showed an average standard deviation of 0.0005 percent Cl^-, which is a large improvement over the value of 0.0026 percent given by Lankard and others (5).

Concrete Sample	Cl^- Content	Concrete Sample	Cl^- Content
1		2	
Portion 1	0.0236	Portion 1	0.0439
Portion 2	0.0244	Portion 2	0.0432
Portion 3	0.0237	Portion 3	0.0439
Portion 4	0.0232	Portion 4	0.0431
Portion 5	0.0239	Portion 5	0.0444
Range	0.0012	Range	0.0013
Standard deviation	0.0004	Standard deviation	0.0005

This precision includes variations in the Cl^- contents of the individual portions, in the extraction and titration, and in the determination of the endpoint. The variation in the determination of the endpoint had a standard deviation of approximately 0.0003 percent Cl^-, as determined by multiplicate titrations of aliquots from each of several extracts prepared from the same concrete samples.

Accuracy

Because of difficulty in preparing test specimens without any material loss during their mixing and curing, the accuracy of the original potentiometric titration pro-

Table 3. Cl^- analysis of prepared concrete specimens by potentiometric titration, atomic-absorption spectroscopy, and neutron-activation analysis.

Concrete Specimen	Cl^- Added (%)	Measured Cl^- Content (%)			Difference (% Cl^-)		
		PT[a]	AA[b]	NAA[c]	PT[a]	AA[b]	NAA[c]
S1	0.0100	0.0107	0.0078	0.0127	+0.0007	-0.0022	+0.0027
S2	0.0200	0.0206	0.0185	0.0216	+0.0006	-0.0015	+0.0016
S3	0.0300	0.0310	0.0278	0.0297	+0.0010	-0.0022	-0.0003
S4	0.0400	0.0393	0.0379	0.0368	-0.0007	-0.0021	-0.0032
C1	0.0061	0.0066	0.0058	0.0068	+0.0005	-0.0003	+0.0007
C2	0.0121	0.0118	0.0110	0.0117	-0.0003	-0.0011	-0.0004
C3	0.0182	0.0179	0.0159	0.0160	-0.0003	-0.0023	-0.0022
C4	0.0243	0.0243	0.0203	0.0202	0.0000	-0.0040	-0.0041
Avg absolute difference	—	—	—	—	0.0005	0.0020	0.0019

[a] PT = potentiometric titration.
[b] AA = atomic absorption spectroscopy.
[c] NAA = neutron activation analysis.

Figure 6. Analysis of Cl^- in prepared concrete specimens by potentiometric titration procedure.

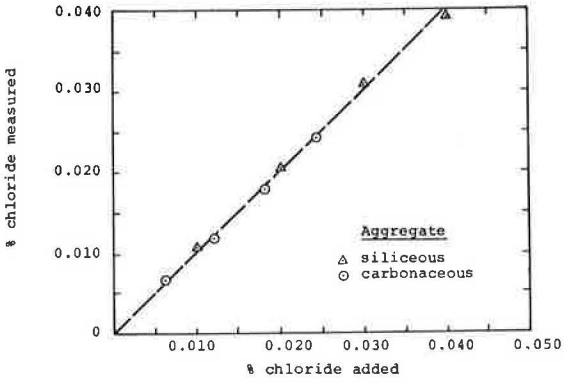

Figure 7. Analysis of Cl^- in prepared concrete specimens by atomic-absorption spectroscopy.

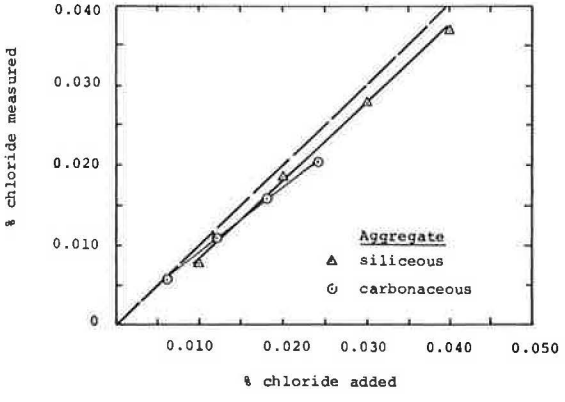

Figure 8. Analysis of Cl^- in prepared concrete specimens by neutron-activation analysis.

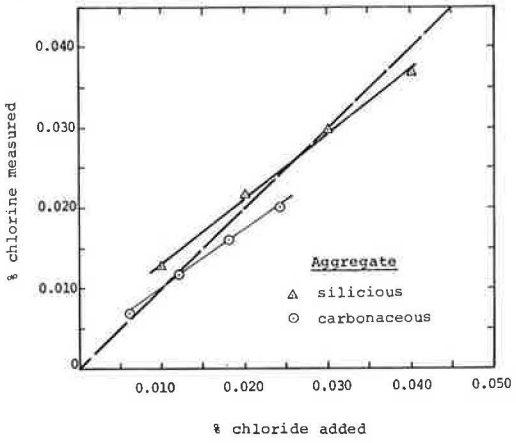

cedure was estimated by using samples having Cl^- contents considerably higher than the corrosion threshold value of 0.030 percent Cl^- suggested by Clear (6). However, because decisions about expensive repairs are made on the basis of Cl^- contents found to exceed the corrosion threshold, it is important to know the reliability of the analytical procedure used, particularly near the threshold level. To estimate the accuracy of the improved procedure at the threshold level, we compared its results to those of two procedures adapted from well-established analytical techniques (7)—atomic-absorption spectrometry and neutron-activation analysis. For the comparison, two series of test specimens—one using a siliceous aggregate and one using a carbonaceous aggregate—were prepared by adding Cl^- in increments. Then, each of the specimens was analyzed by all three procedures.

The results, shown in Table 3, indicated that the smallest average absolute difference in Cl^- content was obtained by using the potentiometric titration procedure. These values are probably fairly good indications of the accuracy of each of the procedures.

In Figures 6, 7, and 8, the Cl^- contents measured by the three procedures and corrected for a blank determination are plotted separately against the Cl^- added to the specimens. Figure 6 shows that the results obtained by the potentiometric titration procedure clustered around the 45° dashed line, which indicates excellent agreement and no discernible aggregate effect.

The Cl^- content measured by the atomic-absorption procedure (Figure 7) averaged about 11 percent lower than the known Cl^- added. In addition, this procedure apparently was affected by the nature of the aggregate in the test specimens, as indicated by the existence of two lines. In the neutron-activation procedure (Figure 8), the aggregate effect appeared to be more pronounced than in the atomic absorption procedure, and this procedure showed positive differences with samples having relatively low known-Cl^- contents and negative differences with those having relatively high Cl^- contents.

CONCLUSIONS

1. The use of the Gran method of endpoint determination eliminates the difficulty that unstable potential readings cause in the $\Delta E/\Delta V$ method.
2. The use of the Gran method eliminates the need

to spike solutions of concrete samples having low Cl^- contents with a known amount of Cl^- before titration to facilitate endpoint determination.

3. The use of the Gran method improved the precision of the potentiometric titration procedure.
4. The average absolute difference of 0.0005 percent Cl^- between measured Cl^- and known added Cl^- contents, as determined by analyzing several test specimens, is probably a good indication of the accuracy of this improved potentiometric titration procedure.
5. Among the procedures tested, the improved potentiometric titration procedure showed the best agreement among the test specimens. In addition, this procedure showed no discernible effects of the particular siliceous and carbonaceous aggregates used to prepare the specimens.

ACKNOWLEDGMENTS

The work described in this paper was supported by Highway Planning and Research funds administered through the Federal Highway Administration. All opinions and conclusions expressed are ours and do not necessarily reflect the view or policy of the Federal Highway Administration or the Virginia Highway and Transportation Research Council.

REFERENCES

1. H. A. Berman. Determination of Chloride in Hardened Portland-Cement Paste, Mortar, and Concrete. Journal of Materials, Vol. 7, 1972, p. 330.
2. G. Gran. Determination of the Equivalence Point in Potentiometric Titration, Part 2. The Analyst, Vol. 77, No. 11, 1952, p. 661.
3. H. A. Berman. Determination of Low Levels of Chloride in Hardened Portland-Cement Paste, Mortar, and Concrete. Journal of Testing and Evaluation, Vol. 3, No. 3, 1975, p. 208.
4. T. Anfalt and D. Jagner. The Precision and Accuracy of Some Current Methods for Potentiometric Endpoint Determination With Reference to a Computer-Calculated Titration Curve. Analytica Chimica Acta, Vol. 57, 1971, pp. 165-176.
5. D. R. Lankard and others. Neutralization of Chlorides in Concrete. Battelle Memorial Institute; Federal Highway Administration, First Quarterly Rept., Nov. 1973.
6. K. C. Clear. Evaluation of Portland-Cement Concrete for Permanent Bridge-Deck Repair. Federal Highway Administration, Interim Rept. FHWA-RD-74-5, Feb. 1974.
7. G. G. Clemeña, J. W. Reynolds, and R. McCormick. Comparative Study of Procedures for the Analysis of Chloride in Hardened Concrete. Virginia Highway and Transportation Research Council, Rept. VHTRC 77-R7, July 1976.

Publication of this paper sponsored by Committee on Performance of Concrete—Physical Aspects.

Comparison of Performance of Concrete Bridge Decks in British Columbia

A. J. Montador, Vancouver Region of the British Columbia Ministry of Highways and Public Works

The bridges of the freeways south and east of Vancouver, British Columbia, were chosen as a sample of concrete bridge decks in the area. They are of similar ages and quality of supply of ready-mixed concrete and subject to the same weather, salting, and traffic conditions. They have the following types of decks: monolithic, monolithic recapped, two layer on precast box beams, and two layer on cast-in-place concrete; the two-layer decks used either cement grout or two-part epoxy as bonding agents. The use of site-mixed versus plant-mixed concrete is related to the performance of the bridge decks. Six observations are made why two-layer decks are more satisfactory than monolithic decks, and 16 recommendations for construction of two-layer decks are given. It is concluded that (a) two-layer decks are more durable than monolithic concrete decks and guarantee a minimum coverage of the steel, (b) the placement of the overlay requires rigid quality control of the site-mixed concrete, and (c) application of the two-part epoxy bonding agent requires constant technical attention.

There are more than 2600 bridge and overpass decks in British Columbia, of which 650 are exposed concrete. Of the latter, 570 are monolithic and 80 are of two-layer deck construction. Of the monolithic concrete decks, 140 have concrete resurfacing, 30 are in immediate need of resurfacing, and a further 100 will need resurfacing in the next 3 or 4 years. Some of the older bridges that are still in use were built before 1920, and some of the newer bridges have been resurfaced with concrete just a few years after being opened to traffic.

The weather conditions cover a freezing-index range of from 100 to 500 degree days (1), and the traffic volumes vary from very light to 20 000 vehicles/lane/d. The concrete aggregate used in British Columbia varies from a granular material taken from a river bank to a high-quality aggregate produced to size and standard in modern plants. The concrete quality is variable and depends on the location of the bridge site and the plant and expertise available. The types of concrete deck used are (a) 20 700-kPa (3000-lbf/in^2) monolithic, (b) resurfaced monolithic, (c) two layer with precast box beams as the structural deck, and (d) two layer with 20 700-kPa concrete as the structural deck, both with a concrete running surface. Either cement grout or two-part epoxy is used to bond the overlays to the structural decks.

This report presents a comparison between the behavior of monolithic decks and two-layer decks in respect to site conditions, concrete used, method of placement, types of structure, chloride content of the concrete (2), bonding method, and deck performance.

SAMPLING OF BRIDGE DECKS

Of the total bridge population of British Columbia, all those with concrete riding surfaces from two freeway systems south and east from Vancouver were chosen for study. These bridges were chosen because (a) they are approximately the same age (constructed between 1959 and 1964), (b) they are subject to similar weather and traffic conditions, (c) they were made from good-quality ready-mixed concrete, and (d) they contain a variety of types of bridge decks. A total of 73 bridges were studied.

The average annual rainfall in the Vancouver area varies from less than 900 mm (35 in) in the south to more than 1800 mm (70 in) along the mountains (3). The annual number of days of measurable precipitation varies from 160 in the south to 180 along the mountains (4).

The maintenance practice for freeway salting is to do the bridges first because they tend to ice up and become unsafe. When overnight freezing is anticipated, salt is applied once before the heavy evening traffic, once during the night, and once early in the morning. During snowfalls, salting is relatively continuous. Generally, there are about 12 snow d/year (a range of 10 to 18) and 50 to 100 freeze-thaw cycles/year.

One of the bridges in the sample, the Port Mann Bridge, crosses the Fraser River and is subject to wind chill. Its salting period begins at least a month before and ends a month after salting of the other bridges. Its traffic density is approximately 15 000 vehicles/lane/d. More than 10 percent of the automobiles use studded tires between October 31 and March 31.

The following procedures were used during the construction period for the bridges in this study:

1. Aggregates for concrete were produced in modern plants in the area;
2. Material from glacial outwash was crushed, washed, screened, and stockpiled in various sizes;
3. The resulting aggregates were of sound, durable particles and free from deleterious substances;
4. The sand varied somewhat in gradation, but was within the ASTM specifications for variation in fineness modulus;
5. The ready-mix plants in the area were modern and all had quality-control service available to any customer;
6. The concrete was centrally batched, mixed, and truck agitated or centrally batched and mixed in trucks en route to the site;
7. Trucks and plants were maintained to produce consistently mixed concrete; and
8. Admixtures for air entrainment were available at most plants.

DETAILS OF BRIDGE-DECK CONSTRUCTION

The bridges in the study have monolithic decks, concrete-resurfaced monolithic decks, or two-layer decks with a 34 500-kPa (5000-lbf/in^2) concrete wearing surface. The two-layer decks can be further subdivided into structural or precast substructures with either two-part epoxy or cement-grout bonding agents.

Monolithic Decks

The monolithic decks were cast in place from ready-mixed concrete supplied in truck mixers. The concrete was produced to the following specifications and was transported to the deposit position by either buggies or crane and bucket (1 kPa = 0.145 lbf/in^2 and 1 mm = 0.039 in).

Specification	Value
Strength, kPa	20 700
Slump, mm	100
Entrained air, %	5

Vibrators were used to consolidate the concrete. The minimum steel cover was specified to be 40 mm (1.5 in), but some of the decks were later found to have less than 20 mm (0.75 in) cover. The concrete surface was screeded to elevation. Generally, the concrete was finished by using a burlap drag and cured by using a curing compound or saturated burlap.

The records show that

1. The concrete was produced to a low coefficient of variation with strengths greater than 20 700 kPa and air entrainment of 3 to 6 percent by volume,
2. Excessive vibration of the concrete for the deck surfaces usually overworked the concrete,
3. Quality control of the construction was rather loose, which resulted in sacrifice of surface concrete quality (for example, calcimine brushes were used extensively to apply water during the finishing process).

By 1971, some of the decks were showing signs of distress, and it was necessary to decide whether to repair or resurface. The main reasons for deterioration were spalling and pop-outs over the reinforcing steel. If the pop-outs were minor, the bridge deck could be patched. However, usually the patches came out, or the concrete deteriorated around them and the deck became rougher. When considerable reinforcing steel was exposed, the deck was resurfaced (Figure 1). Thus, the criteria used for determining whether decks should be resurfaced were ride and safety.

Some of the resurfacing has shown distress for which inspection and a review of diaries indicates the following causes:

1. A poor bond resulted when the grout dried out before the paving was placed;
2. The overlay hardened before the curing was applied;
3. The concrete was retempered in the ready-mix trucks waiting for the paver; and
4. Large calcimine brushes were used to supply finishing water, which increased the water-to-cement ratio of the overlay surface. Thus far, no resurfaced sections have been replaced, but some have been patched and show signs of failing in bond and around the patches.

The chloride contents and bond strengths of the bridges cored are shown below (1 kg/m^3 = 0.062 lb/ft^3 and 1 kPa = 0.145 lbf/in^2).

Type of Structure	Chloride Content: At Surface (kg/m^3)	Chloride Content: At Rebar (kg/m^3)	Bond Strength (kPa)
Monolithic	1.69 to 14.0	0.69 to 14.40	–
Monolithic overlay (cement)	0.69 to 14.17	3.22 to 14.00	0 to 1199.68

Figure 1. Deck in need of resurfacing.

Type of Structure	Chloride Content At Surface (kg/m^3)	Chloride Content At Rebar (kg/m^3)	Bond Strength (kPa)
Precast beam (epoxy)	3.59 to 11.68	0.29 to 0.46	1909.83 to 1937.41
Precast beam (cement)	0 to 2.25	0.19 to 9.91	241.31 to 1999.41
Structural concrete (cement)	0.10 to 14.32	1.20 to 4.86	620.5 to 2757.9
Structural concrete (epoxy)	0.23 to 11.05	0.07 to 0.52	827.4 to 2089.1

Five-cm (2-in) diameter cores were pulled perpendicular to the bond surface to determine the bond strength. The high concentration of chloride in the lower concrete is probably residual salt from the application of deicing salts before the deck was resurfaced.

Two-Layer Decks Over Box Beams

These bridges were built with precast beams erected at the site and later covered with a concrete riding surface. After the beams were placed, they were posttensioned laterally, and then the ducts were grouted. The upper surface of the box beams became the subdeck surface. This surface was sand blasted, washed, and blown dry with oil-free compressed air to give a good surface for the bonding agent.

Some of the longer box beams had excessive camber. To establish the required deck alignment, the depth of the overlay was varied from more than 5 cm at the beam ends to less than 2.5 cm at their centers. Consequently, two mix designs were used for the concrete overlay. Both used 34 500-kPa concrete having 6 to 8 percent air and 2.5 to 5-cm slump; the shallow sections were constructed with 9.5-mm (3/8-in) coarse aggregate and 298 kg (656 lb) of cement, but the deeper end sections were constructed with 19-mm (3/4-in) aggregate and 278 kg (612 lb) of cement were used.

The bonding agent for the deep-section concrete was cement grout, and that for the shallow-section concrete was a two-part epoxy mixture that gave higher bond strength for the thinner overlay. The concrete was supplied by a ready-mix plant. The surface was struck and finished by using two channels mounted back to back with a vibrator mounted on the top of the channels. This apparatus rested on rails or curbs that had already been cast to the final deck elevation and was dragged over the decking concrete by a man at each end. The compressive strengths of cylinders cast of the surfacing concrete were all greater than 34 500 kPa. The concrete surfacing was cured by using burlap covered with 76 mm (3 in) of sand, kept saturated 24 h/d for 3 d, and then covered with polyethylene for a further 4 d.

Today, about 14 years later, the areas of apparent distress over the box beams are bond failures near the ends that are up to 1 m (3 ft) across on one structure and longitudinal cracks along the seams between the box beams on all the structures. The longitudinal cracks are evident in the winter by long icicles hanging over the freeway. Resurfacing is not yet required, but the bond-failure area has been patched and shows signs of breaking away around the patches.

Two-Layer Decks Over Structural Concrete

In this category, there are minor subdivisions. All the cast-in-place structural concrete was supplied from a ready-mix plant. The design mix and the placement procedure were the same as for the monolithic decks. The surface of the structural deck was rough finished. The surfacing of the decks was either ready-mixed concrete with cement grout or two-part epoxy bonding agent or site-mixed concrete with two-part epoxy bonding agent. The placing, finishing, and curing of the ready-mixed concrete and both bonding agents were similar to the procedures used for the overlay of box beams described above.

Thus far, there is only minor bond failure on one deck of this two-layer type.

The chloride contents and bond strengths for two-layer decks using ready-mixed concrete for the overlay and cement grout for the bonding agent are shown in the table above.

The Port Mann Bridge was constructed over the Fraser River as part of the freeway east of Vancouver in 1963. The total length of the approach spans is more than 1200 m (4000 ft). Special provisions were followed for the construction of the viaduct deck (5). Before beginning the overlay, special aggregates were produced locally for the project and stockpiled at the site. They were kept covered to maintain a more constant moisture content. The coarse aggregate was supplied in two sizes: 16 to 10 mm (5/8 to 3/8 in) and 10 to 5 mm (3/8 in to no. 4). The sand was supplied with a fineness modulus range of 2.4 to 2.9. Cement was supplied in bags and stored dry at the site.

The surface of the structural deck concrete was acid etched, stiff-bristle-broom brushed, neutralized with industrial ammonia, and washed with water. The wash water was ponded on the structure away from the expansion joints and gutters and tested with pH paper before being pumped over the side.

The bonding agent used was a two-component, polysulphide-epoxy adhesive. The specifications required that the epoxy supplier be responsible for the bond between the structural deck and the overlay, and the penalty for any bond failure was the replacement of the overlay in the area that failed. It was the responsibility of the contractor to hire an epoxy-bond inspector to oversee the mixing and placing of the bonding agent. This requirement prompted the bonding-agent supplier to put one of its best technicians in charge of placing the epoxy layer. If, due to delay or weather, the epoxy layer set up, another layer of epoxy was applied before the concreting continued.

The concrete for the overlay was made of 16-mm aggregate and 260 kg (570 lb) of cement and had 19-mm slump, 6 to 8 percent air, and a water-to-cement ratio of 0.39. There was a technician at the batch plant and a technician at the mixer paver. A 9100-kg (20-ton) batch plant was used off the structure, and the aggregates were trucked to the mixer paver in 1800-kg (4-ton)

Figure 2. Paving the Port Mann Bridge.

dump trucks, with bins to hold four separate batches. The mixer paver had a capacity of 0.38 m^3 (0.5 yd^3). The concrete was placed one lane at a time. The technician at the paver monitored each batch for aggregate blend, slump, and entrained air.

The epoxy bonding agent was machine mixed on the back of a truck at the site and never spread more than 3 m (10 ft) ahead of the overlay concrete (Figure 2).

After the overlay concrete was placed, it was screeded and vibrated by using a screeder with vibrators mounted 0.6 m (2 ft) in from each end. The concrete was finished by using a 3-m (10-ft), longitudinal, scraping straightedge. A burlap drag finish was applied to the surface, and the overlay concrete was cured by using burlap, kept saturated for 3 d, and then covered with black polyethylene for a further 4 d.

Thus far, there are no areas of distress on the surface of the approaches to the Port Mann Bridge except some stud wear in the wheel paths of the slow lanes. The chloride contents and bond strengths of the Port Mann Bridge approaches are shown in the table above.

Recently, the British Columbia Ministry of Highways and Public Works commissioned an analysis of the durability of the Port Mann Bridge deck (6). On thin sections prepared from the bridge deck cores and magnified 150 times, both the overlay and the structural concrete showed micro cracks, but the entire section through the bonding agent had no cracks. The epoxy bonding agent is apparently acting as a seal, keeping the salt away from the reinforcing steel in the structural deck. The amount of chloride in the structural concrete also indicates that, when the epoxy is well placed, it acts as a deterrent to chloride migration.

DECK PERFORMANCE

The performances of the different types of concrete deck areas studied are summarized below (1 m^2 = 10.8 ft^2).

Performance	No. of Decks	Area (m^2)	Percentage of Total Area
Monolithic decks			
Resurfaced or needs to be	26	29 610	66.6
Fair	13	8 574	19.3
Good	9	6 232	14.1
Total	48	44 416	100.0
Two-layer decks			
Resurfaced or needs to be	2	1 916	4.1
Fair	3	4 656	9.9
Good	20	40 601	86.0
Total	25	47 173	100.0

SITE MIXING VERSUS PLANT MIXING

Site-mixed concrete for bridge-deck overlays is preferable to ready mixed for the following reasons:

1. Concrete mixed 5 min before placement is more easily handled than is concrete mixed 30 min before placement because of temperature increases, loss of air, aggregate absorption, and cement hydration in the longer mixed concrete.
2. Concrete produced in mixers at the site allows more rigid quality control and the necessary adjustments than is possible in the production of large loads of ready-mixed concrete.
3. It is more economical to reject a small quantity of concrete than a truckload because less concrete is rejected, replacement time is less, and there is less chance of cold joints.
4. Communication among work persons batching and placing the concrete at the site is quicker and more direct than is communication among those on the site and at the ready-mix plant.
5. Aggregates produced in separate sizes, delivered to the site, and covered have more constant moisture contents and less variability. Errors in batching will be fewer, because only one mix is being used, for only one project, and in small quantities. For special projects, aggregates can be produced to exacting specifications.
6. Site-mixed concrete allows better construction control because (a) the same personnel can spread the concrete and place the saturated burlap and (b) production of the concrete can be controlled more easily (e.g., if the epoxy layer is not far enough ahead of the concrete, the work persons can stop spreading concrete and help spread epoxy, and the mixing will stop with no old concrete in the mixer; if the overlay is starting to set up, the work persons can stop spreading concrete and help apply saturated burlap, and the mixing will stop with no old concrete in the mixer; or if rain or breakdowns cause delays, the mixing will stop with no concrete in the mixer, until the operation can proceed).

OBSERVATIONS—MONOLITHIC VERSUS TWO-LAYER DECKS

Two-layer construction for concrete bridge decks is superior to monolithic construction for the following reasons:

1. The 20 700-kPa (3000-lbf/in^2) concrete used for the monolithic decks is less durable than the 34 500-kPa (5000 lbf/in^2) concrete used for the two-layer decks.
2. If the structural part of the deck is to be covered with a high-quality, carefully controlled, durable overlay, then the concrete for the structure can be placed by using normal quality control.
3. Because the structural deck settles during placement to almost its full deadload deflection, the final profile is more nearly correct when the overlay is placed, and better vertical alignment and better drainage will result.
4. The structural deck allows access to the topping placement for heavier equipment, guarantees no displacement of the reinforcing steel during placement, makes pumps unnecessary, deposits the topping almost in place, and allows drier mixes that consolidate with less vibration because there is no steel in the overlay.
5. The overlay will have few shrinkage cracks and none of the segregation of the structural deck.
6. Placing an overlay on a hardened structural deck guarantees that the thickness of cover of the reinforcing

steel in the finished deck is at least the thickness of the overlay.

SUMMARY AND CONCLUSIONS

Of the concrete bridge decks in two freeway systems in the Vancouver area, which were all built about the same time, with aggregates and concrete from the same sources, and subject to about the same weather conditions and to some of the heaviest traffic in British Columbia, the monolithic structures have the most surface failures. For the overlays on the two-layer bridge decks, site mixing with site-stored aggregates produced more durable concrete decks than did ready-mixed concrete. A two-part epoxy bonding agent used under the supervision of a competent technician produces a more consistent bond than does a randomly placed, unsupervised mix of cement grout. The two-part epoxy bonding agent inhibits the migration of chloride ions to the reinforcing steel. Tire studs and the application of extra water for deck finishing at the time of placement contribute to deck deterioration. Rigid adherence to the principles of batching, mixing, placing, finishing, and curing concrete is mandatory for concrete-deck durability.

1. Well-bonded, two-layer decks are more durable than monolithic decks and guarantee adequate cover of the steel.
2. Rigid quality control of the concrete and bonding agent used for the overlay of two-layer bridge decks is mandatory for satisfactory bond and deck durability.
3. Rigid control of the application of the bonding agent appears to produce a positive bond and inhibit chlorides from reaching the reinforcing steel.
4. Site mixing of deck overlay concrete allows excellent quality control and more expedient placement of the concrete.

RECOMMENDATIONS

1. Bridge decks should be two-layer systems.
2. Concrete for deck overlays should be site mixed, preferably in small batches.
3. Aggregates for bridge-deck overlays should be screened to 16 to 10-mm ($^5/_8$ to $^3/_8$-in) and 10 to 4.75-mm ($^3/_8$-in to no. 4) sizes, stockpiled separately at the site, and covered until used.
4. Cement sufficient for the deck overlays should be stored dry at the site.
5. The overlay should be 34 500-kPa (5000-lbf/in^2) concrete with a maximum slump of 19 mm ($^3/_4$ in), a water-to-cement ratio of not more than 0.35, 6 to 8 percent entrained air, and the minimum sand content that allows placing and finishing.
6. The bonding agent should be two-part epoxy.
7. Placing the epoxy during the overlay of the structural deck requires scrupulous supervision by qualified personnel.
8. The structural deck surface should be thoroughly cleaned down into the matrix and kept clean.
9. The overlay concrete should be spread in even rows in front of the paver and struck perpendicular to the centerline of the bridge.
10. The overlay concrete should be placed longitudinally in single-lane widths.
11. The finishing machine should have some form of surface vibration for consolidation.
12. Any cold joints should be vertical, not sloped (including the longitudinal joint between mats), and the vertical surface should be covered by bonding agent when pouring the concrete begins again.
13. Large [170-L (45-gal)] drums of water should be placed along the paving route at suitable intervals for saturating burlap sheets for curing. The saturated burlap should be applied as soon as the surface is finished.
14. The burlap curing should be kept saturated for 3 d and then covered with polyethylene for 4 d.
15. After curing, the surface should be air dried for 1 d and then sealed.
16. Stringent care should be exercised to ensure good concrete practice in batching, mixing, spreading, consolidating, finishing, and curing of the overlay.

ACKNOWLEDGMENT

Without the research of, discussions with, and access to the files of L. C. Johnson and E. A. Locke of the British Columbia Ministry of Highways and Public Works, the preparation of this paper would have been impossible. Foundation Engineering Company of Canada and C.B.A. Engineering provided invaluable details of the construction practices used for the freeway bridge decks and the Port Mann Bridge approaches respectively.

REFERENCES

1. E. B. Wilkins and W. C. Dujay. Freezing Index Data Influencing Frost Action. Proc., 7th Canadian Soil Mechanics Conference, Associate Committee on Soil and Snow Mechanics, National Research Council, Technical Memorandum No. 33, Sept. 1954.
2. H. A. Berman. Determination of Chloride in Hardened, Fastbound Cement Paste, Mortar, and Concrete. Office of Research, Federal Highway Administration, Sept. 1972.
3. J. B. Wright and C. H. Tranholm. Greater Vancouver Precipitation. Meteorological Branch, Department of Transport, Technical Memorandum, TEC 727, Sept. 10, 1969.
4. Temperature and Precipitation—1941 to 1970, British Columbia. Atmospheric Environment Service, Department of the Environment, Canada, UDC 551 582 (711).
5. N. Hilton. A Two-Inch Bonded-Concrete Overlay for the Port Mann Bridge. Engineering Journal, Vol. 47, No. 5, May 1964, pp. 30-44.
6. B. Romer. Test Report on Cores From the Port Mann Bridge Approaches. LPM Laboratory CH-Bienwilan See, Switzerland; and Ministry of Highways and Public Works, British Columbia, Sept. 4, 1974.

Publication of this paper sponsored by Committee on Performance of Concrete—Physical Aspects and Committee on Construction of Bridges and Structures.

Concrete-Deck Deterioration: Concrete-Filled Steel-Grid Bridge Decks Have the Answer

Vijay Hasija, Reliance Steel Products Company, McKeesport, Pennsylvania
Carl Angeloff, Pennsylvania Department of Transportation, Pittsburgh

The most common cause of bridge-deck distress is the corrosion of the reinforcing steel that results from the intrusion of chlorides into the concrete after repeated deicer applications. However, there are many concrete-filled steel-grid bridge decks in existence that have not been affected by deicing chemicals, although the amount of chloride present is significant and sufficient to initiate steel corrosion. Data on more than about 400 000 m² (4 000 000 ft²) of grid decks built between 1931 and 1969 showed that the performance of such decks has been excellent. The soundness of the concrete has not been affected, and the steel within the concrete shows no rust or corrosion. These decks have withstood severe weather conditions and frequent use of deicing chemicals. The satisfactory condition of these grid decks, in service for over 40 years, is significant evidence of their durability, which has been accomplished without the help of waterproofing membranes, coatings on steel, cathodic protection, or other treatments designed to prolong bridge-deck life.

The deterioration of reinforced-concrete bridge decks is well known to highway bridge designers and maintenance engineers. The Office of Research and Development of the Federal Highway Administration considers that the elimination of bridge-deck deterioration deserves a high priority effort (1). It is generally believed that the most common cause of bridge-deck distress is the corrosion of the reinforcing steel that results from the intrusion of chlorides into the concrete after repeated deicer applications (2, 3, 4, 5). Most research on bridge-deck deterioration has been directed at stopping or abating the intrusion of chlorides into the concrete.

There has been very little or no research on types of deck systems that are not significantly affected by chlorides. One such system is that of steel-grid construction filled with concrete.

The purpose of this paper is to draw attention to the existence of grid systems that have performed well for over 40 years and are still in sound structural condition. An investigation of more than 400 000 m² (4 000 000 ft²) of such decking on bridges built between 1931 and 1969 showed that concrete-filled steel-grid decks have withstood heavy traffic under severe weather conditions (6).

Physical examination of these decks showed that there was no sign of distress and that the concrete was in sound condition. The chloride concentrations found in some of these decks are sufficient to initiate corrosion of the steel grid. However, none of the decks tested showed any surface spalling or corrosion (7).

The durability of concrete-filled steel-grid decks in a chloride-containing environment is illustrated by one of the smallest bridges investigated (Figure 1), which has a deck area of 43 m² (468 ft²). This bridge deck has been in service for 42 years. It has a mean chloride concentration of 6.22 kg/m³ (10.49 lb/yd³) of concrete, but no physical damage or deterioration is noticeable. The deck was built with concrete finished flush with the top of the grid steel, and no wearing surface was ever applied. The surface condition of the deck is shown in Figure 2, in which the heavy lines are the exposed top flanges of the main beams of the steel grid, and the lines perpendicular to them are the tops of the rectangular cross bars. This surface condition is typical for grid decks where no wearing surface was ever used.

PERFORMANCE OF EXISTING CONCRETE-FILLED STEEL-GRID DECKS

Information on the condition of 17 existing concrete-filled steel-grid bridge decks was obtained from the engineers responsible for their maintenance and is summarized in Table 1. These decks have been in service for 12 to 44 years. The history of their performance has been excellent. The soundness of the concrete has not been affected, and the steel within the concrete shows no significant corrosion. However, bridges 11 and 12 have not performed well. On these two bridges, the design did not specify an adequate amount of welding of the grid to the supports and the transverse reinforcement was not sufficient. These decks have had maintenance problems due to broken welds at the supports. The broken welds have had to be repaired, but the decks are still in service.

In general, concrete-filled steel-grid decks have been designed according to the AASHO specifications for highway bridges (8). These specifications do not provide for adequate transverse steel or welding of grids to supports. A review of the design and construction details of the 17 bridges showed certain differences that have influenced the performances of the decks.

CONSTRUCTION OF CONCRETE-FILLED STEEL-GRID DECKS

Steel-Grid Floor System

The typical construction details of a steel-grid floor system are shown in Figures 3 and 4. The system consists of the main load-carrying members (usually rolled I-sections), top and bottom cross bars placed at right angles to the main bars, and metal form pans that are tack-welded to the bottom flanges of the main I-sections to retain the concrete. The grid floor is factory assembled—usually in panels 2.4 m (8 ft) wide and up to 14.6 m (48 ft) long. These panels are then transported to the bridge site and installed on the supports designed to carry the deck to create a working platform for further work such as splicing, bolting, welding, and building expansion dams. No field formwork is required because the metal form pans are already provided. After the miscellaneous work is performed, the concrete is poured and cured according to standard practices. The grid panels can also be precast with concrete if necessary.

The materials used in the construction of grid decks are usually, as specified by ASTM, A7, A7 (0.2 percent copper), A36, or A588 steels.

Grid Beams and Main Members

Specially rolled I-sections have been extensively used as the main stress-carrying members in the concrete-filled steel-grid floors. Optimum sections are used to provide approximately equal positive and negative composite-section properties. The practical design constraints are (a) to provide the least top flange width, (b) to provide a sufficient mass in the bottom flange for good bearing and welding, and (c) to provide a sufficient flange width to retain the metal form pans.

The depths of sections commonly used have been 7.6, 8.9, 10.8, and 12.7 cm (3, 3.5, 4.25, and 5 in). The spacing of the grid beams varies with the loading and span. The masses of the I-sections and their mass distributions also differ even within sections having the same depths. Auxiliary reinforcement is sometimes provided if the rolled sections are widely spaced.

Figure 1. Concrete-filled steel-grid bridge deck built in 1934 (bridge 18).

Figure 2. General surface condition of concrete-filled steel-grid bridge deck with no wearing surface after 42 years service (bridge 18).

Transverse Steel

Transverse steel is commonly provided by constructing the grid system with top and bottom cross bars.

The top cross bars have two important functions. First, they serve to armor the deck and, therefore, play an important role in reducing shrinkage cracks, which significantly increases deck durability. Second, they are a part of the transverse reinforcement of the slab and, therefore, assist in the lateral distribution of concentrated wheel loads. The major function of the bottom cross bars is in the lateral distribution of concentrated wheel loads, which requires that there be sufficient tensile reinforcement to resist flexural stresses in the transverse direction of the slab.

On the existing decks, the bottom cross bars and their spacing vary greatly. Rectangular and round bars have both been used in varying sizes. The bars have been spaced from 15 to 61 cm (6 to 24 in) center to center, with one approximately in the middle half of the span. In the earlier designs, only two bars were used for spans up to 1.83 m (6 ft) wide, but in later designs, three bars are used for spans up to 1.98 m (6.5 ft) wide. The current practice is to space the bars at 20.3-cm (8-in) center-to-center intervals, except within 30.5 cm (1 ft) of the supports.

The amount of transverse steel provided varies widely among the bridges (Table 2). The total transverse reinforcement (top and bottom) based on the gross section of the main steel varied from 15.7 to 35.22 percent. The bottom reinforcement varied from 3.10 to 21.65 percent, and the top reinforcement varied from 8.57 to 24.32 percent. These differences exist because there are no design specifications for transverse reinforcement, and engineering judgments have varied.

No problems have been reported where the total transverse steel exceeded 18 percent. The distribution of the reinforcement between the top and bottom cross bars is found to be compensatory. Good performance has been reported where the bottom reinforce-

Table 1. Existing concrete-filled steel-grid bridge decks.

Bridge No.	Bridge Name	Year Built	Owner	Grid Depth (mm)	Approximate Deck Area (m^2)
1	South 10th Street	1932	Allegheny County, PA	76.2	4 738
2	Upper Black Eddy	1933	Delaware River Joint Toll Bridge Commission	88.9	1 394
3	Highland Park	1937	Pennsylvania Department of Transportation	108.0	10 325
4	Manhattan	1938	New York City	88.9	17 211
5	CT-661 (Middletown)	1938	Connecticut Department of Transportation	88.9	5 017
6	Main Avenue	1939	Ohio Department of Transportation	108.0	35 742
7	East 21st Street	1939	Ohio Department of Transportation	108.0	6 689
8	Erie Avenue	1939	Ohio Department of Transportation	108.0	3 103
9	Bronx-Whitestone	1939	Triborough Bridge and Tunnel Authority	108.0	19 733
10	Charter Oak	1942	Connecticut Department of Transportation	108.0	3 755
11	North	1950	Pennsylvania Department of Transportation	108.0	20 506
12	Penrose	1951	Pennsylvania Department of Transportation	108.0	3 198
13	Patapsco Project	1955	Maryland Transportation Authority	108.0	35 273
14	Walt Whitman	1956	Delaware River Port Authority	127	89 915
15	Mackinac Straits	1957	Mackinac Bridge Authority	108.0	16 500
16	Throgs Neck	1961	Triborough Bridge and Tunnel Authority	127	20 547
17	Verrazano Narrows	1964	Triborough Bridge and Tunnel Authority	108.0	91 986

Note: 1 mm = 0.039 in and 1 m^2 = 10.76 ft^2.

Figure 3. Construction details of typical concrete-filled steel-grid floor.

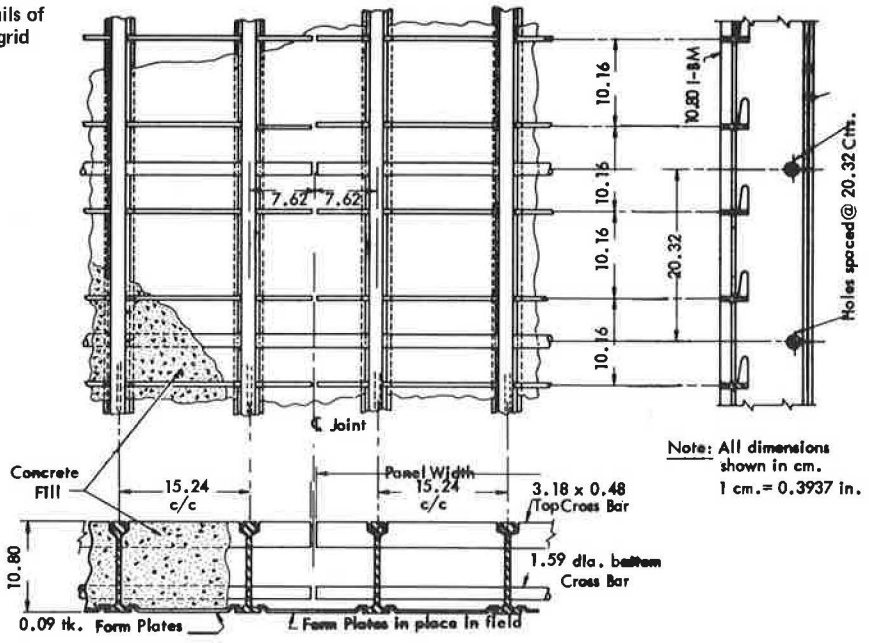

Figure 4. Welding requirements of typical concrete-filled steel-grid floor.

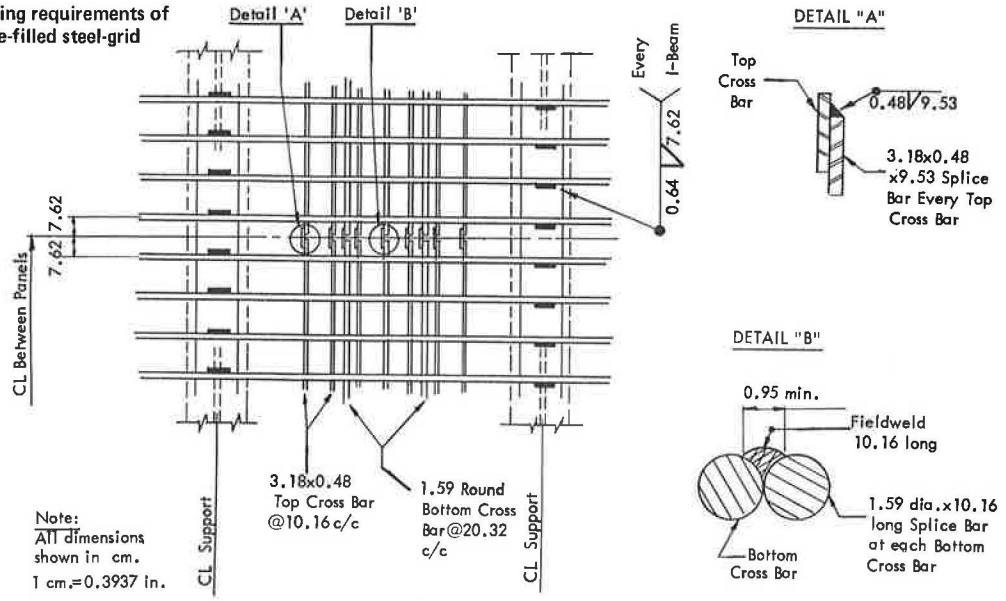

Table 2. Transverse steel and welding on existing concrete-filled steel-grid bridge decks.

Bridge No.	Transverse Steel[a] (percentage of main steel) Bottom	Top	Total	6-mm Fillet Weld[b] (%)
3	8.60	21.00	29.60	14.9
4	12.61	22.61	35.22	49.6
5	3.35	16.95	20.30	13.2
6	3.90	12.62	16.52	19.8
7	5.51	12.60	18.11	24.8
8	5.51	12.60	18.11	24.8
9	17.00	12.60	29.60	16.5
10	10.50	13.39	23.89	19.8
11	3.62	12.60	16.22	13.2
12	3.10	12.60	15.70	13.2
13	12.67	18.90	31.57	26.4[c]
14	15.84	9.64	25.48	75.6[c]
15	8.70	24.32	33.02	52.9
16	17.02	8.57	25.59	90.8[c]
17	21.65	12.37	34.02	70.5

[a] Based on gross areas.
[b] 1% fillet weld = 0.12 in/ft.
[c] Minimum welding where amount varied.

ment exceeded 5 percent of the gross area of the main members. However, when the bottom cross bars were widely spaced [61 cm (2 ft) on centers] and not adequately compensated for by the top cross bars, the deck performance has been unsatisfactory not only where there was less than 18 percent transverse reinforcement, but also where the splicing of cross bars and the welding of grid beams to the stringers was minimal.

Fastening of Grid to Supports

Both welding and bolting have been used to fasten the main beams of the grid decks to the supports. Welding has been popular and economical. Because of this positive connection, the grid floor filled with concrete has a composite action with the supporting steel. To ensure a durable and lasting connection, the weld must be designed to withstand the anticipated stresses.

The amount of welding is another area in which the details differ among the existing decks (Table 2). In the earlier designs, a 6.35-mm (0.25-in) fillet weld,

which gives an average of 18.75 percent (2.25 in/ft) on the stringers, was used. This was later increased to an average of 25 percent (3 in/ft) on the stringer, and current practice is to provide an average of 50 percent (6 in/ft).

These welding specifications are the manufacturers' recommended minimums based on experience. However, design load, stringer size, spacing, and spans should also be considered in determining the size of the welds. However, on the existing concrete-filled steel-grid decks, no failures attributed to fatigue have been reported.

Splicing Adjacent Panels

Splicing of the cross bars is important to maintain continuity and avoid weak links in the slab. In the earlier designs, all the bottom cross bars were welded, but only a few top cross bars were welded. The current practice is to weld all top and all bottom cross bars. Continuity of the main beams in a grid slab has always been maintained by a welded connection, whenever required.

Table 3. Condition of concrete-filled steel-grid bridge decks.

Bridge No.	Year Built	Approximate Deck Area (m^2)	Percentage Spalled	Mean Chloride Concentration (kg/m^3)
18	1934	43	0.0	6.22
19	1940	434	0.0	2.61
20	1958	241	—	0.15
21	1932	4645	0.0	1.72
22	1932	1279	0.0	0.63
23	1937	2880	—	1.12
24	1931	3292	—	3.90
25	1940	8941	—	2.07

Note: 1 m^2 = 10.76 ft^2 and 1 kg/m^3 = 1.69 lb/yd^3

Table 4. Condition of Penn-Lincoln parkway bridges.

Bridge No.	Year Built	Approximate Deck Area (m^2)	Percentage Spalled	Mean Chloride Concentration (kg/m^3)
26	1953	3062	0.0	0.34
27	1953	4852	2.0	0.45
28	1953	3974	—	0.86
29	1953	1450	2.0	3.27
30	1958	4618	—	2.12
31	1958	4618	—	1.83
32	1958	3933	—	4.22
33	1958	6639	45.0	3.55
34	1953	2535	—	6.47
35	1956	124	50.0	2.98
36	1956	2575	25.0	5.55
37	1958	1570	5.0	3.11
38	1951	8012	12.0	4.67
39	1951	3099	70.0	2.59
40	1952	681	32.0	3.27
41	1951	744	—	3.18
42	1951	1175	—	5.64
43	1948	2111	—	5.43
44				
Older portion	1951	439	5.0	3.83
Widened right lane	1971	110	0.0	0.0
45	1950	1079	18.0	3.04
46	1950	479	2.0	4.62
47	1961	557	45.0	4.62
48	1961	3212	5.0	3.27
49	1961	4505	—	5.09
50	1962	1598	7.0	1.61
51	1962	1998	37.0	0.18
52	1962	1971	22.0	4.45
53	1962	604	5.0	0.27
54	1962	604	4.0	0.77
55	1962	1022	3.0	0.12
56	1969	3679	—	0.14

Note: 1 m^2 = 10.76 ft^2 and 1 kg/m^3 = 1.69 lb/yd^3

The details of splicing top and bottom cross bars and grid beams in adjacent panels vary, depending on the engineer's judgment; different details have been used for different bridges. The type and size of cross bars and the nature of the supports govern the splice design.

Those decks where all the top and bottom cross bars were spliced either by welding or by additional lap bars have been trouble free. Simple lap splices with 5.1-cm (2-in) long welds have been as effective as conservatively designed ones.

Concrete and Metal Form Pans

It was not possible to obtain data on the mix proportions and the quality control of the concrete used in the different bridges. But in all cases examined, the soundness of the concrete has not been affected, and spalling has not been observed.

The metal forms used have generally been 0.91 or 1.21-mm (no. 20 or no. 18) commercial-quality steel—sometimes galvanized, but mostly painted on the exposed side. These pan-shaped metal forms have not shown any signs of distress after prolonged use except at places where there is a direct water leakage and, therefore, some rusting. They have been used only to retain concrete and have never been considered to be a part of the structural slab. Some precast decks have been made without permanent metal form pans.

Wearing Surfaces

The grid decks on many of the bridges had had the concrete poured flush with the top of the grid steel. No additional wearing surface was ever applied. Such decks are still in service and, after 30 to 40 years of use, show signs of surface wear mainly in the form of cupping of the concrete enclosed within the cells formed by the main beams and the top cross bars. The depth of the cupping varies from 3.2 to 12.7 mm (0.13 to 0.5 in) below the level of the top of the steel. On some decks, the riding quality has been improved by the application of asphaltic wearing surfaces. On bridge 6, an epoxy system was used to provide a new wearing surface in 1974. On bridge 22, a 25.4-mm (1-in) thick wearing surface of latex-modified concrete was applied in 1973, after 40 years of service without any wearing of the surface. This has worked well and is in good condition.

Some of the grid decks had been constructed with the concrete poured to a depth of 19 mm (0.75 in) above the top of the grid steel. This overfill was inadequate and did not last long under traffic. However, the structural slabs remained unaffected and are still in service.

The grid deck on bridge 17 was overfilled with concrete in one pour to a depth of 44.4 mm (1.75 in) above the top of the grid steel. This has performed excellently.

CHLORIDE CONCENTRATIONS

To assess the effects of deicing salts on the deterioration of two types of bridge decks, 42 reinforced-concrete-slab bridge decks on the Penn-Lincoln Parkway in Pittsburgh and I-79 were sampled, analyzed for chloride concentrations, and evaluated for the physical distress of their riding surfaces. Eight concrete-filled steel-grid bridge decks were similarly tested.

Both the parkway and the I-79 bridges were chosen for study because of the comparative variables associated with their service life. All of each set were similarly constructed, have experienced the same traffic conditions, and, most importantly, have probably had relatively similar quantities of salt applied. However,

the I-79 structures have experienced a shorter salting period than the parkway bridges because of their newer construction. Also, quality control was vastly improved during their construction period. Therefore, a study of these bridges should provide information about the effects of chlorides during an early period in the service life of a bridge deck and of whether or not their concrete, which was made with better quality control, has a greater ability to retard chloride intrusion.

All eight concrete-filled steel-grid decks sampled were in the Pennsylvania Department of Transportation's engineering district 11-0 and had service lives greater than 17 years.

Samples for chloride testing were recovered from a zone 12.7 mm (0.5 in) above the top mat of reinforcing steel for the parkway and I-79 bridges. For the concrete-filled grid decks, the samples were collected at a depth of 38.1 mm (1.5 in) below the top surface of the deck steel. The procedure developed by Berman (9) was used for the chloride analyses.

The results of the chloride tests of the concrete-filled grid decks (bridges 18 through 25) are given in Table 3. The results for the parkway bridge decks (bridges 26 through 56) and the I-79 bridge decks (bridges 57 through 67) are given in Tables 4 and 5 respectively.

The average chloride concentration of the parkway bridges is 2.95 kg/m^3 (4.98 lb/yd^3) of concrete. The decks on bridges 26 through 36 (with the exception of bridges 30, 31, and 32) were all constructed at the beginning of the bare-pavement policy and had the highest mean chloride concentration [3.49 kg/m^3 (5.88 lb/yd^3) of concrete].

Only 3 of the 18 decks in this group had chloride concentrations of less than 1.19 kg/m^3 (2 lb/yd^3) of concrete. Bridge 26, after 23 years in service, had a chloride concentration of 0.34 kg/m^3 (0.570 lb/yd^3) of concrete and showed no surface spalling. No explanation can be offered for this because there were areas of insufficient concrete cover.

Bridges 47 through 55 and bridges 30, 31, and 32 were constructed between 1958 and 1962 and had a mean chloride concentration of 2.37 kg/m^3 (4 lb/yd^3) of concrete. The surface spalls varied from 3 to 45 percent of the traffic lanes. In general, all these decks were in poor condition.

The bridge decks on I-79 were constructed between 1965 and 1973. These decks represent a more advanced period in highway construction techniques. Their mean chloride concentration is 1.0 kg/m^3 (1.68 lb/yd^3) of concrete. Twenty-seven percent of the 22 decks tested showed chloride concentrations greater than 1.19 kg/m^3 (2 lb/yd^3) of concrete. Two of these decks are only 5 years old.

In general, these 22 decks are in good condition. The largest amount of surface spalling is on bridge 57, which has 1 percent of its area spalled and a chloride concentration of 4.81 kg/m^3 (8.11 lb/yd^3) of concrete.

The mean chloride concentration of the concrete-filled grid decks was 2.30 kg/m^3 (3.88 lb/yd^3) of concrete. Although the average chloride concentrations of the parkway and the concrete-filled grid decks are similar, their surface spalling problems differ widely.

None of the steel-grid decks showed any signs of physical distress in their deck surface. On the contrary, all the parkway decks, with the exception of bridge 26, showed from moderate to severe surface spalling. The problems of the parkway decks are one of the reasons for the $130 million parkway safety update project that will eventually replace 95 percent of the reinforced-concrete slab decks of the main-line bridges.

The durability of concrete-filled steel-grid decks in a chloride-containing environment is illustrated by bridge 21 (Figure 5). This deck has been in service for 44 years and had a mean chloride concentration of 1.92 kg/m^3 (2.90 lb/yd^3) of concrete. The overall roadway surface of approximately 4645 m^2 (50 000 ft^2) is in a remarkably good condition, although rust staining is evident on the top surface of concrete.

Table 5. Condition of I-79 bridges.

Bridge No.	Year Built	Approximate Deck Area (m^2)	Percentage Spalled	Mean Chloride Concentration (kg/m^3)
57				
Northbound	1965	1731	1.0	4.81
Southbound	1965	1731	0.5	2.32
58				
Northbound	1965	4047	0.5	1.16
Southbound	1965	4047	0.5	1.33
59				
Northbound	1965	1430	0.5	0.75
Southbound	1965	1430	0.5	2.09
60				
Northbound	1965	4101	0.5	0.77
Southbound	1965	4101	0.5	0.28
61				
Northbound	1972	1534	0.0	0.31
Southbound	1972	1534	0.0	0.32
62				
Northbound	1972	5627	0.0	0.37
Southbound	1972	5627	0.0	0.28
63				
Northbound	1973	2161	0.0	0.45
Southbound	1973	2161	0.0	0.61
64				
Northbound	1973	1944	0.0	0.49
Southbound	1973	1944	0.0	0.41
65				
Northbound	1973	773	0.0	0.47
Southbound	1973	773	0.0	0.60
66				
Northbound	1971	1823	0.0	0.50
Southbound	1971	1823	0.0	0.75
67				
Northbound	1971	2065	0.5	1.70
Southbound	1971	2065	0.0	1.21

Note: 1 m^2 = 10.76 ft^2 and 1 kg/m^3 = 1.69 lb/yd^3.

Figure 5. Tenth Street Bridge, built in 1932 (bridge 21).

CONCLUSIONS

The following conclusions can be drawn from the data presented in this paper.

Research and test data on steel-grid systems have not been available. The only guide for design has been the AASHO specifications. The designs have varied in details, and these have affected their performance. The unsatisfactory performance of two bridge decks has been

traced to inadequate welding of grids to supports, provision of transverse steel, and splicing of adjacent grid panels. These details can be improved by proper research and analysis.

The chloride concentrations found in concrete-filled steel-grid bridge decks are sufficient to initiate corrosion of the steel. However, none of the grid decks tested showed any surface spalling.

The chloride concentrations found in the reinforced-concrete slab decks of the parkway bridges are sufficient to initiate corrosion of the reinforcing steel. The physical condition of the majority of these bridge decks shows that surface spalling is a serious problem.

The chloride concentrations found in the reinforced-concrete slab decks of the bridges on I-79 showed that 27 percent of the decks sampled contained chlorides in amounts sufficient to initiate corrosion of the reinforcing steel. However, since the oldest deck is only 11 years old and all the decks are in generally good condition, these bridge decks are merely undergoing the preliminary phases of steel corrosion, and surface spalls have not had sufficient time to develop.

The single most important conclusion of this study is that concrete-filled steel-grid bridge decks are effective in providing long serviceability in chloride-containing environments. This is accomplished without the help of waterproofing membranes, coatings on steel, cathodic protection, or any other substances designed to prolong bridge deck life. At the same time, the construction of such decks does not require high-caliber quality control.

A review of two bridge biddings in October 1975, indicates that concrete-filled steel-grid decks are economically competitive with reinforced-concrete slab decks. The bid price received for the reinforced-concrete slab decks in the parkway west safety update project [13 350 m^2 (143 560 ft^2) on four bridges] was \$125.60/m^2 (\$11.63/ft^2), including galvanized bars and a waterproofing membrane. The low bid received for the replacement of one 434-m^2 (4669-ft^2) bridge deck was \$139.60/m^2 (\$12.00/ft^2) for a concrete-filled steel-grid deck. Thus, the concrete-filled steel-grid bridge deck may be an economical, lightweight, and durable solution to the problem of bridge-deck deterioration.

ACKNOWLEDGMENTS

We acknowledge the contributions of various engineers who cooperated in providing information and data about existing concrete-filled steel-grid decks. The samples for the chloride test were collected by the bridge inspection staff of District 11-0, and the tests were conducted by the Bureau of Materials and Research, Pennsylvania Department of Transportation. We also acknowledge the cooperation of the Civil Engineering Department of the University of Pittsburgh.

REFERENCES

1. K. C. Clear and R. E. Hay. Time to Corrosion of Reinforcing Steel in Concrete Slabs. Federal Highway Administration, Interim Rept., April 1973, pp. 1-8.
2. D. L. Spellman and R. F. Stratfull. Laboratory Corrosion Test of Steel in Concrete. Division of Highways, California Department of Public Works, Res. Rept. MR-635116-3, Sept. 1968, pp. 1-19.
3. C. F. Stewart. Deterioration in Salted Bridge Decks. In Improving Pavement and Bridge Deck Performance, HRB, Special Rept. 116, Aug. 1971, pp. 23-28.
4. R. F. Stratfull and V. VanMatre. Corrosion Autopsy of a Structurally Unsound Bridge Deck. Division of Highways, California Department of Public Works, Rept. MR-5716-8-72-41, Jan. 1973, pp. 1-17.
5. D. L. Spellman and R. F. Stratfull. Chlorides and Bridge Deck Deterioration. Division of Highways, California Department of Public Works, Interim Rept., Aug. 1969, pp. 1-17.
6. V. Hasija. Concrete-Filled Steel-Grid Floors for Bridges. Reliance Steel Products Co., McKeesport, PA, July 1975, pp. 1-61.
7. C. Angeloff. An Evaluation of the Comparative Effect of Chlorides on the Deterioration of Reinforced-Concrete-Slab and Concrete-Filled-Grid Bridge Decks. Univ. of Pittsburgh, MS thesis, April 1976, pp. 1-62.
8. Standard Specifications for Highway Bridges. AASHO, 1973, Article 1.3.6.
9. H. A. Berman. Determination of Chloride in Hardened Portland Cement Paste, Mortar, and Concrete. Federal Highway Administration, Interim Rept., Sept. 1972, pp. 1-22.

Publication of this paper sponsored by Committee on Corrosion.

Possible Explanation of Concrete Pop-Outs

J. H. Havens and R. C. Deen, Bureau of Highways, Kentucky Department of Transportation

Several years of research relating to damage to concrete and aggregates undergoing freezing and thawing is summarized. Basic principles involving freezing and the attendant pressures are discussed. These principles were applied to the evaluation of concrete in experiments on concretes having low and high air contents. The freeze-thaw characteristics of saturated aggregates relative to their physical properties such as porosity, absorption, and bulk specific gravity were studied by submerging individual particles in prechilled mercury. The pressures associated with pop-outs in concrete were monitored and are discussed in theoretical terms.

Voids occur in concrete through the entrapment and entrainment of air, the occlusion of excess mix water, differences in the specific volumes of reactants and hydration products, leaching of hydration products such as CaO and the use of porous aggregates. Those voids that are easily saturated affect the durability of the concrete unfavorably while those that are less permeable increase the durability. Much water is occluded in concrete in the form of excess mix water and water ab-

sorbed by the aggregate. Concrete that has not been allowed to dry after curing and before the onset of freezing does not perform as well in laboratory tests as does concrete that has been dried, but otherwise is similar. This indicates that a somewhat irreversible fixation or tightening of the mortar structure attends drying so that the concrete becomes less susceptible to resaturation; i.e., the process of drying may close some of the pores. The use of aggregate that is merely moistened, as opposed to soaked or saturated, in the concrete favorably affects its durability—at least in laboratory freeze-thaw tests. Either or both of these effects may be merely the result of delayed saturation.

Dry concrete is unaffected by freezing and thawing: In fact, serious damage is sustained only when a high degree of saturation exists. If the concrete is relatively impermeable, even though it contains a large percentage of voids, saturation is unlikely to occur unless exposure to water is sustained for a long period of time. In natural exposures, periods of wetting alternate with periods of drying, and the durations of the drying periods tend to exceed those of the wetting periods. In the random course of nature, a concrete structure such as a bridge would tend to dry; however, long interim periods of wetness followed immediately by freezing may be extremely damaging.

BASIC THERMAL ANALYSIS

The density of water at 0°C (32°F) is 999.8 kg/m^3 (62.4 lb/ft^3), and the density of ice at 0°C is 917 kg/m^3 (57.2 lb/ft^3) (1). There is an increase in volume of approximately 9 percent when water freezes. If the pores or voids in concrete are completely filled with water and this is frozen, the concrete must dilate or expand proportionally.

Saturation of all voids to 91.7 percent is termed critical saturation, alluding to the degree of saturation beyond which freezing of the water overfills the voids with ice and creates internal expansive pressures. While its theoretical meaning is quite clear, its practical meaning is more in the sense of a statistical average that can be interpreted in two ways: (a) 91.7 percent of the voids are completely filled or (b) all the voids are filled to 91.7 percent of their capacity. The first possibility could be extremely damaging to concrete undergoing freezing; if the second possibility accurately described the condition of the water in the concrete, there would be no damage from freezing.

Analogous Phenomena

To demonstrate some basic principles, preliminary experiments were made on rather idealized models (2). First, water in an open vessel was frozen in air, and a time versus temperature record was made with a thermocouple placed near the center of the volume of water. The resulting thermograph (Figure 1) had a broad step at 0°C with no noticeable depression of the freezing point. Second, a closed vessel or steel bomb was improvised from a 76.2-mm (3-in) diameter pipe nipple and two cast-iron caps. A valve and thermocouple well were tapped into the nipple. The bomb was filled with water and frozen in air as before; the resulting thermograph is also shown in Figure 1. Freezing began at 0°C, the freezing point gradually decreased to -4°C (25°F), and then suddenly the cap ruptured and the temperature increased to 0°C. The pressure at rupture agreed closely with the estimated ultimate strength of the cast-iron caps [48 MPa (7000 lbf/in^2)].

Third, the ruptured cap was replaced, and the bomb was filled with water to 96 percent of its capacity. Here again, the water began to freeze at 0°C, but there was no immediate depression of the freezing point and consequently no immediate increase in pressure. In this case, the development of pressure was delayed until most of the water had frozen. The depression of the final freezing point was 3.3°C (6°F) and the pressure at this point was 43 MPa (6200 lbf/in^2); there was no explosive rupture, but the caps yielded considerably.

Experimental Phenomena

Figure 2 illustrates a typical time versus temperature curve obtained from an oven-dried specimen of concrete undergoing one freeze-thaw cycle. Since the freezing was done in air, the specimen temperature lagged behind the air temperature, and there were no sharp breaks or steps in the cooling curve. On flooding the freezing chamber with water at 4°C (40°F), the temperature of the specimen increased rapidly, but there were no sharp steps or breaks in the curve. Figure 2 also illustrates a typical time versus temperature curve obtained from a highly porous, highly absorptive, highly saturated concrete undergoing one cycle of freeze-thaw. The steps in the freezing and thawing curves occurred at approximately the same temperature—near, but not exactly at, the normal freezing temperature of water. The portions of the curves above and below that step have characteristically different curvatures, and the steps are not merely offsets in otherwise normal cooling and heating curves. The slopes of either or both curves as they approach the step may be described as $\Delta T/\Delta t$, i.e., the incremental change in temperature per increment of time. This factor, when multiplied by the product of the specific heat and the weight of the concrete specimen would give the rate at which heat was being removed from the specimen. The product of the time lapse and the rate of heat removal should correspond approximately to the isothermal change in heat content (ΔH) accompanying freezing of the water in the specimen. From Figure 2, it is also apparent that the freezing step is sloping slightly downward from 0°C, signifying that the water began to freeze at a normal pressure of 98 kPa (1 atm), but finished freezing at -22°C (28°F), which corresponds to the freezing point of pure water at a pressure of approximately 31 MPa (4500 lbf/in^2). Since there is no apparent depression of the initial freezing point, no supercooling or other interference mechanism is evident.

A large part of the water absorbed into concrete at saturation may be regarded as being free water that will freeze and evaporate in much the same way that pure water will; it is this water to which the analysis of freezing-point depression and pressure applies most directly. However, part of the water, in addition to the water of hydration and crystallization, exists in an infinitely more complex state because of internal surface absorption and capillary tensions in the concrete. This part of the water is not expected to have a normal freezing point, and it may be of little or no significance here unless its effects appear as an interference mechanism distorting the prototype thermograph.

The only other serious possibility of an interference mechanism is the effect of dissolved electrolytes on the freezing characteristics of the so-called free water. The most abundant solute in hardened concrete is $Ca(OH)_2$, but its solubility at 0°C is about 1.85 kg/m^3 (0.115 lb/ft^3). If complete saturation and 90 percent dissociation are assumed, this would depress the initial freezing point approximately 0.1°C (0.2°F). Since the solution is saturated, it becomes a eutectic or constant-freezing mixture that should otherwise respond to pressure according to the prototype thermo-

graph. The possible effects of alkali available from the cement may be similarly estimated by assuming 0.6 percent alkali by weight of cement and the maximum free water to be approximately equal to the excess mix water. This quantity of alkali, if available as solute, would depress the initial freezing point a maximum of 1.4°C (2.5°F). Since there are no such initial depressions apparent, the concentration of alkali must be rather small, at least while the greater portion of water is freezing. Alkalies such as NaOH and KOH are much more soluble than $Ca(OH)_2$. In dilute solutions of this type, water freezes into nearly pure ice and concentrates the salts in the remaining solution; this decreases the freezing point of the remaining solution. This type of interference mechanism would cause the freezing point step to curve downward at an increasing rate, and there would be no discrete terminus to the step. A general, but cursory, conception of the effects of pressure and different concentrations of highly soluble electrolytes is compared with the normal freezing curve for pure unrestrained water in Figure 3.

In another experiment, two sets of 152-mm (6-in) cubes were cast using a six-bag mix, a 76-mm (3-in) slump, and a dense limestone aggregate. One set contained 13 percent air; in the other set, the concrete was vibrated to expel the entrapped air and had a final air content of 0.7 percent. The two sets of specimens represent extremes of air contents and were a deliberate attempt to magnify the effects of the air contents on the thermographs. Three thermocouples were cast into these specimens to measure their freezing points. One specimen from each of the two sets was moist cured for 5 weeks before the beginning of freeze-thaw, and these specimens failed to exhibit any indication of a freezing-point step even after 30 cycles. The other specimens of each set were cured 14 d and immersed in water for 24 h before the beginning of freeze-thaw. These specimens showed a progressive broadening of the step and a progressive differentiation between the air-entrained and the non-air-entrained concretes, indicating that the rate of absorption of water by the non-air-entrained concrete was much greater. Freeze-thaw was continued to 77 cycles, at which time the non-air-entrained specimens were virtually ruined. Thermographs of the first, fortieth, and seventy-seventh cycles are shown in Figure 4.

The failure of the two concrete specimens that were cured 5 weeks to exhibit a significant thermal step, even after 30 cycles of freeze-thaw, offers an example of highly retarded or delayed saturation. Continued curing and hydration tend to desiccate the smaller interstices of the cement gel and reduce the free water content of the concrete. Continued curing would likewise densify and strengthen the mortar against subsequent ingresses of water. Thus, the mere number of freeze-thaw cycles that a concrete specimen is able to withstand before saturation becomes critical is probably not as significant as the time duration of the conditions causing absorption of water and eventual saturation. It is suggested, therefore, that the number of regular cycles or the time preceding the development of a significant thermal step and freezing-point depression may be a significant basis for evaluating concrete durability.

Figure 1. Typical thermographs.

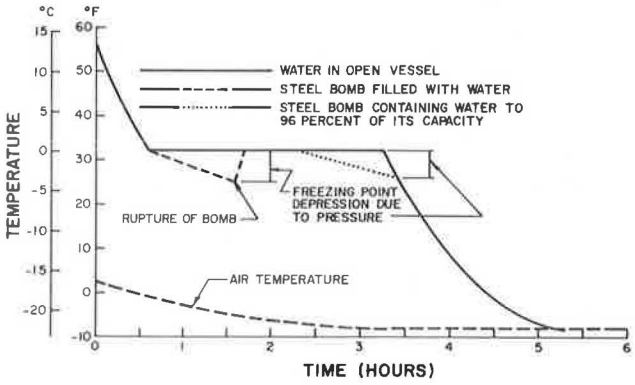

Figure 2. Typical time versus temperature curves of concrete undergoing single freeze-thaw cycle.

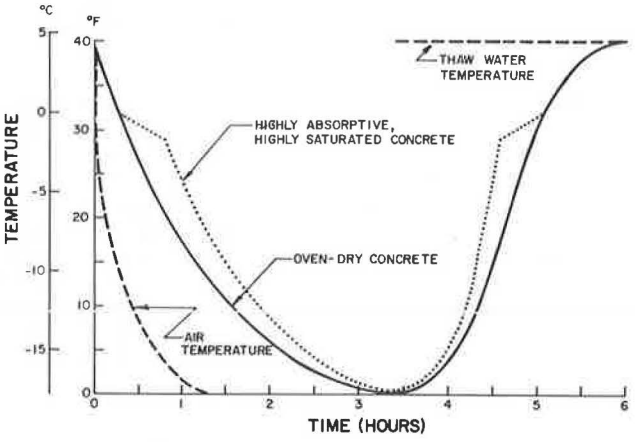

Figure 3. Probable effects of solutes on time versus temperature curve.

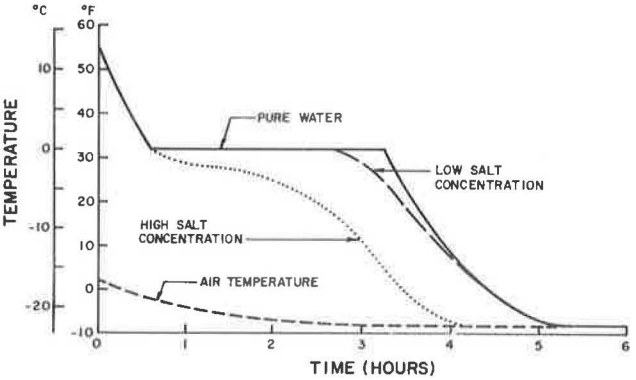

FREEZE-THAW RESISTANCE OF AGGREGATES

The present methods for testing aggregates use composite samples, and the results of such tests provide average values. For example, the average value of absorption obtained from a composite sample may have a low value indicating a sound aggregate; however, if each particle were analyzed, it might be found that a portion of the aggregate was so highly absorptive as to be detrimental to concrete. The percentage of these deleterious particles in an aggregate is also important. Logically, in determining the soundness of an aggregate sample, the freeze-thaw testing should be conducted on a per-particle basis. Each particle should be saturated at the onset of testing and kept saturated during testing. For study purposes, the degree of saturation may be varied. Maximum saturation definitely establishes the ultimate susceptibility of the aggregate to damage from freezing and thawing.

Figure 4. Time versus temperature curves of concrete containing 0.7 and 13 percent air moist-cured 14 d and soaked 24 h.

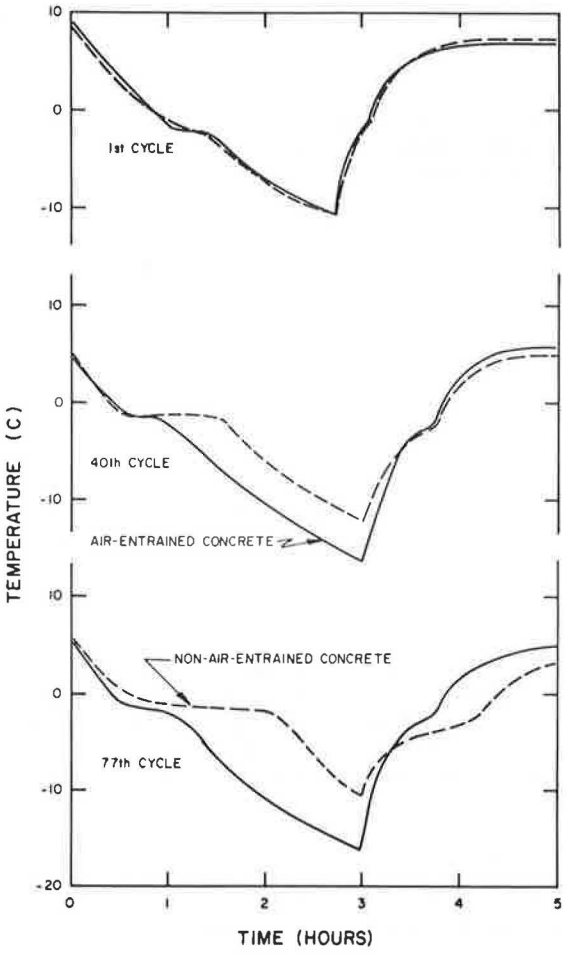

Figure 5. Cumulative percentage of fractured particles.

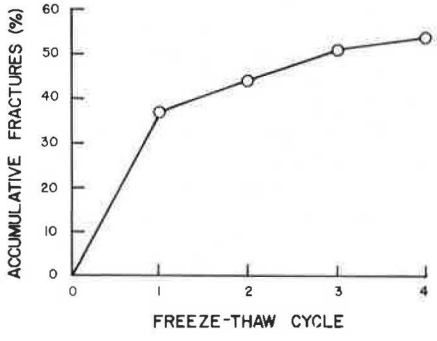

Figure 6. Relation between particle size and percentage of fractured particles after exposure to four freeze-thaw cycles.

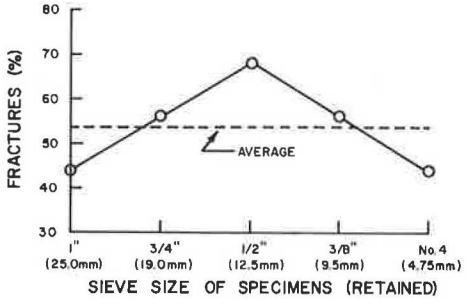

Phenomena

To obtain objective data—definitive relations between the effects of freezing and thawing and such physical properties as porosity, absorption, and bulk specific gravity—pertaining to the freeze-thaw characteristics of aggregate, the following conditions were required (3): (a) a freezing medium in which each aggregate particle could be frozen quickly so that the quickly frozen surface would form a seal or shell about the particle and retain the pore water and (b) a medium that would not contaminate the pore water. Chilled mercury was chosen as the freezing medium—it has a high thermal conductivity, it is immiscible with water, and it has a low freezing point. The test consisted of submerging the aggregate particle in prechilled mercury. Preliminary testing showed that if a particle did not show visual distress at the end of four cycles—which could be performed in a matter of minutes—it would withstand innumerable cycles.

A saturated gravel that represented a variety of rock types and possessed a wide range of physical properties was secured from a glacial outwash deposit and kept inundated to ensure saturated conditions. The primary constituents of the aggregate sample were dolomites, cherts, limestones, sandstones, siltstones, and various igneous and metamorphic rock particles. Although usually acceptable for concrete, this gravel contained both sound and unsound particles and provided an appropriate assortment of particles.

After grading according to five sizes ranging from 4.75 to 38.1 mm (no. 4 sieve to 1.5 in), each particle was numbered. For each particle, the saturated-surface dry weight and the bulk volume, by mercury displacement, were measured before the freeze-thaw tests, and the bulk specific gravity was calculated. The freezing was accomplished by submerging each particle in cold mercury [-30 to -35°C (-22 to -31°F)] for 5 min. The mercury was contained in a glass cylinder enclosed in an insulated container of dry ice (solid CO_2). At the end of each freezing cycle, the particle was removed from the mercury, placed in a container of water, and allowed to thaw. At the end of each thawing cycle, the particle was examined visually and any distress resulting from the freezing and thawing was recorded.

Absorption values for each particle were determined after the freeze-thaw testing. Each particle (or major piece) was dried to a constant weight at 110°C (230°F). The absorption of each particle was calculated from

$$w = 100(W_T - W_S)/W_S \quad (1)$$

where

w = absorption (percent),
W_T = saturated-surface dry weight of particle (or major pieces), and
W_S = oven-dried weight of particle (or major pieces).

Porosity calculations were made by using

$$\eta = 100G_{SSD}\, w/(100 + w) \quad (2)$$

where η = porosity (percent) and G_{SSD} = bulk specific gravity (saturated-surface dry). (This equation applies only for saturated aggregates.)

The accumulated number of fractured particles at the end of each freeze-thaw cycle, expressed as a percentage of the total number of particles, is shown in Figure 5. Of the total number of fractures, approximately 70 percent occurred during the first freezing cycle. The small increases in the accumulated percentage of frac-

tured particles that occurred after succeeding cycles are probably due to fractures that were undetected at the end of the first freezing cycle and required additional cycles before they became visible.

The percentage of fractured particles at the end of the fourth cycle of freeze-thaw, for each particle size tested, is shown in Figure 6. The largest percentage of fractured particles occurred in the 12.5-mm (0.5 in) size; the smallest percentages occurred in the 25 and 4.75-mm (1-in and no. 4) sizes. The average percentage of fractured particles of all sizes combined was 53.6. The 25-mm particles were mostly igneous and metamorphic rock particles that, by their mode of formation, are less porous than water-lain sedimentary rocks. Most of the 12.5-mm particles were porous cherts and dolomites. Most of the 4.75-mm particles were quartz.

The relation between the soundness of the test particles and their adjusted porosity values is shown in Figure 7. As expected, the more porous particles were less durable than the less porous particles. All particles having a porosity of more than 11 percent fractured in the freeze-thaw test; less than 25 percent of the particles having a porosity of less than 2 percent fractured.

The relation between the percentage of fractured particles and the absorption values of the test particles is also shown in Figure 7. All particles having absorptions of 4 or more percent failed when subjected to freezing and thawing. Very few specimens having absorptions of less than 1 percent failed. Between these extremes, the percentage of particles failing increased as the absorption increased.

Theory

The ability of a rock fragment to withstand the internal pressures that accompany freezing is controlled by certain inherent properties of the fragment. These properties can be understood in terms of Timoshenko's explanation (4) of Lame's solution for the radial and tangential stresses in a thick-walled, spherical container under internal and external pressures. If the exterior confining pressure (P_o) is zero, Timoshenko's equation for radial stresses (σ_r) at the extreme outer fiber is

$$\sigma_r = 0 \tag{3}$$

Figure 7. Relation between porosity and absorption and percentage of fractured particles after exposure to four freeze-thaw cycles.

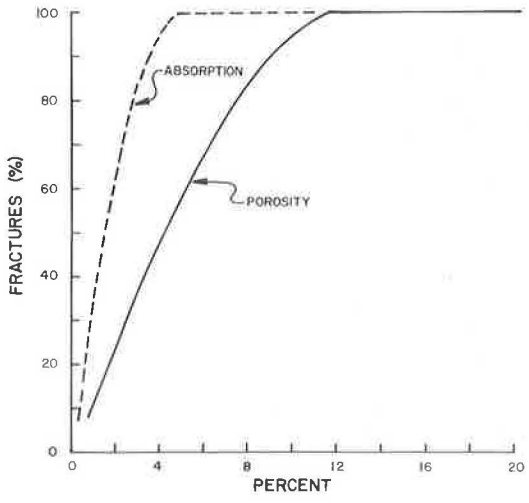

For tangential stresses (σ_t), Timoshenko's equation reduces to

$$\sigma_t = 3P_i a^3/2(a^3 - b^3) \tag{4}$$

where

P_i = internal pressure,
a = inner radius of sphere, and
b = outer radius of sphere.

If

$$V_v = 4\pi a^3/3 = \eta V_t \tag{5}$$

and

$$V_t = 4\pi b^3/3 \tag{6}$$

where

V_v = volume of voids,
V_t = total volume of sphere, and
η = porosity = V_v/V_t are substituted in Equation 4, it becomes

$$\sigma_t = 3P_i\eta/2(1 - \eta) \tag{7}$$

σ_r along the outer edge of the spherical container is zero, and σ_t at the same point, which is a tensile stress, is dependent on the porosity and tensile strength of the container and independent of its size or total volume.

If σ_t is replaced by the tensile strength (σ_u), Equation 7 becomes

$$P_u = 2\sigma_u(1 - \sigma)/3\sigma \tag{8}$$

where P_u = maximum allowable internal pressure. The tensile strengths of the gravel particles were not determined, but similar materials have tensile strengths ranging from 0.7 to 7 MPa (100 to 1000 lbf/in^2). If the tensile strength is known, the maximum allowable internal pressure for various porosity values can be calculated. Porosity-pressure curves for tensile strengths of 2, 4, and 6 MPa (300, 600, and 900 lbf/in^2) are shown in Figure 8.

The determination of the internal pressure accompanying the freezing of water within a hollow sphere can also be approached from a theoretical standpoint. If the temperature-volume changes of the sphere, water, and ice are neglected, the volume of ice (V_I) within the cavity, assuming all the water freezes, is

$$V_I = 4\pi a^3 S(1 + \beta)(1 - P_i K)/3 \tag{9}$$

where

S = degree of saturation,
β = volume increase accompanying freezing of water, and
K = bulk modulus of ice.

The tangential strain at any point within the sphere is given by

$$\epsilon_t = \delta/r = (\sigma_t/E) - \mu(\sigma_r/E) \tag{10}$$

where

ϵ_t = tangential strain,
δ = radial displacement,

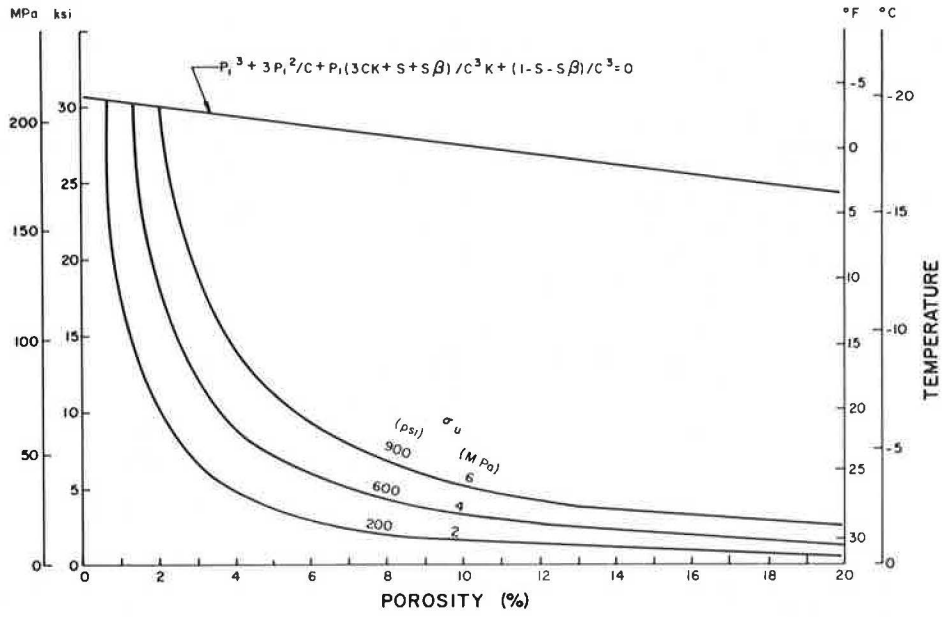

Figure 8. Suggested theoretical relations for varying tensile strengths.

E = Young's modulus of elasticity of sphere,
μ = Poisson's ratio of sphere, and
r = radial distance.

By assuming that $P_o = 0$ and substituting for V_v and V_t, the increase in the radius of the internal cavity or void due to an internal pressure reduces to

$$\delta = aP_i(1 + \mu + 2\mu - 4\mu\eta)/2E(1 - \eta) \quad (11)$$

The volume of the cavity (V_c) under internal pressure will thus increase to

$$V_c = 4\pi a^3(C^3P_i^3 + 3C^2P_i^2 + 3CP_i + 1)/3 \quad (12)$$

where $C = (1 + \mu + 2\mu - 4\mu\eta)/2E(1 - \eta)$. The volume of the ice within the cavity must be equal to the volume of the cavity. By equating the two and rearranging, it follows that

$$P_i^3 + (3P_i^2/C) + [P_i(3CK + S + S\beta)/C^3K] + (1 - S - S\beta)/C^3 = 0 \quad (13)$$

The internal pressure was calculated for various porosity values by using the following values: $\mu = 0.365$, E = 6.9 GPa (1 000 000 lbf/in^2), K = 8.3 GPa (1 200 000 lbf/in^2), S = 1.00, and $\beta = 0.0917$. This plot is superimposed on the maximum allowable internal pressure curves in Figure 8.

The intercepts of the maximum and the available pressure curves are the maximum safe-porosity values. At porosities greater than these, rupture will occur at less than the maximum available pressure. Pressure is dependent on temperature, and as the porosity increases, less pressure—and consequently less severe temperatures—will cause failure. Figure 8 also shows the theoretical relations among disruptive temperature, porosity, and tensile strength. For a given tensile strength, the disruptive temperature increases as the porosity increases, and rupture may occur at a temperature slightly below freezing if the porosity is high.

The range over which critical porosity occurs is a manifestation of the inherent tensile strength of the aggregate. Whereas it must be presumed that tensile strength varies in inverse proportion to porosity, the inherent tensile strength varies within a wide range that depends on the mineralogical nature of the aggregate. Hence, the force opposing the expansion accompanying freezing—and therefore the limiting pressure—is governed by the restraining strength of the aggregate or the confining vessel. Logically, an encasement medium such as mortar or concrete will provide additional restraint against the forces emanating from a dilating particle of aggregate. Thus, restraint increases with depth of embedment. A saturated particle of aggregate in concrete may be viewed as being a center of compression, and the surrounding concrete may be viewed as a thick-walled shell or vessel. Of course, at near-surface locations, the restraint is unbalanced, and pop-outs or cracking will result if the dilating pressures are critical.

PRESSURES ASSOCIATED WITH POP-OUTS

Pop-outs and deep-seated deterioration are generally associated with high absorptivity and high saturation. Aggregate particles of all sizes are capable of inducing damaging pressures. Particles that are near the surface may produce pop-outs even though the dilating pressures are relatively low because the surrounding shell of concrete offers only minor restraint.

Phenomena

To gain a better understanding of the mechanisms associated with these signs of distress, failures were induced by subjecting voids of varying diameters and depths below the concrete surface to hydrostatic pressure (5). Concrete specimens [254 by 254 by 102 mm (10 by 10 by 4 in)] were cast from six-bag concrete containing limestone coarse and fine aggregates. The specimens were moist cured at 25°C (77°F) 28 d. Each specimen was then drilled with a flat-faced masonary bit to form a cylindrical hole in the center of one of the 254 by 254-mm surfaces. The hole depths ranged from 63.5 to 93.4 mm (2.5 to 3.875 in) and provided depths of burial ranging from 28.1 to 3.2 mm (1.5 to 0.125 in). The diameters of the bits used for drilling were 6.4, 9.5, 12.7, 19.1, 25.4, and 34.9 mm (0.25, 0.375, 0.5, 0.75, 1, and 1.375 in). A 6.4-mm (0.25-in) high-pressure tube and rubber gasket assembly was placed in each specimen to within 19.1 mm (0.75 in) of the bottom of the void. The tubing and

gasket were held in place with high-strength epoxy cement. In all cases, the void depth was 19.1 mm, and only the void diameter and the depth of burial were varied.

A hand-operated pump capable of producing a maximum pressure of 34 MPa (5000 lbf/in^2) was connected to the pressure tubing, and glycerin was pumped into the artificial void at such a rate that the pressure zone was limited essentially to the pressure cavity. [This method has also been used by Bache and Isen (6) to illustrate failure patterns.] The time required to attain the final pressure was approximately 10 s. The characteristics of a resultant pop-out are illustrated in Figure 9. The pressures required to produce pop-outs in the various specimens are shown by the series of curves in Figure 10, which present data obtained from tests on 150 specimens. Results obtained had a remarkably high degree of duplication. For similar depths of burial, greater pressures were required to produce pop-outs in the smaller diameter cavities than were required for the larger cavities. Figure 10 indicates that a cover of about 23 mm (0.9 in) would be necessary for protection against failure from the pressures expected within a 6.4-mm (0.25-in) cavity, and a cover of approximately 31.8 mm (1.25 in) would be needed for 34.9-mm (1.375-in) cavities. All the pop-outs were predominantly conical, and thinning was more pronounced along the outer surface perimeter of the larger pop-outs. Failure widths for the 19.1 and 25.4-mm (0.75 and 1-in) cavities at varying depths of burial are shown in Figure 11. Failure angles were computed from the fitted curves and are shown in Figure 12. The failure angle is significantly related to the cavity diameter and the depth of burial.

Figure 9. Test specimen showing pop-out.

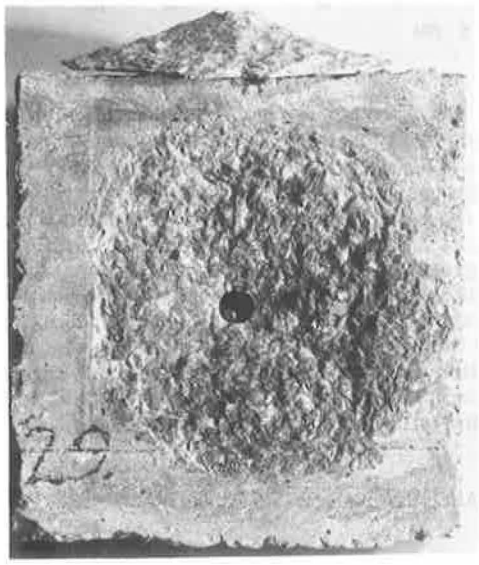

Specimens containing cavities that were more deeply buried split into two sections as shown in the sketch inserted in Figure 13. The pressures required to produce this type failure varied with the cavity diameter but were independent of the depth of burial—that is, above the limit of pop-out failure. The pressures to induce failures of this type did not vary appreciably with the depth of burial because the area of resistance to failure was constant [102 by 254 mm (4 by 10 in)] for all specimens. The limiting depth of burial for a given cavity diameter at which the mode of failure changes is governed by the specimen dimensions, and pop-outs would occur at greater depths of burial in specimens larger than those tested here. Splitting-type failures are represented on the curves in Figure 10 in the zones of zero slope. Failures of this type can be considered as the deep-seated deterioration commonly associated with deeply embedded and highly absorptive aggregate particles. High dilating pressures are necessary for these failures because the restraint on the particles is greater.

Additional tests were conducted by casting water-filled spherical capsules in concrete specimens of the same size as described above. A copper-constantan thermocouple was placed in the center of each sphere of water, and the voltages were amplified and recorded, making possible temperature measurements within $\frac{1}{4}$°C (0.14°F). The pressures accompanying the confined freezing of water within the spheres were computed from

Figure 10. Relations among pop-out pressure, void diameter, and depth of burial.

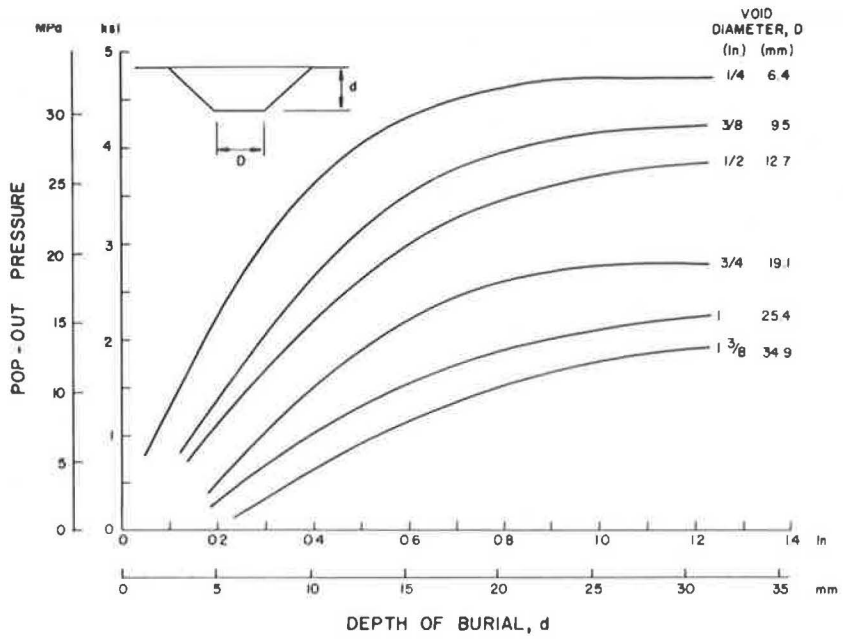

Figure 11. Relations among depth of burial, void diameter, and pop-out width.

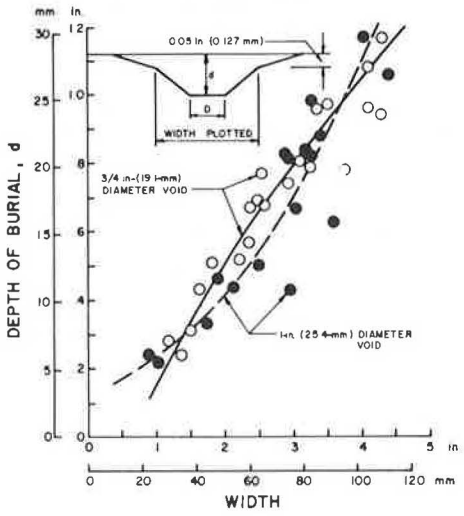

Figure 12. Relation between failure angle and depth of burial.

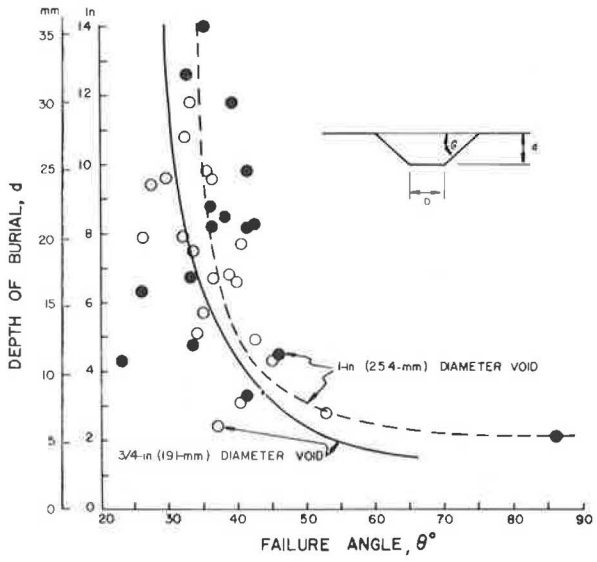

the temperature data. The temperature at failure was -4.0°C (24°F), and the accompanying pressure was 50 MPa (7200 lbf/in^2). After rupture, the pressure decreased, and the freezing point returned to normal. Freezing thereafter was isothermal. These events occurred over a series of successive cycles rather than within a single one. This was interpreted as a manifestation of progressive damage.

Theory

Within a semi-infinite mass, there is a free-field stress distribution. When the continuity of an assumed homogeneous material such as concrete is interrupted by the presence of a porous and saturated aggregate particle undergoing freezing, stresses near the particle are no longer equal to the free-field stresses because there is a discontinuity of strains or deformations at the aggregate-matrix interface. Because of this discontinuity, the induced differential pressures alter the at-rest stress conditions that existed before freezing.

Figure 13. Pressure necessary to produce splitting failure in deeply buried voids.

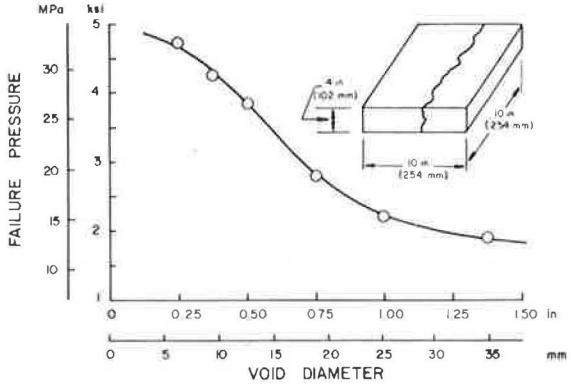

Figure 14. Passive pressures and pop-outs.

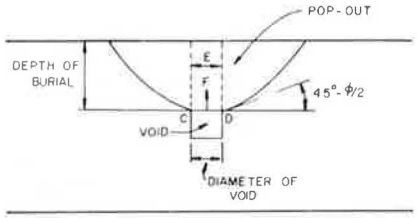

Shear stresses are therefore mobilized within the concrete matrix and, if the shearing strength of the concrete is exceeded, the material may fail in the form of a pop-out.

When a freezing aggregate particle is contained in a concrete mass, relative displacements between the particle and the surrounding matrix will occur, and shearing stresses will be mobilized along those planes that experience shearing distortions. Because of the extremely high pressures that sometimes are developed in freezing aggregate particles, the modulus of the porous particle may be assumed to be greater than that of the surrounding concrete matrix. The resulting conditions may be, in a general way, assumed to be analogous to the phenomenon of stress transference called passive arching.

The application of theoretical solutions implies that the material behaves elastically, but such behavior may depart from ideal at high pressures. However, elastic solutions are good approximations when small displacements are involved. At large displacements, the stresses in some regions will reach the yield stress, and the stress distribution that finally results may be quite different from the stress distribution determined by considering only elastic equilibrium. In Figure 14, the movements of the concrete matrix above plane CD are denoted by arrows E and F. The material just above CD tends to move upward because of the high pressures induced by the freezing and expanding water within the aggregate. The material to the sides of the aggregate particle tends to move laterally, creating a condition analogous to the passive pressure state, i.e., the lateral stresses that occur at the limiting stage of lateral compression. If the deformations proceed far enough and the depth of burial is sufficiently small, the failure surface may propagate to the surface of the concrete mass and result in a pop-out. Rankine's theory gives the passive pressure as

$$P_p = \gamma d \tan^2(45° + \phi/2) + 2c\tan(45° + \phi/2) \qquad (14)$$

where

P_p = passive pressure,
γ = unit mass,
d = depth of burial,
c = cohesion, and
ϕ = angle of friction.

If typical values of 2.4 Mg/m^3 (150 lb/ft^3) for the unit mass of concrete, 7.8 MPa (950 lbf/in^2) for the cohesion, and 47° for the friction angle are used, the passive pressures calculated by Equation 14 are about 33 MPa (4800 lbf/in^2). Because the depth of burial is small, the effect of d in Equation 14 is extremely insignificant. The passive pressures determined from Equation 14 are about the same order of magnitude as the compressive strength of the concrete.

By assuming that passive pressures act over a rectangular surface with dimensions equal to the depth of burial and the void diameter (perpendicular to the plane of the figure), the passive forces can be calculated from Figure 14. If the coefficient of passive pressure is assumed to be 3, the forces acting at the top interface between the void and the concrete mass can be determined, and from this vertical force and the diameter of the void, a calculated value of the void pressure can be obtained. The table below summarizes such calculations for the ranges of depth of burial and void diameter investigated (1 mm = 0.039 in and 1 MPa = 145 lbf/in^2).

Depth of Burial (mm)	Void Diameter (mm)	Void Pressure (MPa)	
		Calculated	Observed
25	25	14.1	14.8
13	25	7.0	9.0
25	35	10.1	8.7
13	35	5.0	6.6
25	6	54.1	32.4
13	6	27.1	27.9

The agreement between the calculated void pressures and the void pressures observed to cause pop-out failure is extremely satisfactory in all except one case, the 25.4-mm (1-in) depth of burial for a void diameter of 6.4 mm (0.25 in).

On the basis of the calculations given above, it seems reasonable to consider the passive-pressure concept as adequate to explain the mode of failure for pop-outs. However, the case of the 6.4-mm diameter void buried 25.4 mm beneath the surface may be different; thus, pressures originating at depths of three or four or more times the cavity size cannot significantly exceed the compressive strength of the concrete.

SUMMARY AND CONCLUSIONS

Aggregates having an absorption greater than 4 percent are likely to rupture on freezing; aggregates having an absorption less than 1 percent are generally unaffected by freeze-thaw. A composite sample of aggregate particles may collectively absorb less than 4 percent water by mass and still contain individual particles having absorptions significantly greater. Absorption tests based solely on composite samples are not adequate in this respect. The degradation of composite samples subjected to saturation and quick freezing cycles could provide a measure of the proportions of sound and unsound particles. Alternatively, each particle within a composite sample could be tested for absorption and the proportions of deleterious material determined statistically.

Concretes can contain as much as 20 percent voids. Theoretically, the critical volume of water in a void is 91.7 percent of saturation (capacity). It is intuitively apparent that the system of voids in a mass of concrete is infinitely complex. It would be possible, therefore, for certain cavities or pores to be critically saturated while others were relatively unsaturated. Here again, gross absorption alone fails to define the state of saturation (unless saturation is complete in all respects). Forced saturation renders concretes and aggregates susceptible to damage through freezing. The entrainment of air causes concrete to be infinitely more difficult to saturate—probably by disconnection of the voids or by the back pressure of air in minute spherical voids. Aggregate particles are usually not immunized in this way and tend to saturate preferentially. Nevertheless, it seems reasonable to conclude that any mechanism by which saturation is delayed or rendered improbable increases the durability of concrete exposed to freezing weather.

REFERENCES

1. N. E. Dorsey. Properties of Ordinary Water-Substance. Reinhold, New York, 1940.
2. J. H. Havens. Thermal Analysis of the Freeze-Thaw Mechanism in Concrete. Engineering Experiment Station, Univ. of Kentucky, Bulletin 59, 1961.
3. J. W. Scott and G. R. Laughlin. A Study of the Effects of Quick Freezing on Saturated Fragments of Rocks. Division of Research, Kentucky Department of Highways, Feb. 1964.
4. S. Timoshenko. Theory of Elasticity. McGraw-Hill, New York, 1934.
5. J. W. Scott, G. R. Laughlin, and J. H. Havens. Freeze-and-Thaw Characteristics of Aggregates. Proc., 16th Annual Highway Geology Symposium, Engineering Experiment Station, Univ. of Kentucky, Bulletin 76, Sept. 1964.
6. H. H. Bache and J. C. Isen. Modal Determination of Concrete Resistance to Pop-Out Formations. Journal, ACI, June 1968.

Publication of this paper sponsored by Committee on Performance of Concrete—Physical Aspects.

Case Histories of Unsatisfactory and Abnormal Field Performance of Concrete During Construction

Bryant Mather, U.S. Army Engineer Waterways Experiment Station,
Vicksburg, Mississippi

Case histories are given relating to concrete produced in connection with the construction of three different projects. One was a major building, the second was an airfield pavement, and the third was a highway bridge deck. The projects are located in three different states on the East Coast of the United States. These case histories have in common that a major part of the problem in each was low strengths of test cylinders. In the first case, defective concrete containing the wrong aggregate and made to the wrong mixture proportions was removed and replaced. In the second case, the problem was traced to the presence in the aggregate of aluminum particles from the bodies of the dump trucks in which it had been transported. In the third case, there were many causes of loss of control of the concrete properties; an instance was found of greater variation of air content in a smaller volume than ever reported previously. In this case, the safety factor in design allowed the concrete to remain in the structure.

CASE 1: BUILDING

This case history began in August 1973. In the construction of a reinforced-concrete building for which a 34.5-MPa (5000-lbf/in^2) concrete had been specified and a mixture proportioned by an approved commercial testing laboratory was being used, the tests on the mixture gave values of more than 41.4 MPa (6000 lbf/in^2), but on the job there were many results in the 24 to 31-MPa (3500 to 4500 lbf/in^2) range.

The concrete in question had been placed between April 10 and June 16. Air temperatures during and after this period had been as high as 46°C (115°F), but by using ice, the temperature at which the concrete was placed was kept to a maximum of 29°C (85°F). Some probe tests and some core tests had been made by the contractor before the beginning of this study. The cylinder-test data were evaluated, and a program of core sampling and rebound-hammer testing was developed and carried out. The table below shows the 28-d cylinder-test results for the three strength classes of concrete involved (1 MPa = 145 lbf/in^2).

Strength (MPa)

Nominal	Observed
28	22.5, 24.4, 26, 27.5, 27.8, 27.8, 27.9, 28, 28.1, 30, 30.4, 34, 40.8
34.5	19.6, 23.9, 23.9, 24.2, 24.3, 24.4, 27.3, 37.6, 27.9, 28.6, 29.8, 29.9, 30.2, 30.8, 31.8, 32.6, 32.6, 33.6, 34.3, 34.4, 34.5, 34.6, 34.7, 34.7, 34.8, 34.8, 35, 35.5, 36, 36.2, 36.7, 37.9, 38.2, 42.6, 46.2, 47
38	20.6, 22.3, 30, 33.3, 34.2, 38.2, 38.2, 39, 42.8, 43.4, 46.5, 50.3

These results are summarized below.

Nominal Strength (MPa)	n	$\bar{X}$ (MPa)	R (MPa)	Percentage Below Nominal Strength
28	13	28.3	18.4	31
34.5	36	32.5	27.5	55
38	12	36.6	29.7	42

The following table shows the results of strength tests on cores drilled from portions of the structure represented by specific cylinder-test results.

Strength (MPa)

Nominal	Cylinder	Core
28	22.5	23.2, 21.5
	26	28.2, 24.8
	27.8	24.4, 37.2
	27.9	29.9, 27.7
	30	25.7
	30.4	37.2
34.5	19.6	25
	23.2	33.1, 26
	24.2	24.5
	32.6	42.6
	33.6	35.8
	34.3	30.5
	34.4	40.8, 48.1, 30.7
	46.2	34.3
	47	41.8
38	20.6	18.6
	22.3	19.8, 21
	30	20.3
	33.3	29.9
	34.2	30.8, 29.1
	38.2	25.1, 38.1
	46.5	33.2
	50.3	54.4

These cores represented concrete 60 to 124 d old when tested. In 5 of 21 locations where the cylinder strength was below the specified level, the core strength was above; in 5 of 12 locations where the cylinder strength was above the specified level, the core strength was below.

Rebound-hammer tests were conducted on areas adjacent to the locations of the pairs of drilled cores. Calibration curves were made for the rebound-number versus core-strength relation for each class of concrete (Figures 1, 2, and 3).

The calibration curves were used to predict the range of probable core strengths at a 99 percent confidence level in locations not represented by cores. The table below shows the predicted core strengths in such areas.

Nominal Strength (MPa)	Range (MPa)		Nominal Strength (MPa)	Range (MPa)	
	High	Low		High	Low
34.5	6.2	37.5	38	3.72	34.8
	6.2	37.5		3.72	34.8
	10.3	37.8		4.62	34.8
	11.5	37.8		4.62	34.8
	12.4	37.9		4.68	34.8
	13.1	37.9		6.21	34.9
	14.1	38.0		11.3	35.4
	18.7	38.4		12.4	35.7
	21.2	38.7		12.8	36.4
	22.3	38.8		15.2	36.7
	23.0	39.0		15.9	37.0
	24.1	39.3		18.4	38.5
	24.1	39.3		20.7	41.3
	26.8	40.3		22.1	43.3
	31.5	45.3		22.6	46.4

Figure 1. Core strength versus rebound-number calibration: 28-MPa mixture.

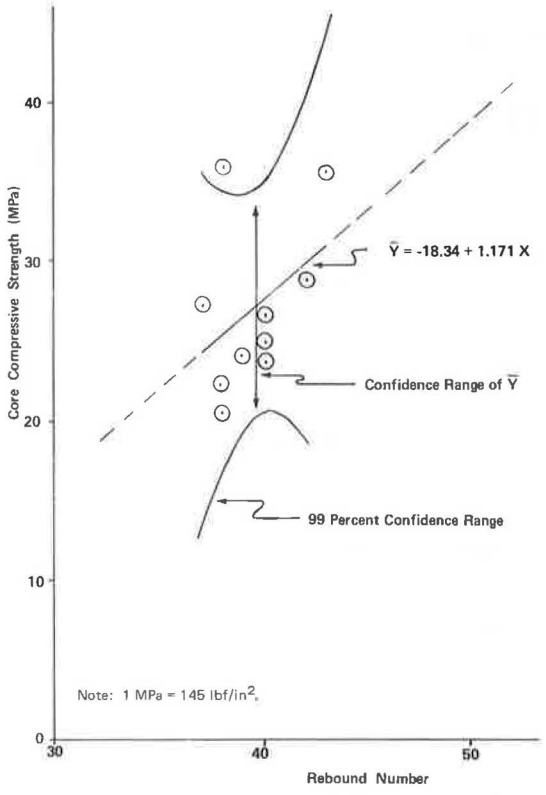

Figure 2. Core strength versus rebound-number calibration: 34.5-MPa mixture.

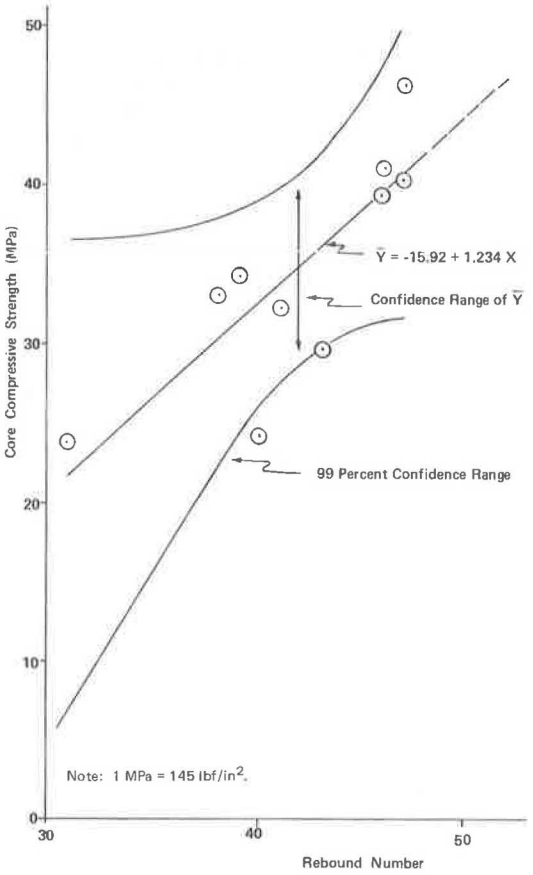

Figure 3. Core strength versus rebound-number calibration: 38-MPa mixture.

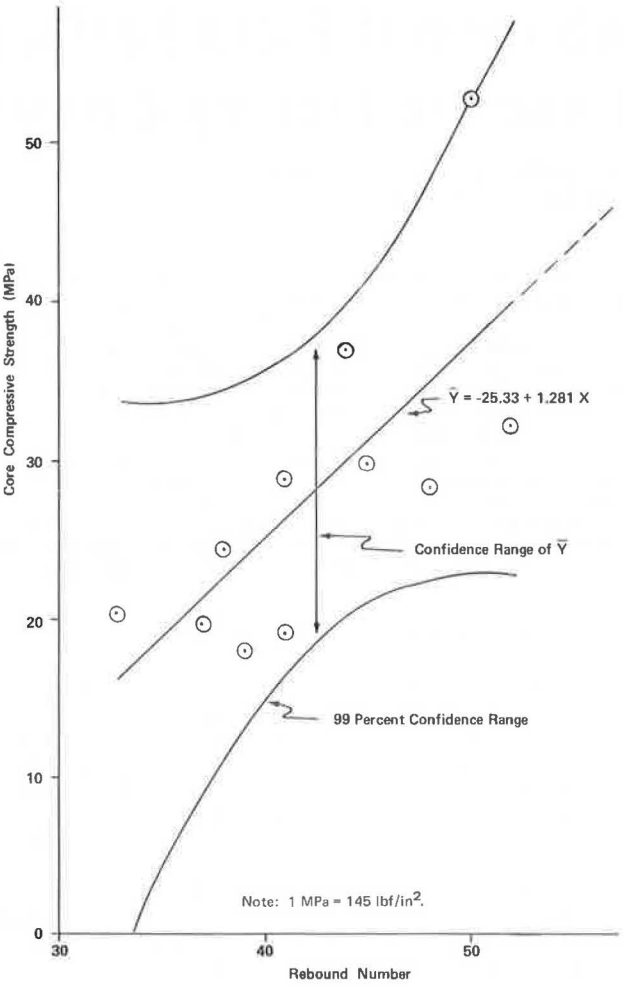

Nominal Strength (MPa)	Range (MPa)		Nominal Strength (MPa)	Range (MPa)	
	High	Low		High	Low
34.5	32.0	46.3	38	22.6	46.4
	32.8	51.3		22.6	48.0

In the case of the 34.5-MPa concrete, there were no areas in which the rebound values indicated, within 99 percent probability, either that the concrete must be stronger or that it must be weaker than its nominal value. However, in the case of the 38-MPa (5500-lbf/in^2) concrete, while in no area did the rebound values indicate a 99 percent probability that the concrete was at least nominal strength, in 11 of the 17 areas tested, there was a 99 percent probability that it was less than nominal strength. Additional rebound-hammer tests were made but are not included here.

The procedure followed was to evaluate areas based on the cores by using the following standard (1):

> Concrete in the area represented by the core tests will be considered structurally adequate if the average of the three cores is equal to at least 85 percent of [the ultimate compressive strength] f'_c and if no single core is less than 75 percent of f'_c.

On the basis of the core-test results and a few areas where the cylinder-test results indicated low strengths, which were confirmed by rebound-number estimates,

20 of 29 columns specified to contain 38-MPa (5500-lbf/in^2) concrete were determined to be not in compliance with respect to strength. A few core samples were laboratory tested to determine cement and air content. The results (given below) for samples having specified cement and air contents of 439 kg/m^3 (752 lb/yd^3) and 4 percent respectively make it clear that the deviation of strength, at least in certain cases, from that required by the contract and capable of being produced from the approved mixtures, resulted from unauthorized changes in aggregate type, aggregate grading, and cement content from those expected for these mixtures (1kg/m^3 = 0.062 lb/ft^3).

Strength (MPa)		Cement Content (kg/m^3)	Air Content (%)
Nominal	Core		
34.5	24.5	233	8.7
	40.8	603	3.7
38	20.4	316	2.2
	37.5	628	5.7

Figure 4 shows cores of concrete containing the approved aggregate. Figure 5 shows cores of concrete containing inferior aggregate from a different source and of a different grading.

This experience suggests a method for using a nondestructive test—i.e., the rebound hammer—to estimate the range of strength of concrete in a structure. In this case, the contractor was notified as to the known extent of nonacceptable concrete by drilling and testing cores, and he then removed and replaced those portions of the structure.

Figure 4. Cores from concrete made with approved aggregate.

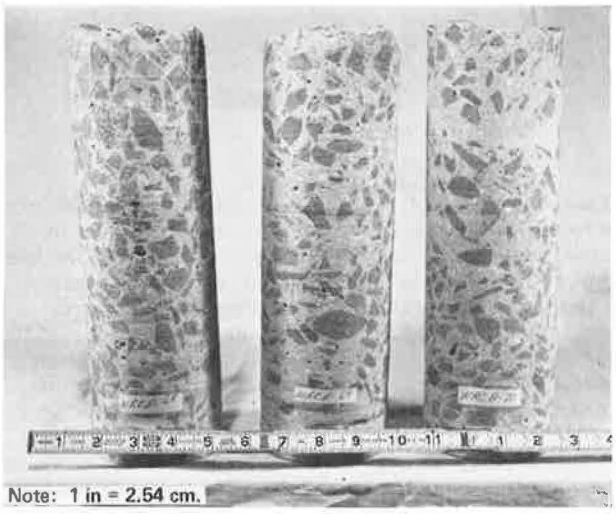

Figure 5. Cores from concrete made with inferior aggregate.

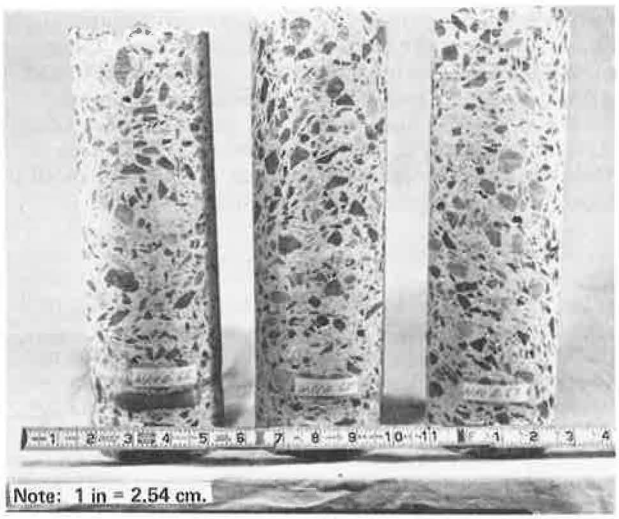

CASE 2: AIRPORT PAVEMENT

This case history began in February 1974. The problem was described as involving unusually large fluctuations in flexural-strength results for no apparent cause. Initially, it seemed that the following assumptions could be made:

1. Since the problem was encountered with both type 1 and type 1P cement, it is apparently not a function of cement type.
2. Since the aggregates used have a long history of satisfactory ability to produce concrete having a high flexural strength, the problem is apparently not a function of the intrinsic quality of the aggregate.
3. Since many specimens were of satisfactory strength, the problem appears to relate to specific batches or specific specimens.

Figure 6. Aluminum particles from aggregate stockpile.

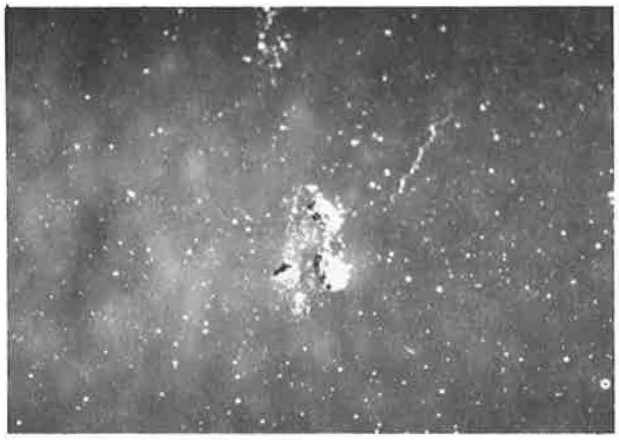

Figure 7. Hydrogen evolution by aluminum particles in alkaline solution.

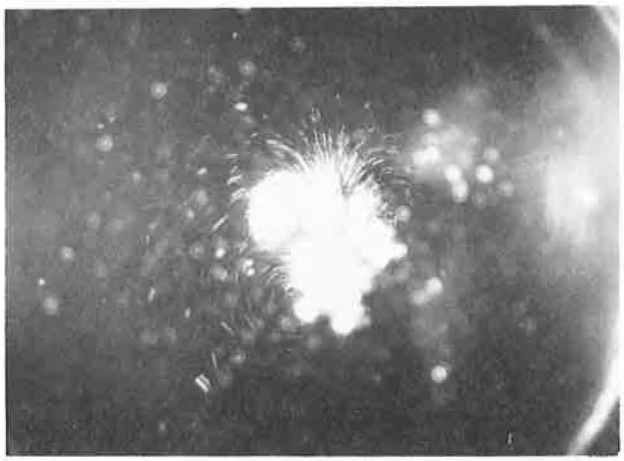

Figure 8. Slice through full thickness of core showing zones of different air content: (a) 12 percent and (b) 3 percent.

Figure 9. Enlarged view of 12 percent air-content zone (Figure 8a).

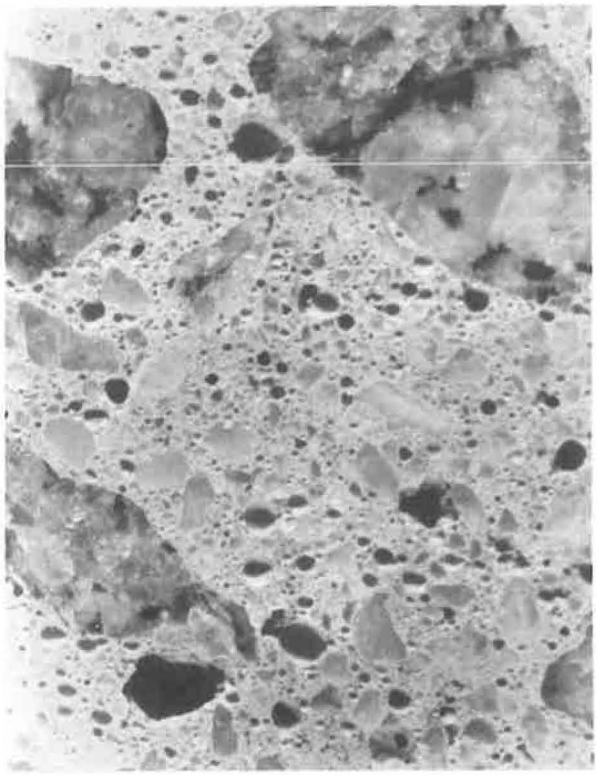

Figure 10. Enlarged view of 3 percent air-content zone (Figure 8b).

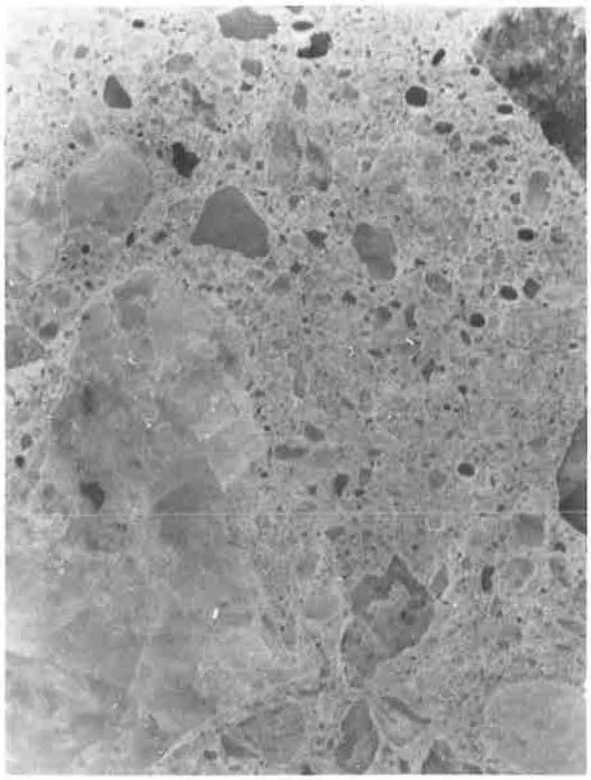

On these assumptions, the first possibility considered was based on a case history of concrete having an increased gas-bubble content after placement that had been pumped through aluminum pipe, but no pumping was involved here. However, the aggregate was a hard, tough, angular, crushed granite that was transported by truck for a considerable distance from the production site to the project site in large aluminum-body dump trucks, and an analogous mechanism might be involved. By March 18, work was resumed, it having been found that satisfactory strengths were obtained when the coarse aggregate was rewashed after delivery to the project site.

Meanwhile, it was established that grains of metallic aluminum were present among the fines accompanying the coarse aggregate as it was dumped into stockpiles at the job site (Figure 6). It was also confirmed that these particular aluminum particles evolved hydrogen gas when immersed in an alkaline solution (Figure 7) and that there is a direct relation between decreased flexural strength and increased air content of hardened concrete as determined by microscopic examination. So far as is known, this is the first recorded case of generation of hydrogen gas in concrete by aluminum particles present as a contaminant in the aggregate after transportation in aluminum-body trucks.

CASE 3: BRIDGE DECK

The third case began in August 1971. At first, the problem was one of bridge-deck deterioration, but by September, it had become one of quality assurance for a replacement deck. The replacement was done during the winter of 1971/1972 and used more than 2270 Mg (50 000 cwt) of cement and 680 Mg (1 500 000 lb) of reinforcing steel. The first mixture proportions selected used a type 3 cement to give a 7-d design strength of 31 MPa (4500 lbf/in^2), i.e., an average of 35.2 MPa

(5100 lbf/in^2). Problems were encountered because the type 3 cement had been selected merely to reduce the duration of the required period of wet curing. The specifications were changed to membrane curing, type 1 cement, and a 28-d design strength of 31 MPa. In November, about a month after placement was begun, problems with the 28-d strength were encountered. The concrete had been dry batched, hauled about 37 km (23 miles), mixed, discharged into a pump, pumped to the deck, spread, consolidated, finished, and coated with curing compound. The problems involved control of slump and air content and seemed related to the length of time between batching and discharge and to be aggravated by the procedure of putting all the air-entraining admixture in half of the wet sand that goes over half of the stone and under the first half of the cement. An extensive series of tests using the rebound hammer and core drill were made, and 45 cores were tested in the laboratory. The core strengths averaged 19 MPa (2750 lbf/in^2) and ranged from 12 to 27.4 MPa (1710 to 3970 lbf/in^2). Three job-made cylinders had strengths of 22.7 to 46.2 MPa (3300 to 6700 lbf/in^2) and cement contents of 288 to 625 kg/m^3 (5.1 to 11.1 bags/yd^3). Other cores were tested for air content and frost resistance. The air contents of nine cores ranged from 5.7 to 10.2 percent, but one having a value of 7.2 percent (Figure 8) had two zones, one with an air content of about 12 percent (Figure 9) and the other with an air content of about 3 percent (Figure 10). By May 1972, the average core strength had increased from about 17.9 MPa (2600 lbf/in^2) at 3 months age to about 20.7 MPa (3000 lbf/in^2) at 7 months age.

REFERENCE

1. Building Code Requirements for Reinforced Concrete Concrete. ACI, 1971, paragraph 4.3.5.1.

Publication of this paper sponsored by Committee on Performance of Concrete—Physical Aspects.

Map Cracking in Limestone-Sweetened Concrete Pavement Promotes D-Cracking

Carl F. Crumpton and John E. Bukovatz, Research Division,
Kansas Department of Transportation

A Portland cement-concrete pavement constructed in north central Kansas in 1963 showed map cracking near the sawed transverse joints by 1970. The pavement had been built using Republican River sand gravel, which is known to be reactive, and 30 percent Towanda limestone from near Milford, Kansas, had been added to the concrete mix as a sweetener to prevent the map cracking. The limestone did not prevent the map cracking, but was not otherwise involved in the deterioration that occurred before 1970. By 1972, however, after the surface near the joints was opened by the map cracking, the limestone aggregate particles became directly involved through the freeze-thaw deterioration type of the D-cracking. By 1974, deterioration was rapidly spreading outward from the transverse joints and blowups at the joints were requiring considerable repair. The synergistic effects of map cracking during the summer [with an average of 5000 degree hours, above 29.4°C (85°F)], and D-cracking during the winter (with more than 68 freeze-thaw cycles) promoted even more rapid deterioration and joint blowups. The progress of the deterioration was followed by the study of pavement cores obtained in 1970, 1972, and 1974.

For many years, a standard method for the prevention of serious map cracking in Kansas concrete has been to allow the addition of 30 percent limestone sweetener to unapproved sand-gravel materials. (Unapproved indicates that the sand gravel is known to be reactive and produce map cracking or that no information is available concerning its service record either in the field or from laboratory tests.) The sweetener is used with either type 1 or type 2 cement.

In 1963, a 17.7-km (11-mile) long two-lane pavement was constructed in north central Kansas. The contractor chose an unapproved Republican River sand-gravel material from Scandia, Kansas, with a fineness modulus of 3.52 and a specific gravity of 2.62 as the basic aggregate. For the sweetener, he chose Permian Towanda limestone from Milford, Kansas. This limestone coarse aggregate was all through a 38.1-mm (1.5-in) sieve and had a fineness modulus of 7.24, a specific gravity of 2.47, and a water absorption of 4 percent. The particular limestone used is one of the better ones available in Kansas in terms of its resistance to the freeze-thaw type of D-cracking. Even so it has produced D-cracking (1), and would be rejected in many states. Studies made by the Corps of Engineers in their investigations of aggregates for the Milford Dam showed that the Towanda limestone was physically superior to most of the coarse aggregates from sources economically available (5). Thus, the limestone chosen seemed the best of those readily available. The aggregate mix ratio was the standard 70 percent sand gravel and 30 percent limestone sweetener. The contractor used a type 1 cement that was near a type 2 and had the following properties:

Property	Value (%)
Total alkali	0.59
C_3A content	8.9
Autoclave soundness	0.33
C_3S content	51.5
C_2S content	23.4
MgO	2.35
SO_3	1.82

The concrete mix used 368.1 kg/m^3 (620.4 lb/yd^3) of cement with a 0.47 water-to-cement ratio. The concrete was air entrained with a target value of 6.5 percent. Two admixtures were used separately in some

sections of the pavement on an experimental basis. Lignosulfonic and hydroxylated carboxylic acid type, water-reducing set retarders were each added at a rate of 2 percent (2 oz/sack of cement). Where these were used, the water-to-cement ratio was reduced to 0.44, and the cement content was reduced to 340.2 kg/m^3 (573.4 lb/yd^3). Control sections of pavement were placed where the set retarders were not used. The concrete mix was typical for the proportions used, with a slump of about 44.45 mm (1.5 in) and a unit mass of 81.89 kg/m^3 (138 lb/ft^3). Everything appeared to be normal, and no problems were anticipated from the concrete for many years.

The first hint of a developing problem was in 1964. In the D-cracking survey made late that year, this pavement, which was less than 2 years old, exhibited many short transverse cracks that showed a distinct but narrow band of staining (1, Figure 7). Most of the joints themselves showed little or no staining. Water was present at the pavement surface seeping from many cracks and joints. Otherwise, the pavement was in good condition (1, Figure 8).

Staining is a matter of concern but not necessarily an indicator of serious problems to come. However, by 1969 the joints showed heavy stain that appeared to be D-cracking and by 1970, there were dark stains adjacent to the joints. Cores from such badly stained areas usually have many cracked limestone particles and nearly parallel horizontal cracks mostly limited to the lower half of the core.

Cores were obtained from near several of the heavily stained transverse joints. Close examination of their top surfaces showed a fine pattern of cracking, but internally the cracks were primarily vertical and extended only a short distance downward into the concrete. There were no cracks in the lower halves of the cores. Gel was found in many of the cores, which showed that a reaction was taking place. It was obvious from the cores that the limestone coarse aggregates were not directly involved in the deterioration. They were sound, and the short surface cracks went around rather than through them. There was no evidence in the cores that freeze-thaw damage had occurred. The Republican River sand gravel used contained its usual volume of reactive particles, such as opaline siltstone, opaline sandstone, opaline limestone, and glassy volcanics (4). Steam treatment of some of the cores produced more gel, which showed that the reaction was not complete.

The evaluation of the cores in 1970 led to the conclusion that the problem was one of map cracking, rather than one of D-cracking. This is supported by the 1970 report of Bukovatz and others (2), who found that Towanda limestone (from same quarry as that used here) used as a control was itself not effective in preventing alkali-aggregate expansion. Thus, although the limestone coarse aggregate was not directly involved in the cracking, it was indirectly involved because it was not adequately functioning as a sweetener.

Within 2 years, there was a distinct pattern of cracks roughly parallel to the sawed transverse joints at several locations. These cracks were interconnected by a pattern of short cracks. This crack pattern was not typical of D-cracking, but it was present only near the transverse joints and transverse cracks, primarily at the joints. Thus, it was present at typical D-crack locations. The best description of the pattern is modified map cracking (8) or hybrid map cracking and D-cracking (11).

A new set of cores was taken in 1972, many 0.3 m (1 ft) or less from the locations of the 1970 cores. Those taken from the cracked areas showed that the internal concrete was much deteriorated, including freeze-thaw deterioration of the limestone aggregate that was limited to the top halves of the cores. In addition to the previously existing vertical cracks, there was now a set of roughly parallel horizontal cracks in the upper halves of the cores. The limestone aggregates were now badly cracked. Several cores broke at the level of the mesh, with the cracking primarily above that level. Thus by 1972, it was evident that D-cracking was also involved in the deterioration process.

With both modes of deterioration, map cracking and D-cracking, operating synergistically during 1973, 1974, and 1975, there was rapid deterioration, and blowups at the joints became a common occurrence. By the end of 1974, only 3 percent of the more than 900 joints were still good. Seventy percent of the joints showed staining and cracking, and the remaining 27 percent had required repairs varying from asphalt patching to complete replacement of the concrete at the joint because of pavement blowups.

Cores were obtained again in 1974. The D-cracking conditions were more widespread by then and deeper into the concrete. The concrete next to the joint had progressed to the stage of hybrid map cracking and D-cracking at which freeze-thaw deterioration was also occurring. Farther away from the joint, but still within the stained surface area, map cracking was occurring in the surface, but freeze-thaw deterioration of the limestone aggregates had not yet begun. Cores taken some distance from the joint and outside the stained area showed some evidence of map cracking through surface crazing and minor internal gel deposits. There was no indication of freeze-thaw damage in the nearly sound concrete areas outside the stained zone. A series of cores taken successively farther away from the sawed joint showed the deterioration history as it had been observed through time near the joint.

First, there is a fine surface crazing that can be seen only by close scrutiny. This is accompanied by, or more often preceded by, the staining of the surface near the joints. The staining is a result of deposits left at the surface through evaporation of water that seeps to the surface near the joints. This continuous wetting and drying at the surface by water coming from below causes surface map cracking to occur because of the reactive sand gravel and the ineffective sweetener.

After the surface is opened by the map cracking, water can enter from above more readily, and water from below has easier access to a greater number of limestone coarse aggregate particles. These then soon become critically saturated, and freeze-thaw deterioration in the form of D-cracking begins. This means that deterioration continues summer and winter alike.

Map cracking occurred in this pavement, even though the total alkalies of the cement were less than 0.6 percent and a limestone sweetener was used. Gibson had observed several years ago that the Republican River sand gravel, when used as a single aggregate, has produced severe cracking in concrete constructed with cement having an alkali content of less than 0.60 percent (3). He reported at the same time, however, that the most economical and satisfactory method to stop this map cracking was to add 30 percent durable, absorptive crushed limestone. At that time, he was unaware that this particular source of Towanda limestone is not effective as a sweetener, which was first reported by Bukovatz and others in 1970 (2).

The particular quarry from which the limestone sweetener was obtained has been closed by the construction of Milford Lake. However, it is not known whether other limestone sweeteners in use may also fail to prevent map cracking. There are other locations at which D-cracking began at the surface and

worked downward to the bottom of the slab, and some of these will be studied to see whether a reactive sand-gravel material was used in them.

The water-reducing, set-retarding admixtures did not appear to influence the development of either map cracking or D-cracking. The pavement condition is approximately the same where either set retarder was used and where none was used. Therefore, they apparently neither contributed to nor hindered the development of deterioration.

The area in question has an average precipitation of 686 mm/year (27 in/year), but a pan evaporation rate of about 1626 mm/year (65 in/year) (4). It is subjected to an average of 5000 summer degree hours above 29.4°C (85°F) in a normal year (7). This high number of degree hours is experienced only in central and eastern Kansas, southeastern Nebraska, central and western Missouri, most of Oklahoma outside the panhandle, and north central Texas. The highest average number of such degree hours, more than 7000, is experienced only in portions of Kansas and Oklahoma. The maximum expected in these areas is more than 12 000 degree hours above 29.4°C (7).

The mean annual snowfall on the pavement is about 610 mm (24 in) (6, Figure 4), and more than 68 freeze-thaw cycles can be anticipated each year (9, Figure 2). In 1974, an average of 1500 passenger vehicles and 500 large trucks traveled the road daily (10).

It is reasonably certain that the high summer temperatures, the many freeze-thaw cycles, and the salt and melted snow all contributed to the deterioration. The daily pounding by heavy trucks would add to the problem by loosening and removing the cracked surface concrete. However, the occurrence of blowups because of internal expansion has done the most damage. The plane of splitting of the concrete in the blowups was the level of the load-transfer bars.

Thus, the Towanda limestone sweetener failed to prevent the reactive Republican River sand gravel from causing map cracking. The map cracking allowed the limestone coarse aggregate to become critically saturated, and freeze-thaw led to D-cracking. Together, these effects increased the process of pavement expansion, and with the help of water and hot weather, blowups at the joints soon followed.

REFERENCES

1. J. E. Bukovatz, C. F. Crumption, and H. E. Worley. Study of D-Cracking in Portland Cement Concrete Pavements. Field Phase. State Highway Commission of Kansas and Federal Highway Administration, Rept. 1, 1973.
2. J. E. Bukovatz, W. H. Wendling, and H. E. Wallace, Jr. Expanded Shale Used as an Admixture for Sand-Gravel Aggregate Concrete. State Highway Commission of Kansas and Federal Highway Administration, 1970.
3. W. E. Gibson. Field Experience With Alkali-Aggregate Reaction in Concrete: Central United States. HRB, Res. Rept. 18-C, 1958, pp. 6-7.
4. D. W. Hadley. Field and Laboratory Studies on the Reactivity of Sand-Gravel Aggregates. Portland Cement Association, Journal of the Research and Development Laboratories, Vol. 1, No. 3, Sept. 1959, pp. 17-33.
5. K. Mather, A. D. Buck, and W. I. Luke. Alkali-Silica and Alkali-Carbonate Reactivity of Some Aggregates From South Dakota, Kansas, and Missouri. HRB, Highway Research Record 45, 1964, pp. 72-109.
6. Pavement Traffic Marking Materials and Application Affecting Serviceability. NCHRP, Synthesis of Highway Practice 17, 1973.
7. R. G. Nevins. Environmental Control for Health, Comfort, Productivity, and Learning. Research Foundation of Kansas, Jan. 1968.
8. W. M. Stingley, J. D. McNeal, and R. L. Peyton. The McPherson Test Road: Tenth-Year Report. Proc., HRB, Vol. 39, 1960, pp. 191-204.
9. V. R. Sturrup and T. G. Clendenning. The Evaluation of Concrete by Outdoor Exposure. HRB, Highway Research Record 268, 1969, pp. 48-61.
10. Traffic Flow Map. Planning and Development Department, State Highway Commission of Kansas, and Federal Highway Administration, 1974.
11. L. V. White and R. L. Peyton. Condition of Concrete Pavements in Kansas as Affected by Coarse Aggregate. Proc., HRB, Vol. 25, 1945, pp. 129-146.

Publication of this paper sponsored by Committee on Performance of Concrete—Physical Aspects.

Resilient Response of Railway Ballast

Reid M. Knutson, University of Kansas
Marshall R. Thompson, Department of Civil Engineering, University of Illinois at Urbana-Champaign

The resilient responses of five typical open-graded aggregate materials (dolomitic limestone, blast-furnace slag, granitic gneiss, basalt, and gravel) that are used for railway ballast were measured in a triaxial cell. Three levels of compaction and seven stress levels were used. The results were used in regression analyses to develop equations relating the resilient modulus of a specimen to its first stress invariant. They were also used in correlation analyses attempting to relate the resilient response to the physical properties (particle index, specific gravity, Los Angeles abrasion, gradation, flakiness, soundness, and crushing index), but no consistent relations were established. It is concluded that (a) the resilient response of a specimen is essentially independent of its stress history, (b) the resilient moduli of no. 4 and no. 5 ballast-gradation specimens are

usually lower than that of a well-graded aggregate, (c) the resilient moduli of open-graded ballast materials are virtually insensitive to changes in gradation or compaction level, and (d) the variable that most directly influences the resilient moduli of granular materials is stress level.

Although the concept of resilient modulus has gained acceptance and been widely applied to highway and airfield aggregates and soils, information is lacking about the resilient response of the typical open-graded aggregate materials that are used for railway ballast. This paper presents information about the resilient behavior of open-graded materials and relates the results to material and sample properties.

BACKGROUND

Railroads use ballast to support the rail-tie system and provide a free-draining medium. One of the problems related to the performance of ballast materials is the excessive elastic deformation caused by the rapid application and removal of heavy wheel loads.

Excessive elastic deformations in the ballast and subgrade can shorten the life of the rail tie because of the fatigue that results from increased bending stresses. In addition, the ride quality of both freight and passenger cars is reduced if the elastic deformations in the conventional railway-track support system (CRTSS) are excessive.

Modern analytical models can be used to improve the present experience-oriented design of rail-tie support systems. However, before these techniques can be applied, adequate input in the form of the response parameters of ballast materials must be obtained. Thus far, such information has not been available. The response of ballast materials depends on the applied state of stress, and to accurately predict the structural response of the CRTSS, the test method used to evaluate the granular materials should simulate in-service, dynamic stress conditions.

There have been several investigations (1, 2, 3, 4, 5) of the repeated-load behavior of granular materials, but little work has been done involving open-graded aggregates such as ballast.

Repeated-load triaxial testing of a variety of types of aggregates appears to be the most appropriate method for investigating the resilient behavior of ballast materials. Previous investigations in which actual loading conditions were closely simulated have given results that are excellent for convenient application to techniques of finite-element structural analysis.

MATERIALS

Five materials commonly used for ballast were studied, and comparisons of their repeated-load behavior and their natural properties were made. The materials selected were dolomitic limestone from Kankakee, Illinois; blast-furnace slag from Chicago; granitic gneiss from Columbus, Georgia; basalt from New Jersey; and gravel from McHenry, Illinois.

The materials were sieved, and the various size fractions were stored in separate containers for recombining into the desired gradations.

Characterization Tests

To relate the results of the repeated-load tests to the physical properties of the materials, the following standard tests (9, 10, 11, 12) were performed on each type of material.

Property	Test
Particle index	ASTM D 3398-75
Specific gravity	ASTM C 127, AASHTO T 85
Los Angeles abrasion	ASTM C 131, AASHTO T 96
Gradation parameter	Hudson and Waller
Flakiness index	British Standard 812-15
Soundness	ASTM C 88, AASHTO T 104
Crushing value	British Standard 812-34

The results of these tests are summarized in Table 1.

Gradation

To examine the effects of different gradations of ballast on the resilient response, three different ones were tested. Two standard American Railway Engineering Association gradations, no. 4 and no. 5, were selected by using the center values of the recommended gradation bands, and a third gradation was based on the use of the Talbot equation with an exponent of $\frac{2}{3}$. Because one of the main considerations of ballast is that it be free draining, the results obtained through the use of the Talbot equation were maintained only through the 4.75-mm (no. 4) sieve, and to ensure a high permeability, no material finer than the 1.18-mm (no. 16) sieve was used. This gradation was labeled well graded. A conservative estimate of the permeability of the well-graded material is 1500 m/d (5000 ft/d).

Figure 1 shows the three gradations used in the testing program.

EQUIPMENT

A U.S. Army Engineer Waterways Experiment Station triaxial cell design was modified, and the cell was fabricated at the University of Illinois. Because of the large size of the aggregate to be tested, the cell was constructed with an inside diameter of 279 mm (11 in) to provide the capability for testing 203-mm (8-in) diameter cylindrical specimens 406 mm (16 in) high.

The confining pressure was supplied by air pressure and was not cycled during the tests. The repeated deviator stress was applied by a hydraulically actuated piston; control was by a closed-loop electronic system. Input for the load control was provided by a function generator connected through electronic controls to the hydraulic actuator.

Several investigators (2, 4, 6) have experimented with changes in the duration of the repeated load and found no significant dependence of the resilient behavior on the duration of load, especially if the duration is of the order of 0.10 to 0.15 s. The effect on resilient behavior of the frequency of applied load has been studied by Seed and others (6), who found that so long as the frequency is in the expected in-service range, the effect on the resilient response is slight.

The spacing of trucks on conventional railroad rolling stock varies, and the pulse caused by the second truck on one car overlaps that of the first truck on the following car. These two factors cause problems in analyzing the in-service frequency and duration of loading of the ballast. Thus, to satisfy the constraints of the equipment and to approximate the in-service conditions, a frequency of 50 applications/min and a haversine load pulse of 0.15-s duration were used. These conditions are equivalent to a train speed of about 129 km/h (80 mph).

The triaxial chamber pressure was monitored by a gauge on the air supply line. The axial load was monitored by a load cell mounted between the hydraulic actuator and the loading rod. A two-channel high-speed strip-chart recorder was used to monitor the output of

Table 1. Characterization tests.

Material	Gradation	Particle Index	Specific Gravity	Los Angeles Abrasion Loss (%)	Gradation Parameter	Flakiness Index	Soundness Loss (%)	Crushing Value
Limestone	No. 5	13.80	2.626	34.2	1.846	17.52	12.3	22.7
	No. 4	13.75	2.626	34.2	1.074	16.78	18.5	22.7
	Well-graded	14.09	2.626	34.2	2.039	17.33	15.3	22.7
Granitic gneiss	No. 4	13.45	2.679	34.7	1.074	14.39	0.25	26.1
Blast-furnace slag	No. 4	15.68	2.133	37.8	1.074	3.59	0.75	37.3
Basalt	No. 5	15.10	2.775	12.3	1.846	19.69	6.14	12.4
	No. 4	15.40	2.775	12.3	1.074	17.33	4.93	12.4
	Well-graded	14.83	2.775	12.3	2.039	16.11	4.86	12.4
Gravel	No. 5	7.54	2.658	23.2	1.846	4.03	5.06	13.8
	No. 4	10.17	2.658	23.2	1.074	5.79	5.78	13.8
	Well-graded	8.86	2.658	23.2	2.039	6.58	5.84	13.8

Figure 1. Gradations of specimens tested.

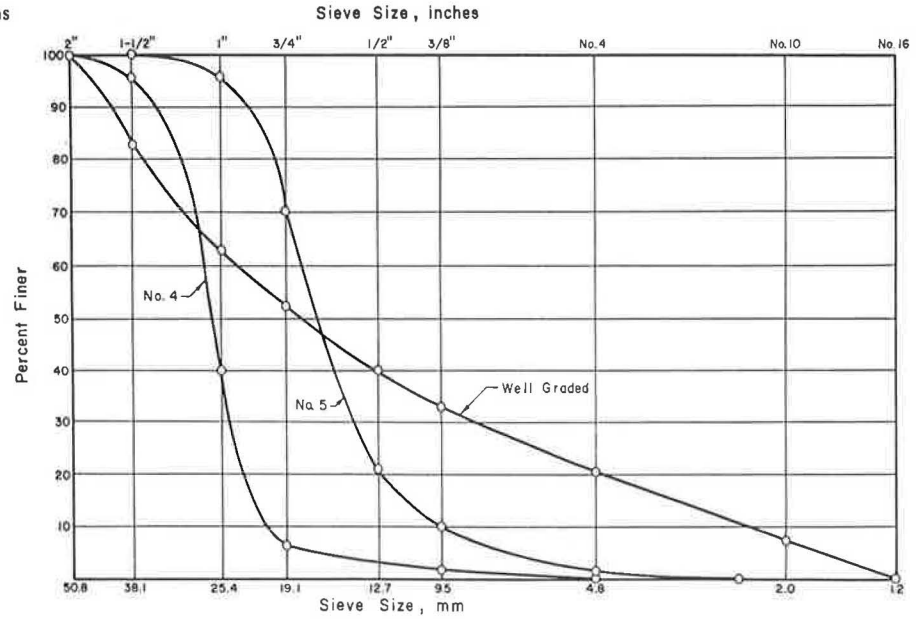

Table 2. Properties of test specimens.

Type of Material	Gradation	Compaction Level	Compaction Density (kg/m³)	Void Ratio
Limestone	No. 5	Medium	1653	0.59
	No. 4	Low	1424	0.84
	No. 4	Medium	1536	0.71
	No. 4	High	1586	0.66
	Well-graded	Medium	1792	0.46
Granitic gneiss	No. 4	Low	1490	0.76
	No. 4	Medium	1562	0.71
	No. 4	High	1639	0.63
Blast-furnace slag	No. 4	Low	1068	1.00
	No. 4	Medium	1137	0.87
	No. 4	High	1173	0.82
Basalt	No. 5	Medium	1722	0.63
	No. 4	Medium	1527	0.82
	Well-graded	Medium	1853	0.50
Gravel	No. 5	Medium	2030	0.31
	No. 4	Low	1640	0.62
	No. 4	Medium	1722	0.54
	No. 4	High	1796	0.48
	Well-graded	Medium	2110	0.26

Note: 1 kg/m³ = 0.062 lb/ft³.

the load cell.

Two methods were used to observe the axial deformations. The first was by the use of two electronic-optical scanners that measured the vertical motion of targets placed at the upper and lower quarter points of the specimen. These targets consisted of one black and one white rectangular strip, 32 by 64 mm (1.25 by 2.5 in) each, held to the specimen membrane by double-sided tape. The chamber pressure ensured that the membrane was molded firmly to the specimen, thereby eliminating slippage between specimen and targets. The movements of the targets were sensed by the optical heads and converted into an electrical signal; the difference in movements was recorded as output on the strip recorder.

A backup for measuring the axial deformations was provided by a linear variable differential transformer (LVDT) mounted at the top of the hydraulic actuator. The LVDT signal was recorded simultaneously with the collimator signal. The LVDT measured deformations over the entire specimen length; therefore, the output included specimen end effects.

TEST PROCEDURE

Because one of the objects of this study was to determine the effects of gradation and maximum size on ballast behavior, two different sample sizes were used. Samples 152 mm (6 in) in diameter were used for the no. 5 ballast-gradation specimens, which have a maximum particle size of 38 mm (1.5 in), and samples 203 mm (8 in) in diameter were used for the no. 4 ballast gradation, which has a maximum particle size of 51 mm (2 in). Thus, the ratio of the diameter of the sample to the maximum particle size was always four. All the prepared samples had a height to diameter ratio of 2 to 1 or more to minimize the end effects on the deformation measurements.

To minimize segregation and to ensure gradation con-

trol, each specimen was weighed out by thirds for each of the size fractions, and each third was placed in a separate container. The material was then washed to remove the fines, drained, and compacted.

Because of the open-graded nature of ballast, vibratory compaction similar to that described by Rostron and others (7) was used. To determine the compaction characteristics of the aggregate and whether it was degraded during compaction, no. 5 ballast-gradation limestone was compacted in the standard split mold for various times by using the vibratory compactor. The results showed that there was little increase in density for compaction times greater than 45 s and that the gradation change (aggregate degradation) due to compaction was extremely small. For example, the amount of material passing the 4.75-mm sieve increased from 2.5 to 4.0 percent after compaction for 45 s/layer, and the increase was less (less than 1 percent) for shorter compaction times.

Because densities are generally not specified when ballast is placed, there was no attempt to attain a predetermined density. Instead, three degrees of compaction were used. For low-density specimens, each layer of aggregate was placed and rodded 10 times; for medium-density specimens, each layer was compacted for 5 s with the vibratory hammer; and for high-density

Figure 2. Relation between E_r and θ for medium-density no. 5 gradation limestone.

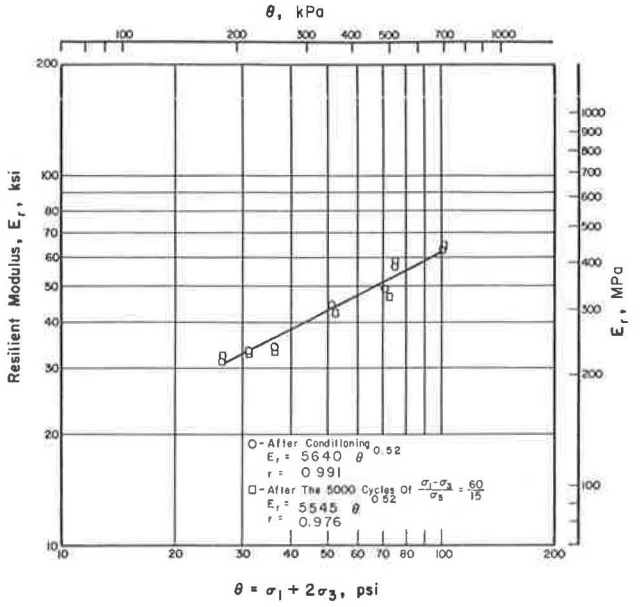

Figure 3. Relation between E_r and θ for low-density no. 4 gradation limestone.

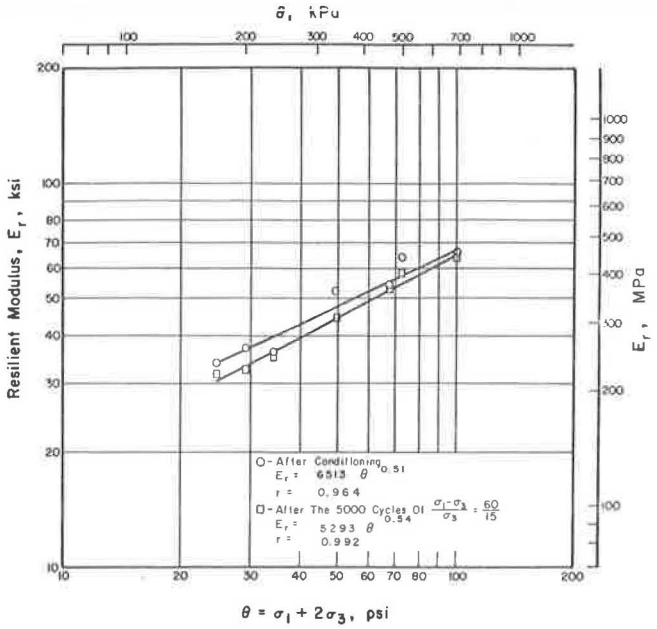

Figure 4. Relation between E_r and θ for medium-density no. 4 gradation limestone.

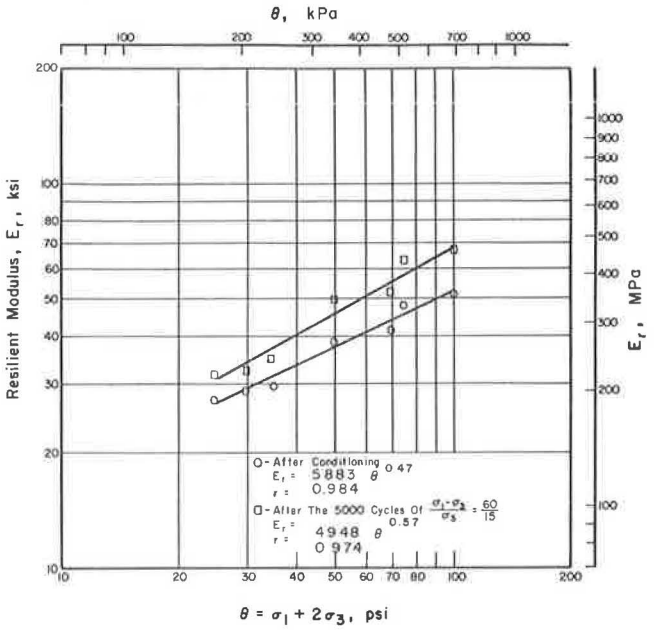

Figure 5. Relation between E_r and θ for high-density no. 4 gradation limestone.

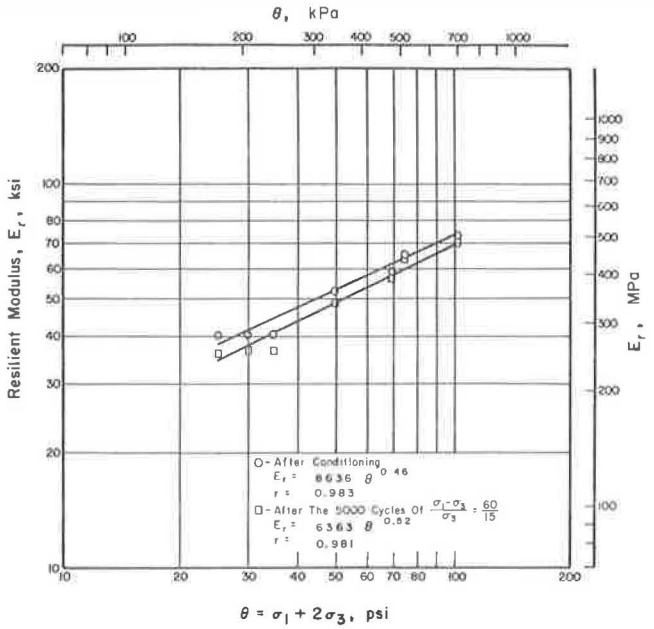

specimens, each of the three layers was vibrated for 45 s.

The compaction was carried out in a split mold clamped to the sample base. A rubber membrane was used inside the mold, and a vacuum was applied through the attached tubing to hold the membrane against the mold. After compaction, the height of the specimen was recorded, the mold was removed, and a second membrane was placed over the specimen because (almost without exception) the original membrane was punctured during compaction.

From a finite-element analysis of CRTSS (8), values were obtained for the stress at various points in the ballast layer. A deviator stress of 310 kPa (45 lbf/in^2) and a confining pressure of 103 kPa (15 lbf/in^2) were selected as representative of the stresses occurring approximately 51 mm beneath a crosstie, and each specimen was conditioned for 5000 load applications. After conditioning, each specimen was tested for resilient modulus at each of seven stress levels as follows (1 kPa = 0.145 lbf/in^2):

Figure 6. Relation between E_r and θ for medium-density well-graded (n = 2/3) limestone.

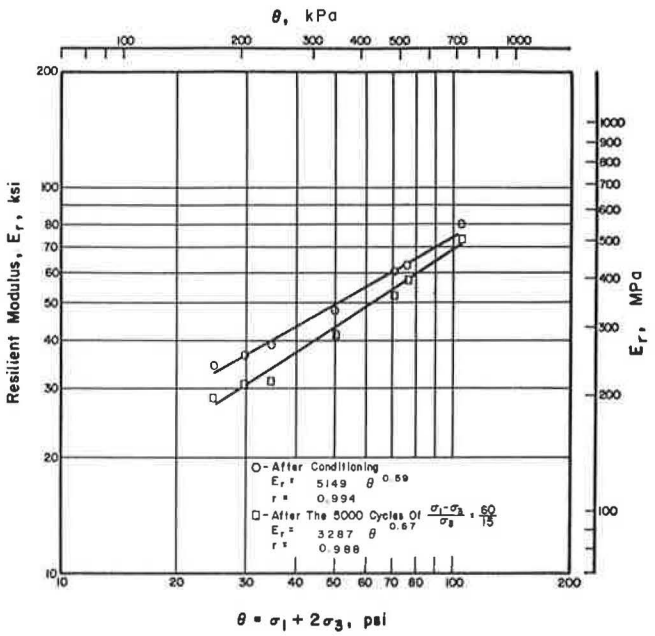

Figure 7. Relation between E_r and θ for low-density no. 4 gradation granitic gneiss.

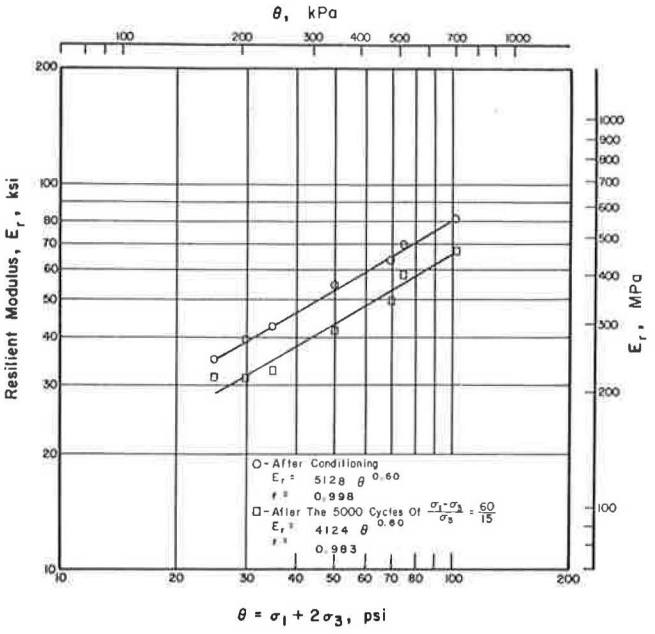

Figure 8. Relation between E_r and θ for medium-density no. 4 gradation granitic gneiss.

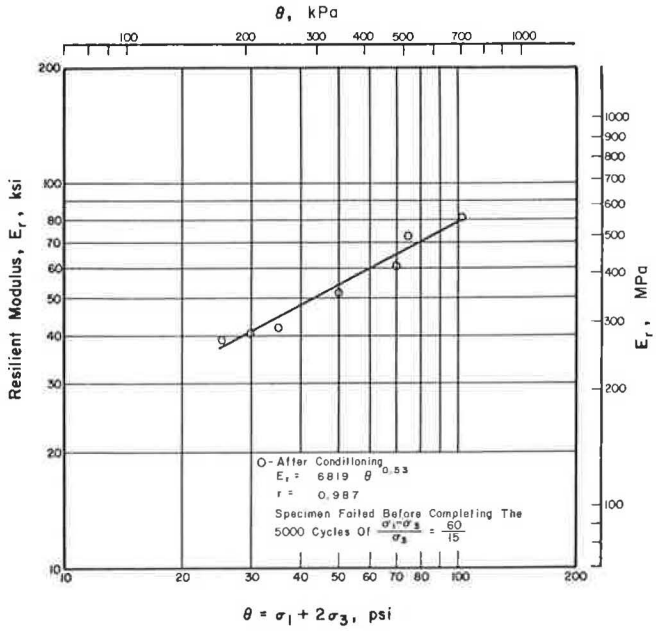

Figure 9. Relation between E_r and θ for high-density no. 4 gradation granitic gneiss.

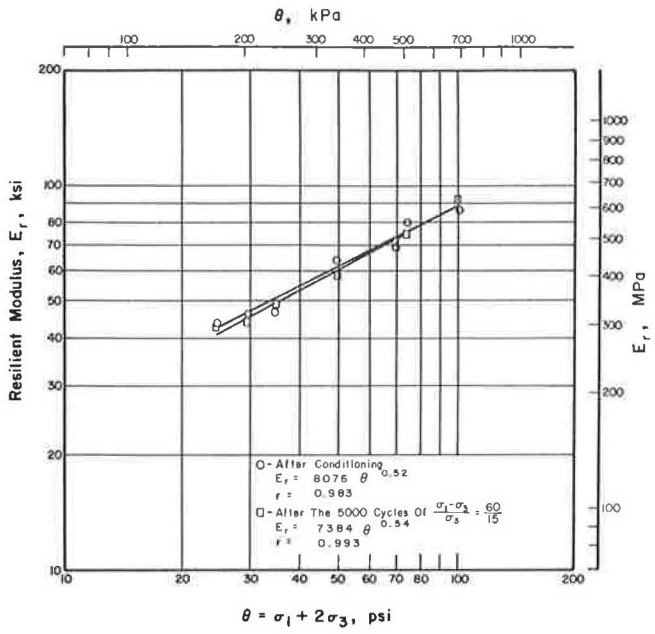

Deviator Stress (kPa)	Confining Pressure (kPa)	Deviator Stress (kPa)	Confining Pressure (kPa)
414	103	138	34
207	103	103	34
276	69	69	34
138	69		

After the first test of resilient response, the specimens were loaded for 5000 cycles at a deviator stress of 138 kPa (20 lbf/in^2) and confining pressure of 34 kPa (5 lbf/in^2) and then for 5000 cycles at a deviator stress of 414 kPa (60 lbf/in^2) and a confining pressure of 103 kPa (15 lbf/in^2). A second resilient-response test was then performed to determine the effects of mixed loading and stress history.

RESULTS

Table 2 summarizes the physical properties of the specimens tested. The most dense specimen, the well-graded gravel, had a density almost twice that of the least dense, the low-compactive-effort blast-furnace slag.

The data collected in the resilient-response tests were used in regression analyses to develop equations

Figure 10. Relation between E_r and θ for low-density no. 4 gradation Chicago blast-furnace slag.

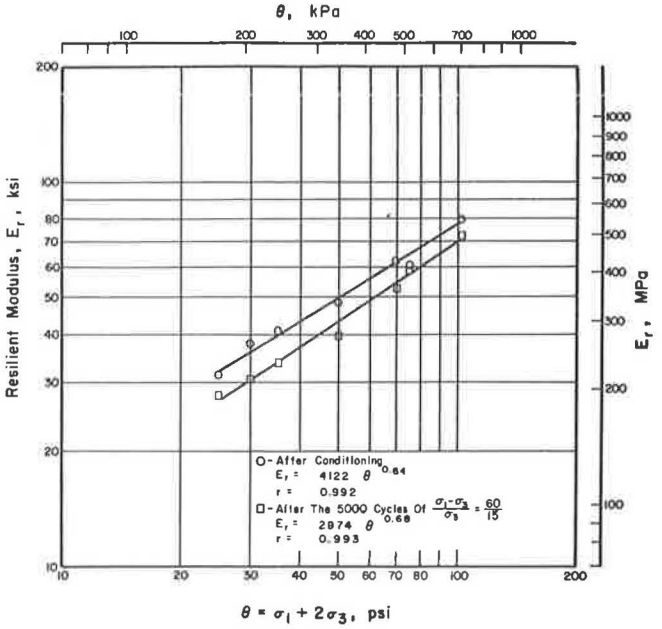

Figure 11. Relation between E_r and θ for medium-density no. 4 gradation Chicago blast-furnace slag.

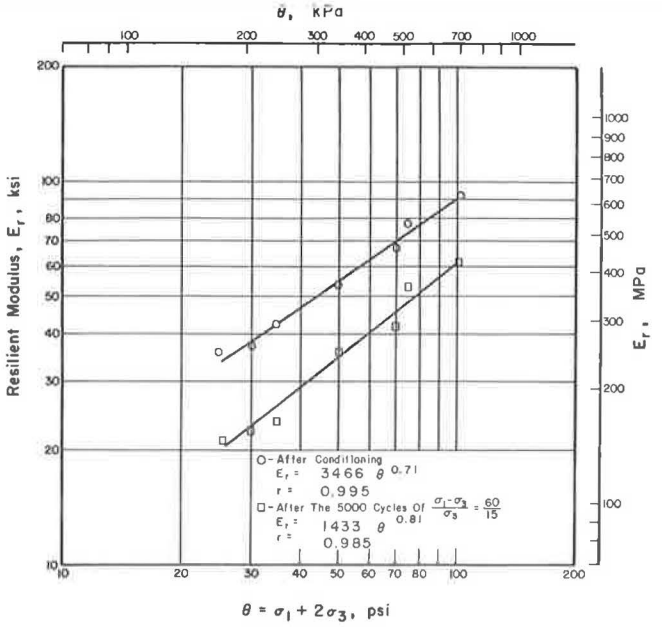

Figure 12. Relation between E_r and θ for high-density no. 4 gradation Chicago blast-furnace slag.

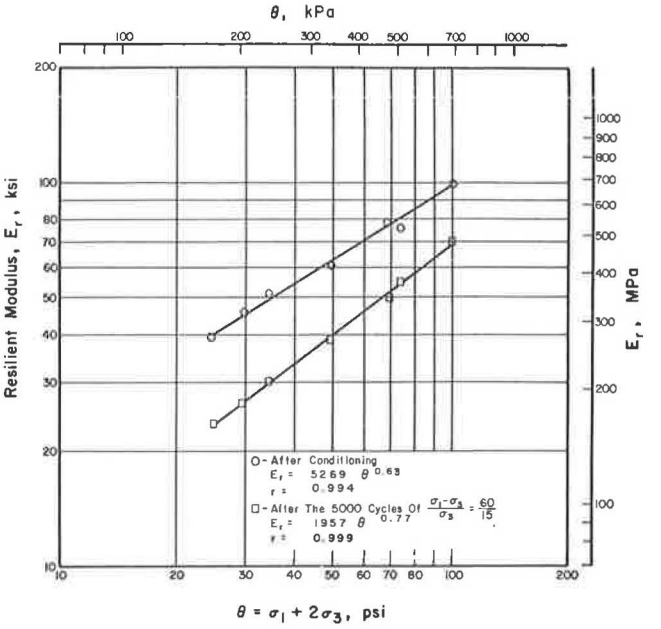

Figure 13. Relation between E_r and θ for medium-density no. 5 gradation basalt.

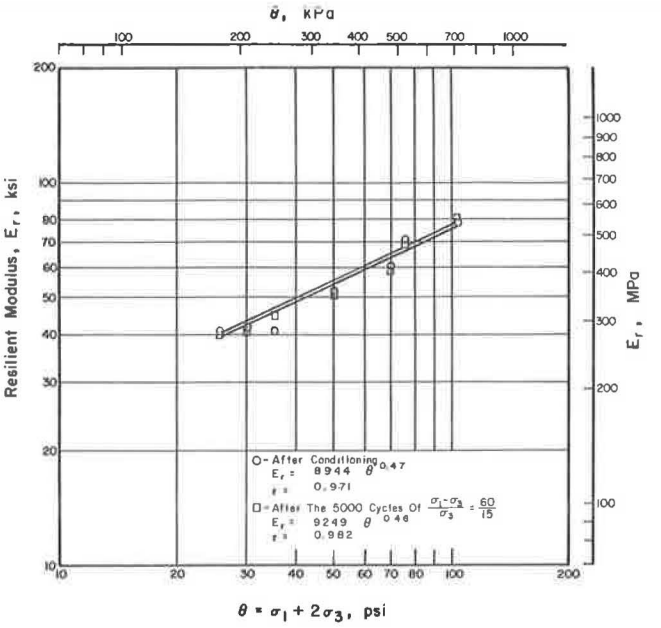

of the following type:

$$E_r = K\Theta^n \quad (1)$$

where

E_r = resilient modulus,
n and K = constants representing slope and intercept respectively on a log-log plot, and
Θ = first stress invariant, i.e., $\sigma_1 + \sigma_2 + \sigma_3$.

($\Theta = \sigma_1 + 2\sigma_3$ in the triaxial test.)

Figures 2 through 20 present the results, including the regression analyses, for the specimens tested. (SI units are not given for the coefficients in the regression results because the analyses were carried out in customary units only.) Two of the specimens failed before completion of the mixed loading sequence, and thus only one set of data is available for those two. All the regression analyses were significant at $\alpha = 0.01$.

The resilient-response data were also used in correlation analyses with the results of the standard characterization tests, but no consistent relations could be established between K or n and the material-

Figure 14. Relation between E_r and θ for medium-density no. 4 gradation basalt.

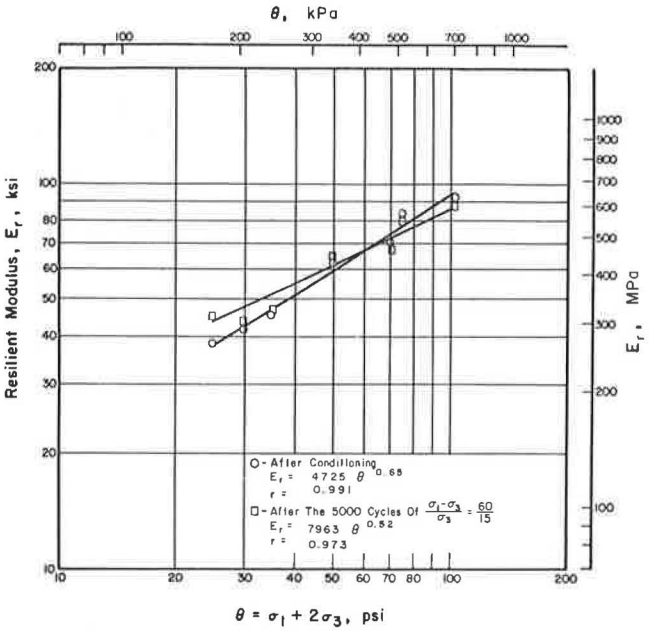

Figure 15. Relation between E_r and θ for medium-density well-graded (n = 2/3) basalt.

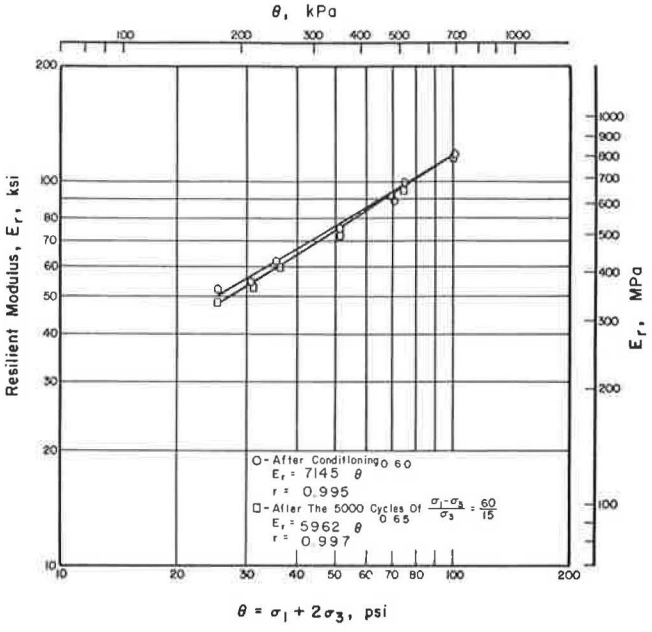

Figure 16. Relation between E_r and θ for medium-density no. 5 gradation gravel.

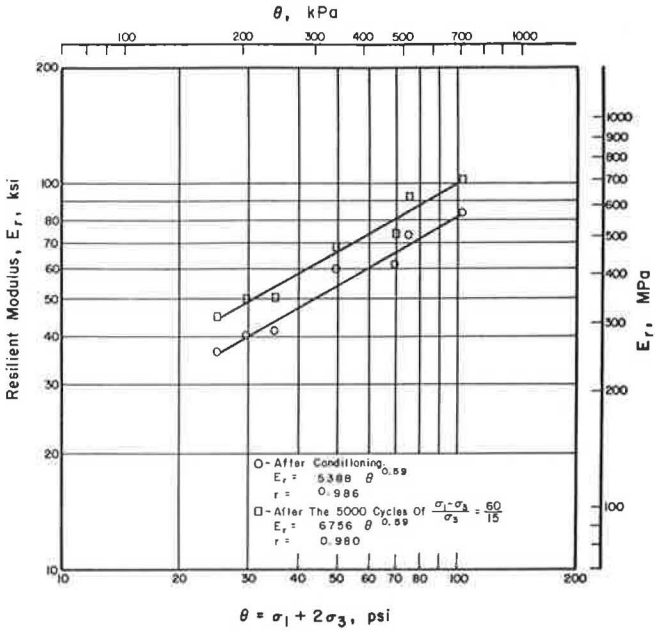

Figure 17. Relation between E_r and θ for low-density no. 4 gradation gravel.

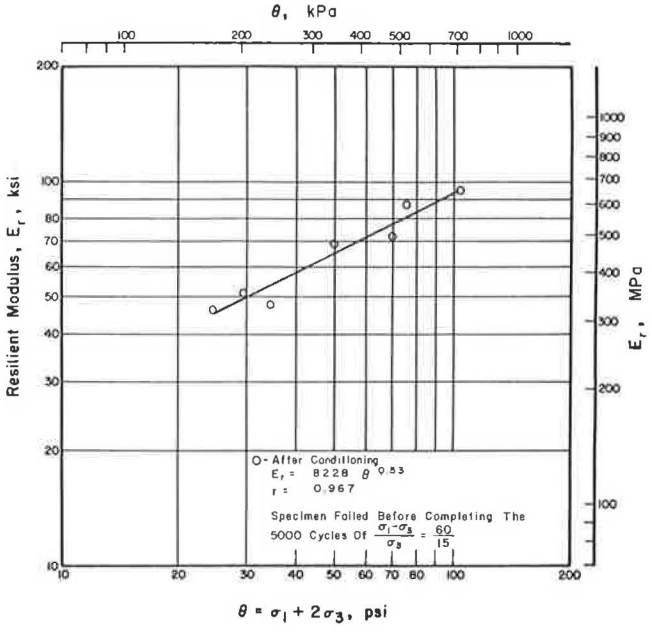

characterization data.

To ensure that the gradation parameter was included on an equal basis, three levels of gradation of three types of material (limestone, basalt, and gravel) were included in the correlation analyses, but neither K nor n were found to correlate significantly ($\alpha = 0.05$) with any of the material properties.

Attempts were also made to determine the effects on the resilient response of the type of material and the gradation through the use of randomized complete block analyses. The effects of loading history and relative density were also investigated.

Because previous research (4) has shown that variations in the values of n and K of the predictive equations for resilient modulus often cancel one another, two values of E_r were calculated at values of Θ of 241 kPa (35 lbf/in^2) and 620 kPa (90 lbf/in^2) and included in the analyses. Thus, the variables included were K, n, E_r at 241 kPa, and E_r at 620 kPa.

To further examine the effect of gradation, three levels of gradation (no. 4, no. 5, and well graded) of three types of material (limestone, basalt, and gravel) were included in the analysis. Only one of the four variables—E_r at 620 kPa—had significant ($\alpha = 0.05$) differences due to gradation. The values of E_r at 620 kPa were further analyzed by using Duncan's multiple range test. No difference was found between the values for the no. 4 and no. 5 ballast-gradation specimens, but both were significantly lower than the values for the well-graded specimens. In general, the effect on resilient modulus of changes in gradation was slight.

The effect of density was included by considering three density levels (low, medium, and high) of four different materials (limestone, granitic gneiss, blast-furnace slag, and gravel). There were no differences among the resilient responses of these materials.

Further analysis of the resilient responses of the specimens to determine the effect of loading history (resilient behavior after conditioning versus after additional loading) showed that none of the four variables (K, n, E_r at 241 kPa, and E_r at 620 kPa) had significant ($\alpha = 0.05$) differences between the two sets of data. Thus, the conclusion that the resilient response of granular materials remains essentially unchanged through a complex loading history is reinforced (2, 3, 4, 5).

To include the effect of type of material, an analysis was made of low, medium, and high-density no. 4 ballast-gradation specimens of limestone, granitic gneiss, gravel, and blast-furnace slag.

There were no differences in the values of K among the four materials considered, but there were significant ($\alpha = 0.05$) differences among the values of n, E_r at 620 kPa, and E_r at 241 kPa. A further analysis was made by using Duncan's multiple range test. Although there were differences among the values for the various types of material, there were no consistent trends. The slag had the highest value of n, and this value was signifi-

Figure 18. Relation between E_r and θ for medium-density no. 4 gradation gravel.

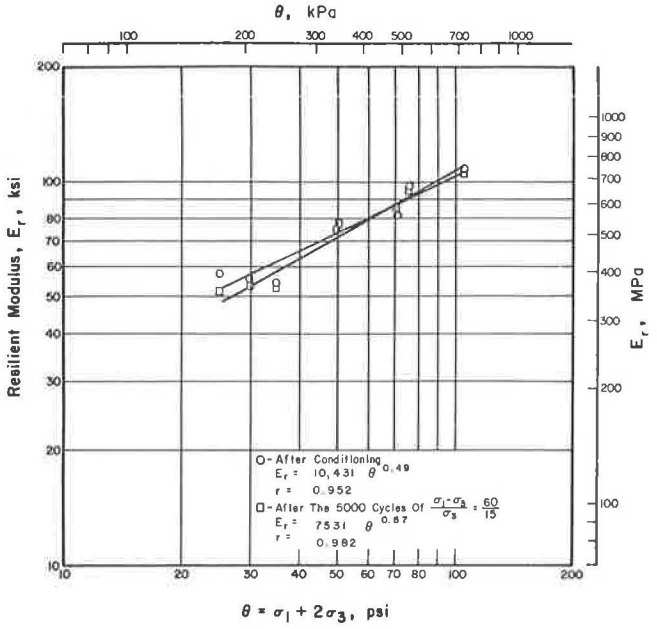

Figure 19. Relation between E_r and θ for high-density no. 4 gradation gravel.

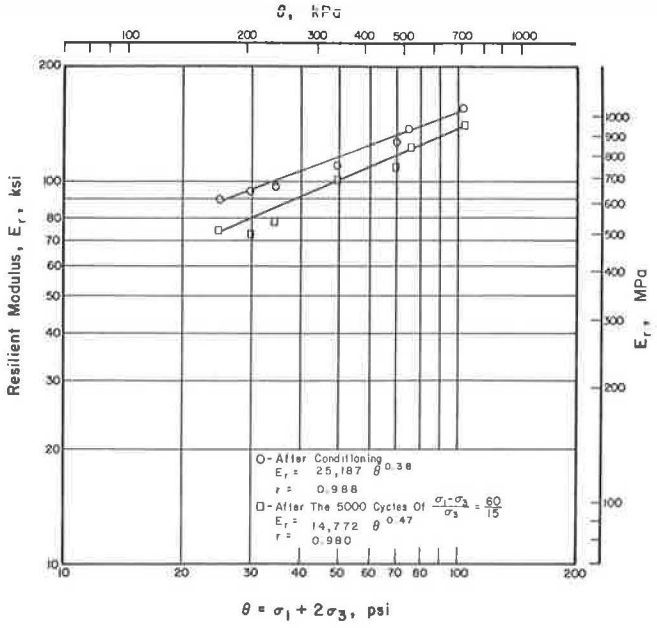

Figure 20. Relation between E_r and θ for medium-density well-graded (n = 2/3) gravel.

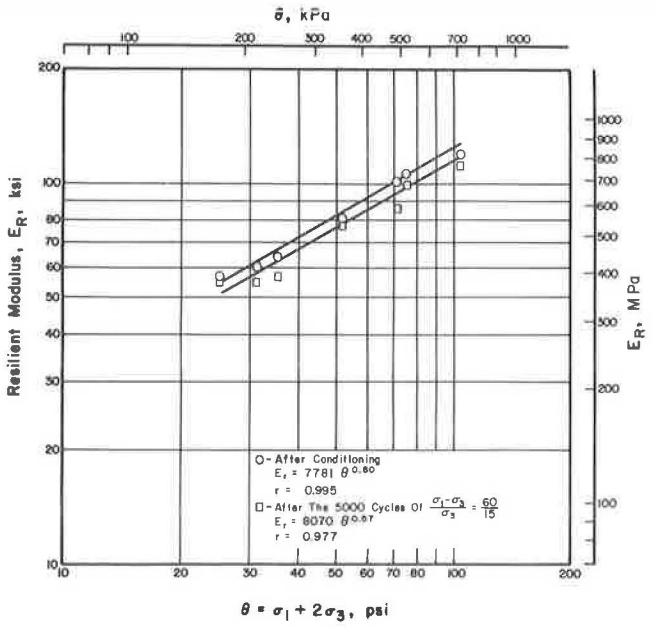

cantly different from that of the other three materials. The gravel specimens had the highest mean values of E_r at 241 kPa and at 620 kPa, and these values were significantly different from those of the other three types of material.

Although the resilient response depends somewhat on the type of material, the lack of consistency in the data prevents making any definite conclusions. The differences in resilient behavior were so slight as to be negligible from the standpoint of the structural response of a CRTSS.

SUMMARY AND CONCLUSIONS

Ballast materials from several sources were tested in the triaxial apparatus. In-service conditions were simulated by the use of a repeated deviator stress and a constant confining pressure. The resilient modulus characteristics were determined; the variables considered included the type of material and its gradation and density, and the stress level. Equations relating the resilient modulus to the first stress invariant were developed, and the results were analyzed with respect to the variables.

The following conclusions were reached:

1. The resilient response of a specimen of open-graded granular material is independent of its stress history so long as the specimen has not been subjected to a stress level that would cause failure.
2. The resilient moduli of no. 4 and no. 5 ballast-gradation specimens are usually slightly lower than that of a well-graded aggregate.
3. The resilient moduli of open-graded ballast materials are virtually insensitive to changes in gradation or compaction level. The dependence of resilient response on type of material is weak and inconsistent, and therefore, no conclusion is drawn with respect to material type.
4. Stress level is the variable most directly influencing the resilient modulus of granular materials. The stress-dependent nature of ballast materials can be characterized by the predictive equation:

$$E_r = K\Theta^n \quad (1)$$

ACKNOWLEDGMENT

This paper is based on the results of a ballast and foundation materials research program conducted by the Transportation Research Laboratory of the Department of Civil Engineering, University of Illinois at Urbana-Champaign. The research was sponsored by a subcontract between the Research and Test Department, Association of American Railroads, and the University of Illinois. This subcontract is part of a larger contract that is a cooperative effort between the Federal Railroad Administration, U.S. Department of Transportation, and the Association of American Railroads on improved track structures. This paper represents our views and positions and does not necessarily reflect those of the U.S. Department of Transportation or the Association of American Railroads.

REFERENCES

1. J. H. Haynes and E. J. Yoder. Effects of Repeated Loading on Gravel and Crushed Stone Base-Course Materials Used in the AASHO Road Test. HRB, Highway Research Record 39, 1963, pp. 82-96.
2. R. G. Hicks and C. L. Monismith. Factors Influencing the Resilient Response of Granular Materials. HRB, Highway Research Record 345, 1971, pp. 15-31.
3. R. D. Barksdale. Repeated-Load Test Evaluation of Base-Course Materials. Georgia Institute of Technology, Atlanta, 1972.
4. J. J. Allen. The Effects of Nonconstant Lateral Pressures on the Resilient Properties of Granular Materials. Univ. of Illinois, Urbana, PhD thesis, 1973.
5. I. V. Kalcheff and R. G. Hicks. A Test Procedure for Determining the Resilient Properties of Granular Materials. ASTM, Journal of Testing and Evaluation, Vol. 1, No. 6, 1973.
6. H. B. Seed and others. Prediction of Flexible Pavement Deflections From Laboratory Repeated-Load Tests. NCHRP, Rept. 35, 1967.
7. J. P. Rostron and others. Density Standards for Field Compaction of Granular Bases and Subbases. NCHRP, Research Results Digest 57, 1974.
8. S. D. Tayabji. Considerations in the Analysis of Conventional Railway-Track Support Systems. Univ. of Illinois, Urbana, PhD thesis, 1976.
9. Annual Book of ASTM Standards. ASTM, 1975.
10. Standard Specifications for Transportation Materials and Methods of Sampling and Testing. AASHTO, 1974.
11. British Standard 812. In Methods for Sampling and Testing of Mineral Aggregates, Sands, and Filters, British Standards Institution, 1967.
12. S. B. Hudson and H. F. Waller. Evaluation of Construction Control Procedures—Aggregate Gradation Variations and Effects. NCHRP, Rept. 69, 1969.

Publication of this paper sponsored by Committee on Coatings, Signing, and Marking Materials.

Abridgment

Snowplowable Raised Pavement Markers in New Jersey

M. V. Jagannath and A. W. Roberts, Bureau of Operations Research, New Jersey State Department of Transportation

Pavement markings are an important source of information to the motorist for safe vehicle control and guidance under almost all circumstances of driving. One of the most difficult problems in recent years has been that of

developing an economical pavement-marking system that adequately delineates the roadway both day and night, in dry and wet weather. A durable reflective marker for areas where snowplowing is common has only recently been developed to a practical level after more than 8 years of cooperative testing. This snowplowable, raised, reflective pavement marker is shown in Figure 1.

DESCRIPTION

Components

The raised, reflective pavement marker specifically designed for use on roads subject to snow removel consists of a casting, a reflector, and reflector attachments. The casting is manufactured with a hardened steel surface and has keels, rails, a web, a seat for the reflector, and notches to retain a spring clip. There are two types of reflector retention methods. One type uses a butyl adhesive pad that is attached between the bottom of the reflector and the casting, and the other type uses a spring-steel wire clip. Reflector shields are used to protect the reflector from hits by tire studs, chains, and stones and are held on top of the reflector by butyl adhesive pads or spring clips.

Experimental Installations

Markers were installed for experimental purposes at three locations in New Jersey at different times. Each installation was carried out in two parts. First, grooves were cut in the pavement with a vertical radial blade and then, at another time, the grooves were dried, cleaned with compressed air, and partially filled with epoxy, and the castings were inserted. Clear markers were placed at alternate gaps on all the lane lines, which are 10 cm (4 in) wide, and have 4.6-m (15-ft) long striping and 7.6-m (25-ft) gaps. On the median (10-cm-wide solid yellow lines), amber markers were placed every 12 m (40 ft). At the exit gores, clear markers were placed outside the 20-cm (8-in) wide lines at 6-m (20-ft) intervals. No markers were placed on the right-hand edge lines (Figure 2).

Visual Characteristics

A raised, reflective marker should provide a visual substitute for the painted line delineation in the rain at night. These markers appeared to become brighter on rainy nights under conditions in which the painted lines become more difficult to see.

DURABILITY

Castings

Pavement markers installed in areas where snowplowing is common should resist damage from snowplow operations and traffic. Snowplow operations were carried out at all three locations using both steel and tungsten carbide insert blades. The steel blades did not damage the castings, but the tungsten carbide insert blades produced some noticeable effects. On US-1, during the winter of 1973/1974, the 520 markers that had been installed in 1973 were plowed 21 times, and during the winter of 1974/1975, the markers that had been installed in 1973 and the 435 that had been installed in 1974 were plowed 11 times, always with steel blades. After three and two winters, 2 and 1 percent of the 1973 castings respectively were either missing or unusable.

Reflectors

Reflector replacement is much simpler and less costly than casting replacement. The durability of a reflector is based on its resistance to damage caused by snowplows, snowplow accessories, and traffic. There was no damage to or loss of reflectors from the use of steel or tungsten carbide insert blades in summer plow and grader tests on I-95. There was damage to reflectors from nose shoes in a test in Trenton that used three versions of modified nose shoes, but there was no damage to reflectors in tests in which plow shoes and plow wheels rode over reflectors. Tire studs and other tire forces have caused reflector loss and damage. The effects of traffic on reflector loss and damage varied according to the type of assembly or model. The types of models are described below.

	Model				
Component	1	2	3	4	5
Casting	Yes	Yes	Yes	Yes	Yes
Adhesive pad B	Yes	No	No	Yes	No
Reflector	Yes	Yes	Yes	Yes	Yes
Adhesive pad D	No	No	No	Yes	Yes
Stud shield	No	No	Yes	Yes	Yes
Spring clip	No	Yes	Yes	No	Yes

In January 1974, 3 months after the 1973 installation of 520 model 3 assemblies on US-1, the markers were plowed 13 times, and 105 reflectors were lost. The missing reflectors were replaced with 49 model 1 on the northbound side and 56 model 2 assemblies on the southbound side. The results of the smaller installation of models 1 and 2 led to a test of all five models in a larger installation. After one winter, none of the models 1 and 4 was lost, but some damage was observed on all the reflectors.

The effects of traffic could have been the major cause of loss of some of the types of reflectors, while studded tires appeared to be the major cause of damage. The reflectors that were protected with shields had less damage from traffic than those without shields.

The fractures and chips on the reflective surfaces facing the motorist were counted and classified by size. The tops of the nonshielded reflectors were chipped to a large extent, while the tops of the shielded reflectors were not damaged. There were one-third more stud marks on the nonshielded reflective surfaces. A rating of the loss of and damage to each reflector model after two winters of use is shown in Table 1. The highest overall rating indicates the type with the least amount of a combination of loss and damage. A reflector with a spring clip requires 30 to 45 s to replace, whereas an adhesive-pad reflector requires 45 to 90 s. Most of the model 4 assemblies lost their shields and, as a result, experienced more damage. The adhesive does not attach well in cold weather. Many of the adhesive-pad reflectors installed in cold weather were lost due to lack of proper adherence to the castings. Considering minimum loss and damage and ease of installation and replacement, the model 5 assembly appears to be the most practical.

CONDITION OF SNOWPLOW BLADES AND ACCESSORIES

Raised pavement markers should not damage snowplow blades and accessories during normal snow-removal operations. These markers did not damage steel blades, whether on truck-mounted or grader-mounted plows, but tungsten carbide insert blades were shattered or chipped

at points where they contacted the castings, and the holding steel was turned forward and made irregular, exposing the damaged tungsten carbide inserts. Both types of blades were in contact with the pavement while plowing.

COST ESTIMATE

The cost of installing and maintaining markers was estimated for one side of a four-lane divided highway with markers spaced 24 m (80 ft) apart on lane lines, 12 m (40 ft) apart on median lines, and 6 m (20 ft) apart on exit-ramp gores and one exit-ramp gore located every 2.4 km (1.5 miles). A computer program was developed to simulate a yearly replacement cycle for reflectors. The estimated cost of installing markers and maintaining reflectors over a period of 10 years is $2378/km ($3806/mile), or approximately $15/marker. The estimated cost of marking a highway, restriping the lane lines twice a year and the median solid line and the gore once a year, over a period of 10 years is $1430/km ($2282/mile). Therefore, the estimated cost in 1975 dollars of using both delineator techniques would be $3808/km ($6088/mile). This is an average annual cost of $381/km ($609/mile) as opposed to $140/km ($228/mile) for striping alone.

DISCUSSION AND FUTURE RESEARCH NEEDS

These markers appear to be adequate for use in areas where tungsten carbide insert blades are not used directly on the pavement. Damage to the inserts can be avoided by keeping the blade off the pavement; otherwise, steel blades should be used. The use of a steel blade bolted over a carbide insert blade as in Sheboygan County, Wisconsin, should be evaluated. Nose shoes could be modified to prevent premature loss of reflectors or the entire nose-shoe assembly could be removed, if it were not deemed advisable to retain the extra metal for protection of the side plate on the leading side of funnel type plows. The function of nose shoes should be thoroughly investigated before modification recommendations are made.

The highways in central New Jersey on which the markers were tested were an expressway and a freeway that are considered major intercity routes—US-1 and I-95—that have a two-way average daily traffic of up to 60 000 vehicles. The snowfall is about 51 cm/year (20 in/year). The markers in these locations are plowed about 10 to 15 times/year, mostly with steel-edged blades resting on the pavement. In 1974, nose shoes were either not used or were modified.

Figure 1. Experimental reflector assemblies.

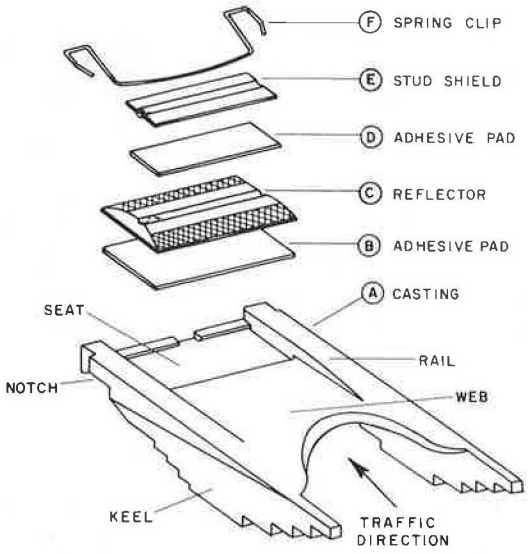

Figure 2. New Jersey system of marker placement.

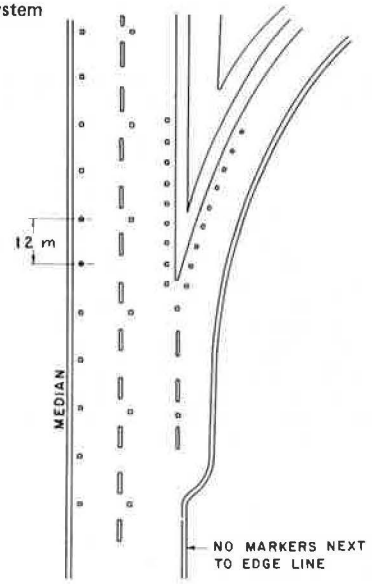

Table 1. Rating of reflector loss and damage after two snow seasons by type of assembly.

Percentage Damage Category	Rating Factor	Model 1 (N = 94) Percentage of Reflectors Lost	Model 1 Rating	Model 2 (N = 88) Percentage of Reflectors Lost	Model 2 Rating	Model 3 (N = 86) Percentage of Reflectors Lost	Model 3 Rating	Model 4 (N = 84) Percentage of Reflectors Lost	Model 4 Rating	Model 5 (N = 82) Percentage of Reflectors Lost	Model 5 Rating
0	1.000	20.21	20.21	23.86	23.86	31.40	31.40	30.95	30.95	46.34	46.34
1 to 25	0.875	23.40	20.48	30.68	26.85	18.60	16.28	21.43	18.75	12.20	10.68
26 to 50	0.625	15.96	9.98	17.05	10.66	9.30	5.81	11.90	7.44	7.32	4.58
51 to 75	0.375	8.51	3.19	6.82	2.56	2.33	0.87	9.52	3.57	3.69	1.38
76 to 100	0.125	14.89	1.86	5.68	0.71	2.33	0.29	11.90	1.49	6.10	0.76
Missing	0	17.02	0.00	15.91	0.00	36.05	0.00	14.29	0.00	24.39	0.00
Overall rating	—	—	55.72	—	64.64	—	54.65	—	62.20	—	63.74

Note: After the first winter, of the original 435 assemblies, 1 casting and 31 reflectors were missing. After the second winter, an additional 4 castings and 61 reflectors were missing. Only steel blades with modified nose shoes were used both winters. Total snow accumulation was 62.5 cm (24.6 in) during the second winter.

About 10 to 12 percent of the passenger automobiles in the area had studded rear tires. These tires seem to be the main cause of reflector wear, and where they are allowed, the use of shields on reflectors is advantageous. Under conditions in which the lifetime of reflectors is short, the ease of replacement when spring clamps are used and the consequent lower labor costs may balance the higher reflector loss of this type of assembly. Further study of large-scale installations of the marker over a period of 3 or more years in several areas with a wide range of snowfall rates and uses of studded tires should provide useful information for predicting annual losses. The relation between the amount of reflector surface damaged and the nighttime visibility of the reflector should be investigated. This information could be used to determine when replacement is warranted.

ACKNOWLEDGMENTS

We wish to acknowledge the assistance given by E. F. Reilly, R. L. Hollinger, J. J. Gertler, and Richard Weed of the Division of Research and Development and the Bureau of Maintenance, New Jersey State Department of Transportation. The technical assistance provided by Larry Smith, Robert Flanagan, and Adam Smorzaniuk of the Amerace Corporation and the funding and active support of the Materials Division of the Office of Research, Federal Highway Administration, is also appreciated.

Publication of this paper sponsored by Committee on Mineral Aggregates.

Test for the Adhesion of Thermoplastic Highway-Marking Materials

James S. Noel and Steven D. Hofener, Texas Transportation Institute, Texas A&M University

A new method for evaluating the adhesion between thermoplastic highway-marking materials and pavement surfaces is described. The specimen consists of a small square block of paving material (e.g., Portland cement concrete, asphaltic concrete, or some other) with a layer of thermoplastic bonded to one surface. An orifice penetrates the block and opens into a small circular area intentionally not bonded. A blister is formed by forcing fluid through the orifice until the diameter of the unbonded area begins to grow. The pressure used to inflate the blister and the height at the center of the blister are simultaneously recorded. From these measured data, the characteristic adhesive strain energy release rate is calculated. The analytical expressions necessary for the calculations are given, as is a discussion of the significance of the results to the highway engineer. Several exploratory tests were performed and the results are reported. The results demonstrate the sensitivity of the test to the adhesion of the thermoplastic to the pavement surface. Thus, the test can be used to quantify the effect on adhesive strength of those field conditions that can be reproduced in the laboratory.

Thermoplastic highway-marking materials have several advantages over conventional paints. These include better durability, improved color retention, and greater nighttime visibility, especially during periods of heavy rainfall. However, they also have disadvantages: (a) a tendency to flake during the winter (1) and (b) a tendency to blister shortly after placement, especially in the southern states. Figure 1 shows both phenomena and the accelerated degradation that results under the action of traffic.

Both of these disadvantages are related to the degree of adhesion between the marking material and the pavement. This adhesive strength varies, depending on the type of pavement, the time of cure, and the environment. The type of pavement is extremely important; the thermoplastics are much more durable on asphalt than on portland cement concrete. On either, the durability can be improved by the application of a chemical bonding agent before placing the thermoplastic.

Many makeshift methods of testing adhesion to pavements have evolved; however, the results are qualitative and can be only used for comparative purposes. Thus, the selection and method of applying these thermoplastics and primers has generally been left to the judgment of the responsible engineer. This judgment is typically developed through field experience and performance testing—a long, costly process.

A laboratory test toward the same end is suggested here. The test is based on the validity of the energy approach to adhesive fracture. A similar test was originally proposed for use with conventional paint in 1961 by Dannenberg (2). The approach has recently been developed and discussed in detail in a series of papers by Williams and his coworkers (3, 4, 5, 6). These studies concluded that there exists a system parameter (γ), the characteristic adhesive fracture energy, that quantitatively reflects the resistance of a bonded surface to the growth of an unbonded area. This parameter may be sensitive to the rate of loading and the temperature, but is independent of geometry. If the stiffnesses of the adherends and the γ are known, a stress analysis of any geometry can be used to establish the critical balance between the change in the potential energy of the system and γ. The following discussion of the analytical expressions for the energy balance of the blister-test geometry is based on the references cited above.

ANALYTICAL APPROACH

Consider an axially symmetric structure consisting of a flat infinite surface covered by a layer of a second material. The covering layer is bonded to the surface, except for a circular area centered about an axis of symmetry. An orifice smaller in diameter than the unbonded area penetrates the substrate (Figure 2a).

To perform the test, a fluid is forced through the orifice, causing the unbonded portion of the covering plate to deform upward, i.e., blister. The fluid used can be either compressible or incompressible. If it is

Figure 1. Thermoplastic stripe on a grooved pavement surface after two winters of service.

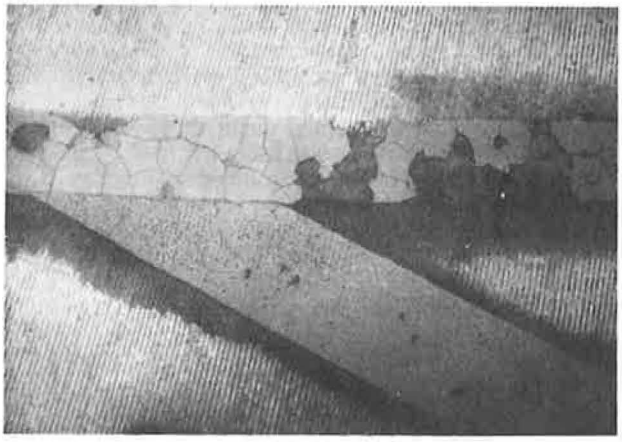

Figure 2. Phases of bond test: (a) initially unbonded area, (b) blister formed, and (c) blister extended.

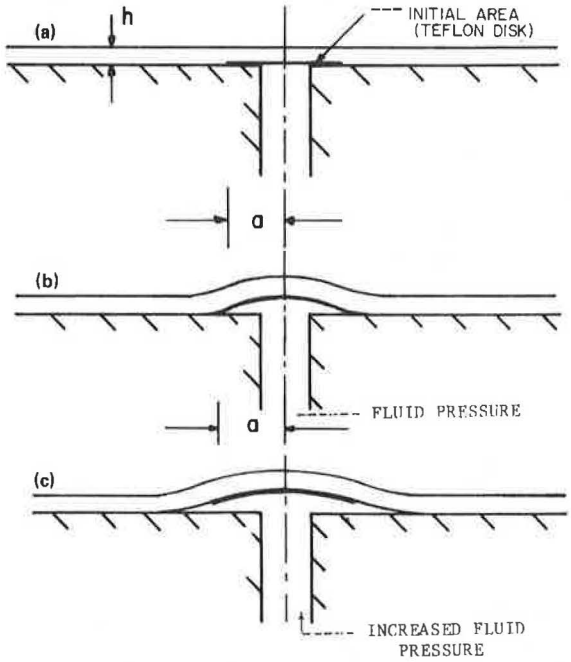

compressible, the analytical interpretation must use traction (pressure) boundary conditions applied to the underside of the blister; if it is incompressible, the analytical expression must use displacement (volume) boundary conditions. The difference between the two is quite important, in a philosophical sense and in the required laboratory technique. But, as shown in the derivations below, the algebraic expressions for criticality are ultimately identical.

The rather simple derivations for fracture in a homogeneous body begin with a functional representative of the potential energy (PE) of the system, including a term for the free surface energy, that can be written as

$$PE = \int_V U dv - \int_S T_i u_i ds - \int_S \gamma ds \qquad (1)$$

where the first term represents the strain energy density (U), integrated over the total volume of the body (V), the second term represents the tractions in the ith direction (T_i) multiplied by the corresponding displacements (u_i), integrated over the free surface area (S), and the last term represents the energy of γ, also integrated over S. This expression is of little physical consequence except that it always assumes a minimum value when the body is displaced into an equilibrium state. Thus, for equilibrium

$$\delta PE = 0 \qquad (2)$$

where the variation is not only of u, but also of a crack shape and size. Accordingly, the theorem of minimum potential energy (7, p. 385) can be rephrased as

> Of all the displacements, and crack configurations, satisfying the given boundary conditions, those which satisfy the equilibrium equations make the potential energy an absolute minimum.

Consequently, an expression for crack-growth criticality can be derived by evaluating the terms of Equation 1, assuming a crack-growth geometry, and taking the derivative with respect to a characteristic crack dimension. The value of zero for this derivative will define the configuration corresponding to the minimum potential energy and, in turn, the equilibrium.. If, at a given crack size, the derivative of the potential energy is decreasing, the crack will grow; otherwise it will not.

EXPRESSIONS FOR CRITICALITY

Consider a blister being inflated (Figure 2b) with a compressible fluid. If the reservoir of pressurized fluid is large, the volume change due to the extension of the unbonded area (Figure 2c) will not significantly influence the pressure. To evaluate the first two terms in Equation 1, it is convenient to use Clapeyron's theorem, which states that for a linearly elastic body (7, p. 86)

> The strain energy of deformation is equal to one half of the work that would be done by the external forces (of the equilibrium state) acting through the displacements from the unstressed state to the state of equilibrium.

This theorem means that the second term in Equation 1 is always twice the magnitude of the first term and, for the constant-pressure system the rate of change of the second term due to crack extension is twice the rate of change of the first. Therefore, if the magnitude of either term can be calculated, the theorem can be used to evaluate the other.

For example, Timoshenko (8) gives the vertical displacements (w) of a circular plate with a fixed outer boundary and uniformly loaded with a pressure (p) to be

$$w(r) = (p/64D)(a^2 - r^2)^2 \qquad (3)$$

where

r = radial coordinate,
a = outside radius of plate, and
D = plate stiffness, i.e.,

$$D = Eh^3/12(1 - \nu^2) \qquad (4)$$

where

E = tensile modulus of elasticity,
ν = Poisson's ratio, and
h = plate thickness.

Equation 3 provides the uniform surface traction (p) and the displacements [w(r)] necessary to evaluate the second term of Equation 1, which becomes

$$\int_S T_i u_i ds = \int_o^a pw(r)2\pi r dr = (\pi p^2/32D)\int_o^a (a^2 - r^2)^2 r dr$$
$$= \pi p^2 a^6/192D \quad (5)$$

Clapeyron's theorem defines the first term as one-half this value, i.e.,

$$\int_V U dv = \pi p^2 a^6/384D \quad (6)$$

The third term, $\int_S \gamma_a ds$, where the subscript a denotes a fracture along a surface of adhesion, is a subject of some contention. When a cohesive fracture occurs, there is little debate; two free surfaces are created, one on each side of the crack tip as it advances through the material. The corresponding concept is not as obvious for an adhesive failure along a bond surface between dissimilar materials. Intuitively, it seems that such a schism might result in one new surface, two new surfaces, or possibly a fractional value between. Following the lead of others to accommodate each of these possibilities, we shall add a coefficient (c) to the third integral with the understanding that it can assume values in the range of $1 \le c \le 2$. In all subsequent calculations, c is assigned a value of 2.

The third integral can now be written as

$$\int_S \gamma_a ds = \int \gamma_a c 2\pi r dr = \gamma_a c 2\pi \int r dr = \gamma_a c \pi a^2 \quad (7)$$

The expression for PE now becomes

$$PE = (\pi p^2 a^6/384D) - (\pi p^2 a^6/192D) + \gamma_a c \pi a^2 \quad (8)$$

and to ensure that the variation with respect to the unbonded area is zero (i.e., that $\delta PE = 0$), $\partial PE/\partial a$ must be zero. Thus,

$$\partial PE/\partial a = (6\pi p_{cr}^2 a^5/384D) - (6\pi p_{cr}^2 a^5/192D) + 2\gamma_a c \pi a = 0 \quad (9)$$

is the energy balance equation defining the critical pressure (p_{cr}) necessary to cause the radius of the blister to begin to grow. If the pressure is insensitive to crack growth, there will be a catastrophic failure and the rapid removal of the entire plastic layer. The criticality equation can be rearranged to

$$\gamma_a = (3/32)/[(1 - \nu^2)/c](a/h)^3(p_{cr}^2 a/E) \quad (10)$$

and used to reduce the experimental test results to give γ_a.

Both the p and the w of the blister should be recorded. These data are then used to determine the effective modulus (E) for evaluating Equation 10. Equation 3, with r = 0, can be rearranged to give

$$E = (3/16)(1 - \nu^2)(a/h)^3 a(P/w) \quad (11)$$

which shows that E is directly proportional to the slope of the recorded p-versus-w curve.

When the blister is inflated with an incompressible fluid, the work done by the surface tractions during the growth of the unbonded area becomes zero. The stored strain energy decreases during growth, rather than increasing as with a compressible fluid. For this situation, the energy balance equation is written as

$$-(6\pi p_{cr}^2 a^5/384D) + 2\gamma_a c \pi a = 0 \quad (12)$$

and the critical pressure has the same value, regardless of the bulk stiffness of the pressurizing fluid (i.e., γ_a is given by Equation 10).

However, once crack growth begins, the subsequent behavior is different for the two types of pressurizing fluids. When a compressible fluid is used (i.e., pressure-controlled conditions), the unbonded area continues to grow without limit, but when an incompressible fluid is used (i.e., volume-controlled conditions), the unbonded area grows only slightly before the pressure decreases to below the critical value. From an experimental standpoint, this means that if an incompressible fluid is used as the loading medium, an incremental growth of

Figure 3. Theoretical solutions for thin and thick plates.

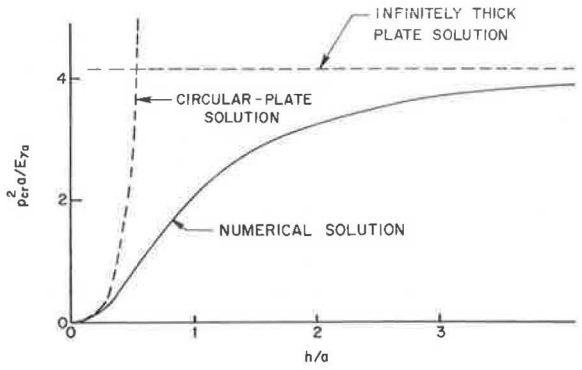

Figure 4. Solutions for small h/a ratios.

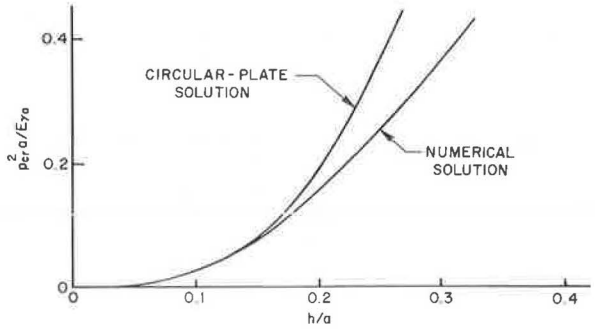

Figure 5. Wood form for casting concrete substrate.

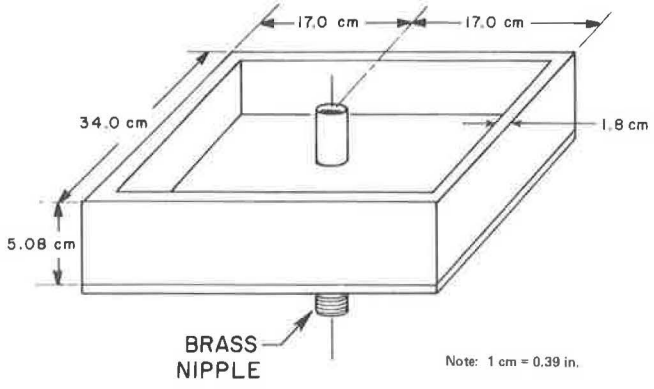

the unbonded area causes a loss of pressure due to the volume increase, and when the pressure drops below the critical value, growth is arrested. Immediately, however, the pressure increases, until it reaches a new critical value, at which time it decreases again, and the cycle is repeated. Thus, numerous data points can be obtained from only one sample. On completion of the test, the dimensions of the initially unbonded area for each cycle can be determined from the striations left on the concrete block.

The closed-form solutions, which are derived from the equations for the deflections of a flat circular plate, lose their validity as the ratio of the thickness to the radius increases. An analytical solution for the limiting case of a very thick plate (i.e., $h/a \to \infty$) has been derived by Mossakovskii and Rybka (9) to be

$$p_{cr} = \left(-[2\pi\gamma_a E(1 - 2\nu)c]/a(1 + \nu)(3 - 4\nu) \times \left\{[(\pi^2/4)\ln^{-2}(3 - 4\nu)] + 1\right\}\ln(3 - 4\nu)\right)^{1/2} \quad (13)$$

or, when $\nu = 1/2$

$$p_{cr} = (2c\pi/3)^{1/2}(E\gamma_a/a)^{1/2} \quad (14)$$

Figure 6. Teflon disk on concrete slab.

Figure 7. Schematic of test apparatus.

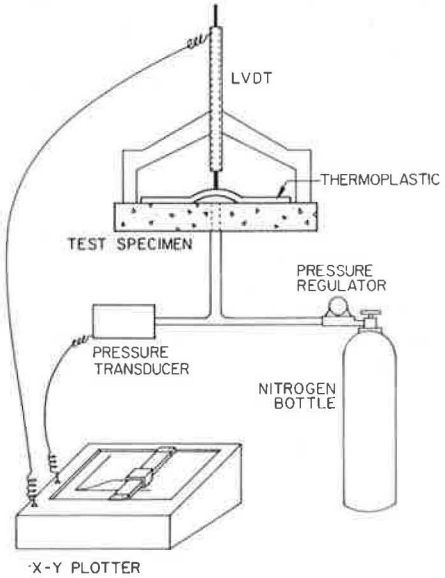

Equations 10 and 14 have been rewritten in a dimensionless format and are plotted, using dashed lines, in Figure 3. The abrupt intersection of these two closed-form solutions has been discussed in detail by both Williams (3) and Jones (4), who concluded that a practical transition curve between these two theoretical solutions is certain to exist.

Figure 8. Specimen before removal of failed thermoplastic.

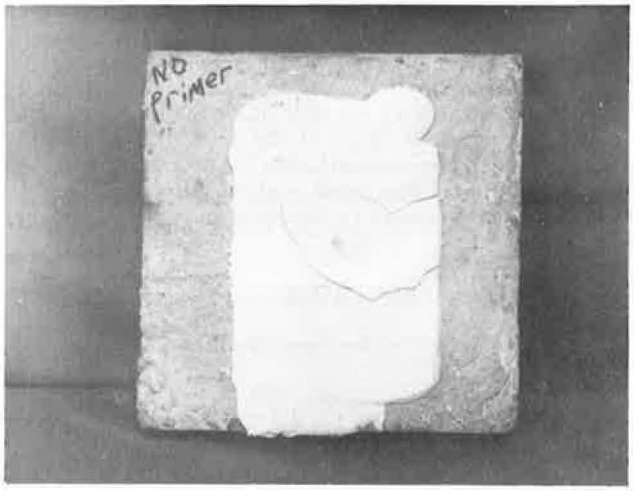

Figure 9. Specimen after removal of failed thermoplastic.

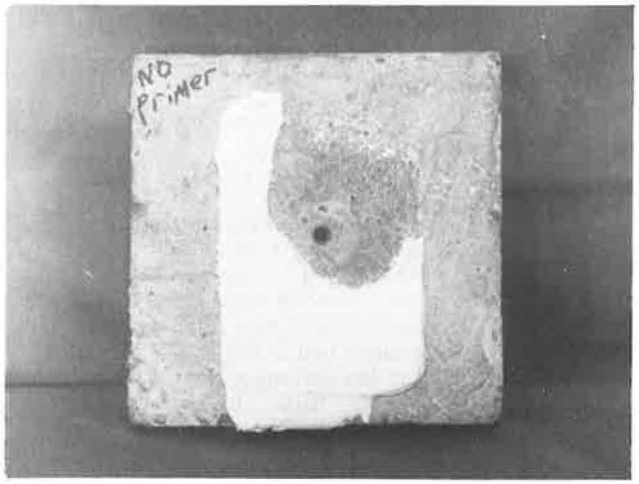

Figure 10. Previously bonded surface of thermoplastic.

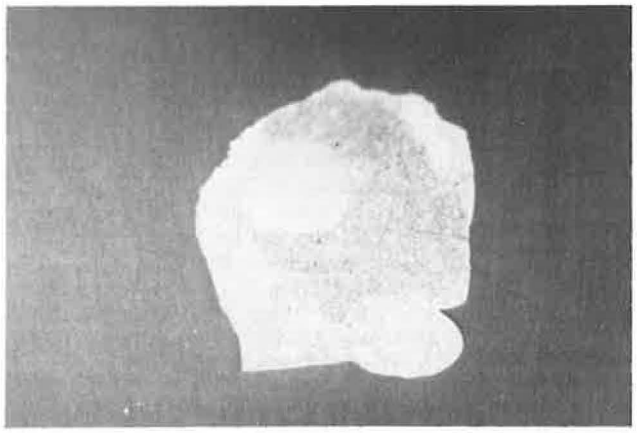

Bennett and others (6) have performed the numerical calculations necessary to define the transitional curve. By using finite elements, they calculated the rate of change of the stored strain energy with respect to the radius of the unbonded area with the pressure held constant, and by putting the numerical derivative equal to γ_a, are able to make the calculations for several h/a ratios and define the shape of the transition (the heavy line of Figure 3).

For the geometries used in the tests described, geometries that are typical of failures observed with actual thermoplastic highway markings, only a small portion of the numerical curve shown in Figure 3 is required. In all test specimens, the radius of the initially unbonded area was 2.22 cm (0.875 in); the thicknesses varied from 0.32 to 0.76 cm (0.125 to 0.3 in), so that the range of the ratio of the thickness to the radius was $0.15 < h/a < 0.35$. This portion of the curve in Figure 3 was enlarged as shown in Figure 4 and used to reduce the test data.

EXPERIMENTAL PROCEDURE

The experimental procedure required the following items of equipment:

1. A 30.5 by 30.5 by 5.1-cm (12 by 12 by 2-in) concrete panel with a 0.64 by 7.62-cm (0.25 by 3-in) (National) taper pipe thread brass nipple cast in the center,
2. A high-pressure bottle of nitrogen as a gas source and a regulator to provide pressures up to 414 kPa (60 lbf/in^2) (an inert gas was used so that the bond integrity would not be influenced),
3. A linear variable differential transducer (LVDT) with a range of at least 1.27 cm (0.5 in),
4. A pressure transducer with a range of 414 kPa,
5. An X-Y recorder,
6. A 5-V dc power source to drive the pressure transducer, and
7. A carrier amplifier for the LVDT.

The first step was to cast the concrete panels. The concrete was made of three parts small aggregate to two parts sand to one part type 1 portland cement, a typical paving mix. One of the threaded ends of the nipple was sawed off and mounted so that it was flush with the top of the form. The threaded end of the nipple extended through a hole bored in the bottom of the form, as shown in Figure 5. The form was filled with concrete until it was flush with the flat end of the nipple. The panels were cured 7 d at 22.8°C (73°F) and 95 percent humidity and allowed to dry at 60°C (140°F) for 7 d to ensure that the presence of water would not affect the test. In two instances, the top of the nipple was not exactly flush with the concrete surface, but this was remedied by carefully hand grinding the extrusion without affecting the surrounding concrete surface.

The panels were then brought back to 22.8°C at 25 percent humidity, and the thermoplastic material was applied. A 4.45-cm (1.75-in) diameter Teflon disk was centered over the nipple, as shown in Figure 6. In the experiments in which a primer was used, it was sprayed on to a thickness of approximately 50 μm (0.002 in). After all preparations were made, the thermoplastic material was centered over the Teflon disk and the air hole and applied at a temperature of 204°C (400°F). It was applied approximately 0.3 cm (0.13 in) thick by using a drawdown process in which the excess thermoplastic was removed with a spatula (laboratory simulation of an actual highway application). The panels and thermoplastic were cured at room temperature for a minimum of 24 h. The test was run in a 32°C (90°F) environment; therefore, the specimens were stored in this environment for another 24 h before testing to stabilize any temperature differentials.

Before the tests were run, the electronic signals being fed to the X-Y recorder were calibrated to a meaningful scale on the graph paper. The LVDT was mounted in a calibration block in which prescribed displacements could be imposed by turning a micrometer barrel. A distance of 2.54 cm (1 in) on the graph was found to correspond to a 0.13-cm (0.05-in) displacement of the LVDT. The pressure transducer signal was calibrated by plugging the open end of the tubing and increasing the pressure in increments of 69 kPa (10 lbf/in^2). Tick marks were made on the X-Y plotter at each increment: 3.05 cm (1.2 in) on the graph were equal to 69 kPa. These scales were used in interpreting the final plots.

In preparing the sample for testing, the LVDT was centered over the initially unbonded area and oriented to measure the vertical displacement of the thermoplastic. The LVDT signal was run through the carrier amplifier and fed to the Y-axis of the recorder. The pressure transducer and tubing from the gas bottle were threaded onto the nipple in a tee connection with the transducer placed as closely as possible to the panel connection to ensure the pressure recorded was essentially that experienced under the blister. The pressure signal was fed to the X-axis of the recorder. The system (Figure 7) was checked for leaks to ensure the accuracy of the plotted data.

After the connections were made, the X-Y recorder was zeroed. The pressure was increased manually at a constant rate of approximately 69 kPa/min at the regulator until leakage or failure occurred. Figures 8, 9, and 10 follow a sample to failure; Figure 8 shows the specimen before the thermoplastic is removed, Figure 9 shows it after the thermoplastic has been removed, and Figure 10 shows the lower surface of the failed thermoplastic. An interesting observation common to all samples is that the lower surface of the thermoplastic is honey combed (Figure 10), even though the exposed side has a glossy finish. The exact thickness of the specimen, a dimension needed for the calculations, was measured with a micrometer.

EXPERIMENTAL RESULTS

Six blister tests were made with the elementary apparatus described above. The resulting curves are shown in Figure 11 in which 11a and 11b show the results for the specimens without and with an adhesive respectively.

To calculate a meaningful value of γ_a between the concrete and the thermoplastic marking material, it is necessary to know the mechanical properties of the two materials. The concrete was assumed to be perfectly rigid so that equations derived above would be applicable. The effective tensile modulus of the thermoplastic was estimated by substituting the deflection of an elastic circular plate subjected to a uniform load normal to its surface into Equation 11. Because the value of the bulk modulus of the thermoplastic is many times greater than that of the tensile modulus, a value >0.49 at 32°C (90°F) was used for Poisson's ratio. Once a and h are known, the effective tensile modulus is seen to be linearly proportional to the slope of the p-versus-w curve. Figure 11 shows that these curves have decreasing slopes all the way to failure. Thus, the question then arises as to what slope should be used to calculate the modulus and, in turn, the adhesive energy release rate. Because an increase in the unbonded area, with the pressure held constant, will increase the stored strain energy, the modulus corresponding to the slope of the p-versus-w curve just before failure was chosen.

Figure 11. Measured pressure versus blister displacement: (a) without primer and (b) with primer.

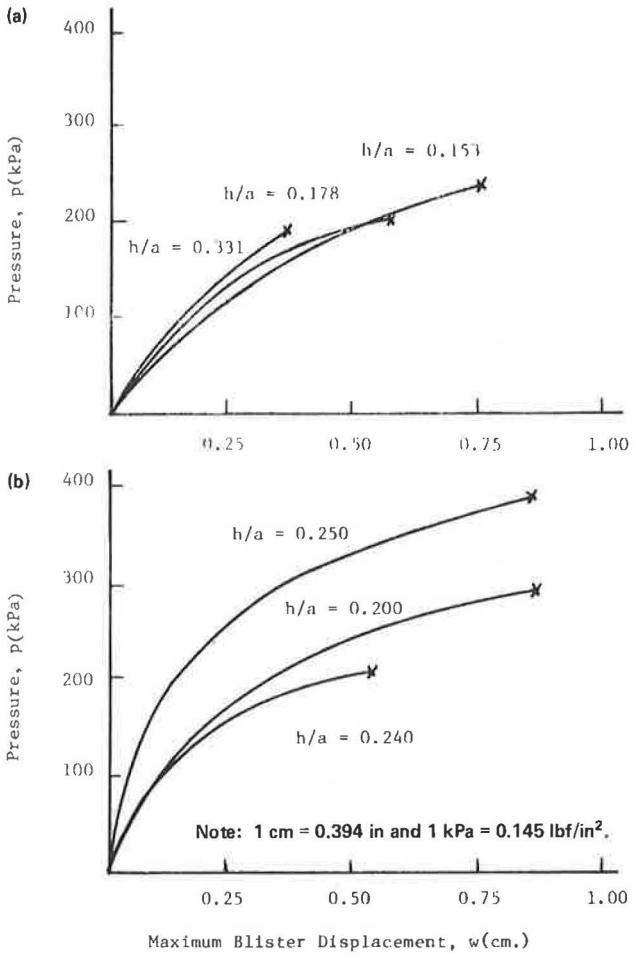

Table 1. Results of blister-peel tests of thermoplastic striping material on portland cement concrete.

Test	h (cm)	Tangent Modulus at Failure (kPa)	Geometric Coefficient	Characteristic Strain-Energy Release Rate (J/m²)
No adhesive				
1	0.340	17 200	0.082	998
2	0.396	8 300	0.120	990
3	0.737	1 900	0.440	1090
With adhesive				
4	0.498	2 800	0.202	2060
5	0.556	3 700	0.254	3960
6	0.445	5 400	0.156	2286

Note: 1 cm = 0.39 in, 1 kPa = 0.145 lbf/in², and 1 J/m² = 0.005 32 in·lbf/in².

When E and the pertinent dimensions are known, γ_a is readily calculated. The numerically derived curve of Figure 3 was entered with the appropriate value of h/a to find the geometric coefficient equal to $p_{cr}^2 a/E\gamma_a$. The γ_a values determined in this manner are shown in Table 1.

CONCLUSIONS

A sensitive test for the adhesion of thermoplastic highway-marking materials to pavements has been successfully demonstrated. The test gives quantitative values for the characteristic strain energy required to force crack growth along the bonded surface. The magnitude of this quantity (γ_a) reflects the ability of a bonded surface to resist the tendency to debond because of either external loadings, such as tires, snow studs, and snow plows, or to internally generated gas pressures.

As shown in Equations 12 and 14, the experimental evaluation of γ_a is a function of the square of the applied pressure at failure; i.e., the parameter is especially sensitive to random experimental errors of the measured value for p_{cr}. However, the results were quite reproducible, particularly when the rudimentary test apparatus used for the demonstration is considered.

The average value of γ_a at 32°C for the thermoplastic applied without an adhesive is 1025 J/m² (5.86 in·lb/in²) and that for the thermoplastic applied with an epoxy adhesive is 2869 J/m² (16.3 in·lb/in²).

Comparison of the results of earlier poker chip tests of the same thermoplastic and pavement combinations with and without the epoxy adhesive is interesting. In those tests, a small poker chip of thermoplastic, 5.1 cm (2 in) diameter by 0.5 cm (0.2 in) thick, was bonded to the pavement, and an aluminum platen, also 5.1 cm in diameter, was then bonded to the top of the thermoplastic. The platen was pulled away from the pavement and the force required to separate the thermoplastic from the pavement measured. At 23°C (73°F), the average bond strengths were 924 and 1530 kPa (134 and 222 lbf/in²) for the poker chip specimens with and without adhesive respectively.

The significance of these tests is unclear, however, because of the complex state of stress generated within the thermoplastic and because the failures often do not originate or propagate along the bonded (thermoplastic to pavement) surface.

The advantages of using γ_a to compare various highway-marking systems are obvious. The test can be performed with a minimum of equipment by relatively inexperienced technicians under a variety of environmental conditions. Either a liquid or a gas can be used for the pressurization, which means that the deleterious effects of entrapped extrinsic chemicals can be evaluated. That γ_a can actually be used to calculate the margin of safety for the bonded surface under specified loads is not without its advantages.

Many unanswered questions remain. Probably the most important is the determination of how γ_a changes as a function of temperature and rate of loading. Another is the determination of how it changes during the curing period just after the thermoplastic is placed. But eventually, the test should provide a sensitive method for evaluating the bond performance of a given thermoplastic highway-marking system. The influence of variables that can be anticipated, reproduced in the laboratory, and defined in numerical terms useful to the engineer is particularly important.

REFERENCES

1. Thermoplastic Pavement Markings. Iowa Department of Transportation, Final Rept., 1975.
2. H. Dannenberg. Measurement of Adhesion by a Blister Method. Journal of Applied Polymer Science, Vol. 5, No. 14, 1961, pp. 125-134.
3. M. L. Williams. The Continuum Interpretation for Fracture and Adhesion. Journal of Applied Polymer Science, Vol. 13, No. 1, 1969, pp. 29-40.
4. W. B. Jones. A Simple Test for Certain Cases of Adhesion. College of Engineering, Univ. of Utah, Rept. UTEC DO-69-010, 1969.
5. J. D. Burton, W. B. Jones, and M. L. Williams. Theoretical and Experimental Treatment of Fracture in an Adhesive Interlayer. Trans., Society of Rheology, Vol. 15, No. 1, 1971, pp. 39-50.

6. S. J. Bennett, K. L. DeVries, and M. L. Williams. Adhesive Fracture Mechanics. International Journal of Fracture Mechanics, Vol. 10, No. 1, 1974, pp. 33-43.
7. I. S. Sokolnikoff. Mathematical Theory of Elasticity. McGraw-Hill, New York, 1956.
8. S. Timoshenko and S. Woinowsky-Krieger. Theory of Plates and Shells. McGraw-Hill, New York, 1959.
9. V. I. Mossakovskii and M. T. Rybka. Generalization of the Griffith-Sneddon Criterion for the Case of a Non-Homogeneous Body. Prikladnaya Matematika I Mekhanika, Vol. 28, 1964, pp. 1061-1069.

Publication of this paper sponsored by Committee on Coatings, Signing, and Marking Materials.

Vehicle Corrosion in Perspective

Michael C. Belangie, Materials and Research Section, Utah Department of Transportation

Early perforation corrosion of American manufactured vehicles was a limited localized phenomenon before the mid-1950s, but a short time after the introduction of unibody construction and sculptured styling in 1955, its occurrence became common throughout most of the United States. The use of deicing salts, which had approximately doubled between 1953 and 1956, was cited in some of the literature of the period as the probable cause. There was little mention of the reduction in sheet-metal thickness that accompanied the change to unibody construction. Anticorrosion measures were nominal in the period immediately following the adoption of unibody construction. The period before the mid-1960s was not typified by major advances in anticorrosion technology, but was a period of trial and error with much of the emphasis being placed on improved anticorrosion design practice. It is doubtful that the improvements made in this period (1958 to 1965) could have counteracted the effect of the sevenfold increase in deicing salt use during 1953 to 1965 if deicing salts were the principal cause. Although it appears that the changes in manufacturing practice were the principle cause of widespread corrosion, the modifications in that practice since the change are producing significantly more corrosion-resistant vehicles. Low-priced, 1955 and 1956 vintage automobiles having unibody construction began to perforate within 6 months in severely corrosive environments. In late 1976, one motor company of Canada began warranting its cars for 36 months against perforation.

It is pertinent to the following discussion to remember the prejudicial character of the deicing salt versus corrosion controversy and that fixed in the minds of many persons in this country is the conviction that deicing salt is the principal cause of automobiles rusting.

The questions addressed here are these. First, Is the opinion that deicing salts are the principal cause of vehicle corrosion damage legitimate? And second, If it is not legitimate, how much of the depreciation in the value of the average automobile can be assessed to deicing salts? These questions are not casual. In January, 1975, the research section of the Utah Department of Transportation became the lead agency in an 11-state pooled-fund study that included Idaho, Illinois, Maryland, Michigan, Minnesota, Montana, New Hampshire, South Dakota, Utah, Virginia, and Washington and the Federal Highway Administration. The purpose of this study was to develop an economic model for snow and ice control activities (1). However, the funding was insufficient to allow the type of economic analysis of vehicle corrosion that would be necessary to effectively determine the portion of increased automotive depreciation costs that can be attributed to deicing salt. As an alternative, an in-depth review of the literature was made. More than 200 publications on vehicle corrosion were collected: Of this number, more than 80 percent were technical, as opposed to economic or summation, documents. Of the technical documents, many came from the Society of Automotive Engineers and the National Association of Corrosion Engineers. The essence of this collection is summarized in an unpublished draft, Vehicle Corrosion, a Synthesis (2).

In developing this synthesis, it became apparent that the document collection could be divided into two sections: those documents or portions of documents dealing with the corrosivity of the environment and those dealing with the ability of the vehicle to resist corrosion. The differentiation is important in evaluating and assigning relative economic costs because it accentuates the fact that both the ability of the average vehicle to resist corrosion and the corrosivity of the environment have varied over time. This makes the assessment of costs due to corrosion considerably more complex than would be indicated by recent economic studies.

An understanding of the market place may be adequate to determine the additional depreciation of the average automobile of a given vintage due to corrosion. However, it is not sufficient to determine the assessment of costs against one environmental factor. To make this assessment, a basic understanding of the variability of the corrosive environment as well as of the changing technology of the average automobile is mandatory.

CORROSIVE ENVIRONMENT

What factors then must be considered if one wishes to assess the cost of a specific corrosion-causing environmental factor, in this case, deicing salts? The size and extent of the corrosive environment is probably a reasonable starting point.

Figure 1 indicates that vehicle corrosion is a worldwide phenomenon. The map shows the noncommunist areas having the potential for a substantial degree of corrosion. Blackened areas indicate the probable use of deicing salts; slashed portions show those areas that do not use salt. Unshaded areas are not exempt from corrosion, but in these areas, it is likely to occur so late in the economic lifetime of the average vehicle as to have relatively little effect on its resale value.

Of the 282 million vehicles registered in noncommunist countries in 1973 (3), approximately 55 percent were in corrosive environments in which deicing salts were apt to be used (blackened areas). Twenty-five percent were in equally corrosive environments in which no deicing salts were used (slashed areas). And 20 percent were in environments where corrosion occurs, but is generally not considered a substantial problem.

Of the 102 million automobiles registered in the United States in 1973 (3), between 46 million and 74

million were in corrosive environments in which deicing salts are used. The lower of these estimates (46 million) was derived from Figure 2 (4, 5) and represents a conservative estimate of the corrosive environment in the continental United States. The larger was derived from Figure 3 (6) and represents a more generous view of the corrosive environment in the United States.

Figure 1. Noncommunist areas having potential for substantial vehicle corrosion.

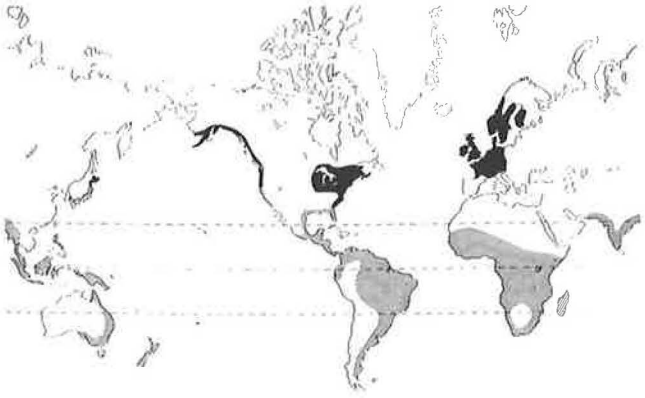

Figure 2. Conservative estimate of corrosion environment in the United States.

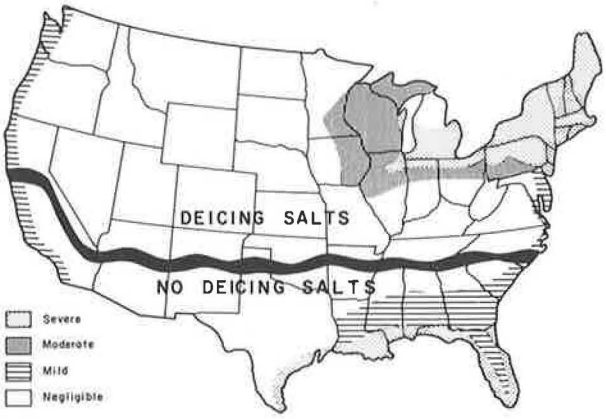

Figure 3. Generous estimate of corrosion environment in the United States.

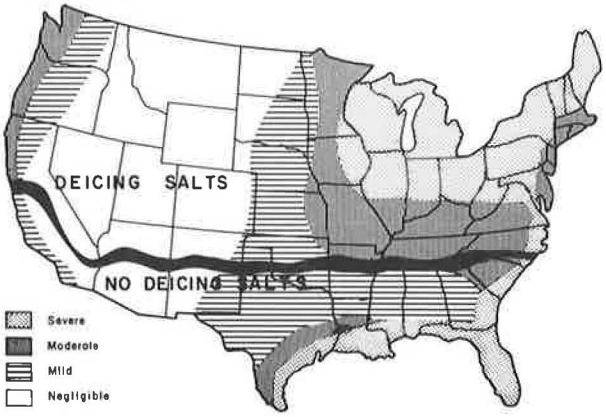

CORROSIVITY OF THE ENVIRONMENT

If this is the extent of the corrosive environment, then what determines the corrosivity of the environment?

The effects of the atmosphere and its pollutants on the corrosion rate are substantial. The atmosphere is both the source and the principal moderator of the corrosion process. It supplies two of the three constituents—water and oxygen—required before corrosion can occur (metal is the third constituent). [Corrosion mechanisms affecting vehicles have been summarized elsewhere (5, 6, 7)].

Fromm's studies (8) in Canada indicated that corrosion rates were four times higher in humid air-polluted environments than in dry nonpolluted climates. His data also showed that deicing salts and air pollution contributed about equally to corrosion damage in the Toronto area. The most severe conditions studied (Toronto and Halifax) are probably more or less typical of the northeastern United States and those states bordering the southeastern shores of the Great Lakes. These severely corrosive areas can be characterized as having high air pollution, high relative humidities, and high uses of deicing salts.

Air pollutants are absorbed into particulates that adhere to surfaces and form point sources of corrosion. Most of the common air pollutants, as well as the deicing salts, are anhydrous and act as moisture reservoirs, allowing corrosive processes on even apparently dry surfaces. Dissolved air pollutants and deicing salts form electrolytes that lower solution freezing points and increase electrochemical activity. Both processes increase corrosion rates. As a paper published by the National Association of Corrosion Engineers (9) states,

> Contaminants from the air occur in such minute quantities that their effect would seem trivial; however, the corrosive rate is at its maximum in dilute acid solutions. Therefore, small quantities of contaminants are the most harmful.

Relative humidity, the presence of dissolved oxygen, and the temperature are some of the principal factors affecting corrosion processes. The effects of these factors have been described by Chance (5):

> . . . it is not necessary to have 100 percent relative humidity to produce condensation on metal surfaces. Hygroscopic impurities in the atmosphere or on the metal surface will cause condensation at much lower values. For certain metals, there is such a thing as a critical relative humidity above which corrosion will proceed at an accelerated rate. For such metals as iron, copper, nickel, and zinc, the critical relative humidity generally falls between 50 and 70 percent. As an example, the corrosion behavior of iron in a 0.01 percent SO_2 atmosphere at various relative humidities is shown in Figure 8 [Figure 4 (10, p. 147)]. Note the dramatic increase in corrosion rate beginning at 60 percent relative humidity.
>
> Dissolved oxygen in solutions has a very definite effect on corrosion rates. In nearly neutral solutions, as in many natural waters, the concentration of dissolved oxygen is the controlling factor that determines corrosion rates. This fact is demonstrated in Figure 7 [Figure 5 (10, p. 81)], which shows the effect of dissolved oxygen concentration on the corrosion of mild steel in slowly moving water containing 165 ppm $CaCl_2$.
>
> An old axiom in reaction kinetics states that reaction rates increase by a factor of two for every 10°C rise in temperature, and it is also generally true that corrosion rates increase with temperature. However, there are other considerations. For example, the dependance of the solubility of oxygen in water on temperature is shown in Figure 6 [(11)]; as the temperature rises, the solubility of oxygen decreases. Diffusion rates increase somewhat to compensate for the loss of oxygen, but the effect on corrosion rates could still be significant.

Our affluent society and the low energy costs of the past have had a direct influence on vehicle corrosion,

Figure 4. Corrosion of iron in air containing 0.01 percent SO_2: effect of critical relative humidity.

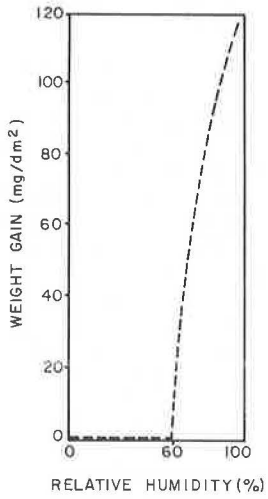

Figure 5. Effect of oxygen concentration on corrosion of mild steel.

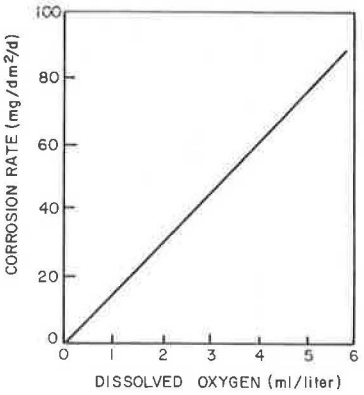

Figure 6. Dependence of solubility of oxygen in water on temperature.

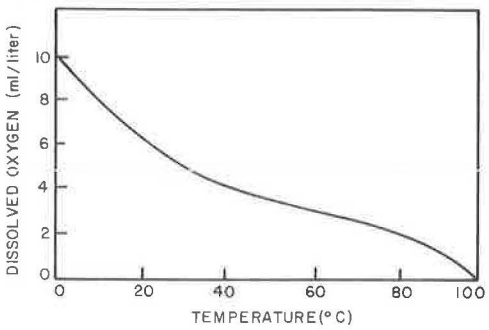

in the form of enclosed and heated garages. The effect on the corrosion rate, as shown in Figure 7 (12), is substantial. The lower lines represent corrosion rates in open unheated storage. The upper lines represent corrosion rates in closed heated garages.

AUTOMOBILE MANUFACTURING (CHANGING TECHNOLOGY)

The question that has generally been either avoided or ignored in assessing vehicle corrosion in economic studies is this: If a product is modified and in the process becomes less able to withstand the environment, is it valid to assess the loss against the environment, or more particularly against one particular aspect of the environment?

Figure 7. Corrosion rates of crevice specimens attached to vehicles in heated and unheated garages.

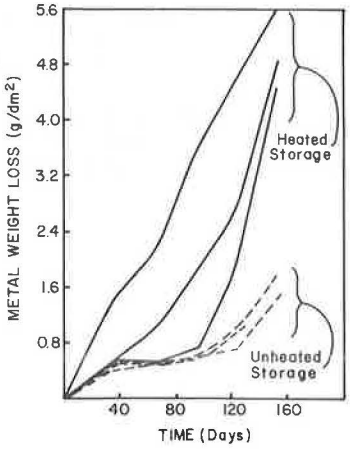

Before the mid-1950s, automotive corrosion was apparently a relatively isolated problem. However, in 1955 the appearance of automobiles changed. Sculptured styling became common and, with it there was a reduction in sheet-metal thickness. Accompanying these changes in body geometry were the beginnings of modification in support structures. Cross-member construction was replaced by unibody construction characterized by relatively light-gauge, formed, sheet-steel members. This reduction in sheet-metal thickness, in both body and support members, is probably the basic reason for the increase in early corrosion perforation that began in American-produced vehicles in the mid-1950s. A subsidiary and initially equivalent probable cause was the lack of anticorrosion measures in both the design and manufacture of vehicles.

The lack of anticorrosion measures can be illustrated by considering the amount of galvanized steel used by the automotive industry. In 1955, galvanized steel was not in common use; in that year, the industry used 25 Gg (27 000 tons). This is equivalent to an average of 2.7 kg/vehicle (6 lb/vehicle) for trucks, buses, and automobiles. Today, approximately 73 kg (160 lb) of galvanized steel are used in the construction of the average automobile. Automotive manufacturing practices before 1970 are summarized elsewhere (5, 13).

Figure 8 is a speculative distribution based on inferences from the documents in the study file. It is an attempt to show the distribution of times at which American automobiles of a given model year would have visible perforation corrosion in a severely corrosive environment. For instance, the extreme left end of the chart indicates that corrosion in 1951 models would follow an approximately normal distribution with corrosion first appearing in some 1951 model automobiles when they were about 1.5 years old.

The average 1951 automobile (according to this speculative distribution) would begin to show perforation corrosion at about 3 years, and some would not perforate until they were 4.5 years old. To the extreme right, the schematic shows a predicted relatively flat distribution. The 1986 models of American automobiles are expected to begin to show corrosion perforation after 4 years of use, and the last of this model year will perforate after 8 years of use.

The dip that begins with the 1955 models and develops into a fairly consistent, moderately skewed distribution represents the adoption of lighter gauge steel and unibody construction by automotive manufacturers, before the development of adequate corrosion-resistant materials. The slow upswing before the mid-1960s is based more on the adoption of good design practices for

Figure 8. Time to corrosion perforation of American automobiles.

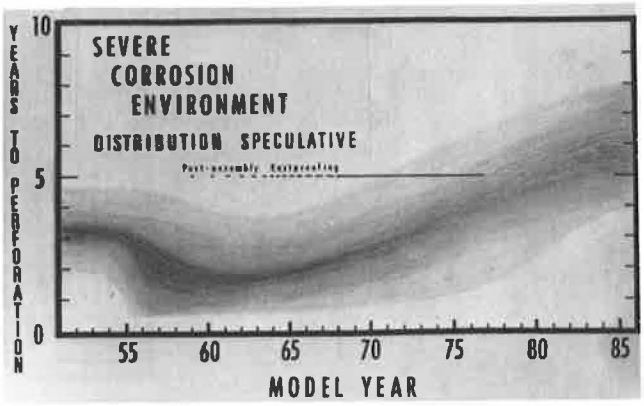

Figure 9. Use of deicing salt in the United States.

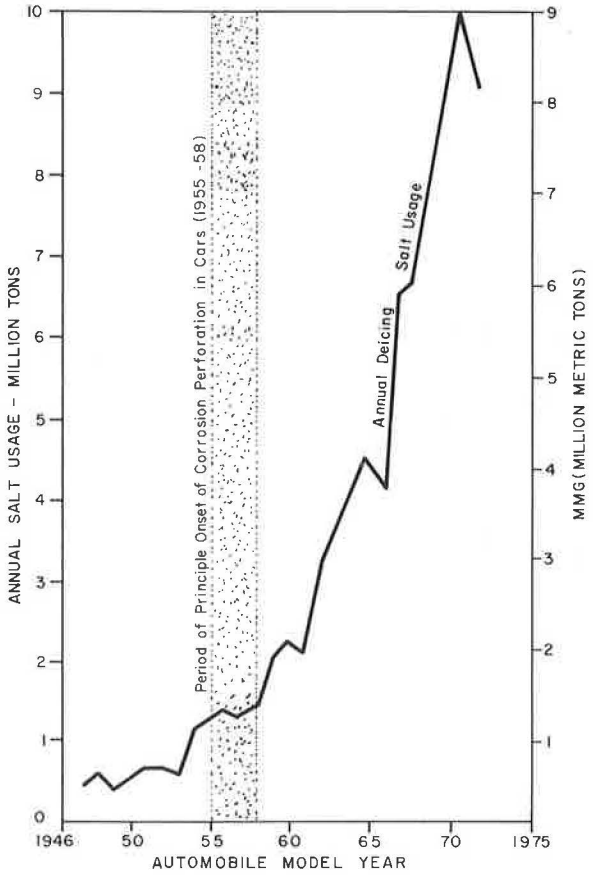

reducing corrosion than on the successful incorporation of new materials.

DEICING SALTS

Figure 9 (14) indicates why the argument that deicing salts are responsible for the increase in corrosion just depicted is questionable. Salt use was fairly constant during the period from 1947 to 1953, at 450 to 635 Gg/year (500 000 to 700 000 tons/year). Between 1953 and 1955, salt use roughly doubled, but it then stayed relatively constant until 1958. This doubling has been used as the justification for implicating deicing salt as the cause of the high incidence of corrosion occurring in 1955 to 1958 model automobiles (shown by the vertical bar).

Galvanized steel is only one of many ways in which an automobile manufacturer improves the corrosion resistance of the product at present. In 1955, the average vehicle (including trucks and buses) contained about 2.7 kg (6 lb) of this material. By 1965, the average automobile contained 46 kg (101 lb), and today it contains 73 kg (160 lb).

If salts were the cause of the sudden increase in corrosion between 1955 and 1958, then why did not automobiles literally fall apart in the years following? If we use 1953 as the base year, salt use had increased sevenfold by 1965. Yet there was no corresponding increase in corrosion damage. Were the changes in corrosion protection so extensive between 1958 and 1965 that this apparently highly corrosive element had been neutralized, or was there some other reason?

This period was not typified by major advances in anticorrosion technology, but was a period of trial and error with most of the emphasis being placed on improved anticorrosion design practice. It is unrealistic to assume that the efforts of the automotive industry in this period—1958 to 1965—could have counteracted the sevenfold increase—1953 to 1965—in deicing salt use, if salts were in fact the principal cause of corrosion.

ANSWER TO QUESTION ONE

Let us return to the original question: Is the opinion that deicing salts are the principal cause of vehicle corrosion legitimate?

Fromm showed that deicing salts and air pollution contribute about equally to corrosion damage. The change in automobile manufacturing procedures beginning in 1955 is well documented. The arguments that fixed the blame for the increase in corrosion between 1953 and 1956 on deicing salt should also be applicable to the subsequent multifold increase in deicing salt use in the following years, and the impact on vehicles should have been significantly greater than it was.

Perhaps the best argument against totally blaming deicing salts comes from a review of areas in which deicing salts are not used, such as the Gulf Coast, that have equally severe corrosive environments. In semitropical and tropical climates, the upper portions of the automobile body are more subject to attack than are the lower portions; in areas in which deicing salts are used, the lower portions are attacked more than the upper (7). If deicing salts were the principal cause of the increased corrosion between 1953 and 1956, then vehicles on the Gulf Coast should have fared better, but they did not.

Thus, the answer of the first question is that deicing salts undoubtedly contribute to vehicle corrosion. But the principal cause of premature corrosion perforation is probably attributable to the method of manufacture adopted by the American automotive industry in the period beginning in 1955.

The improvement in corrosion resistance of the automobile that has occurred since 1958 is also attributable to the automotive industry and its suppliers. Figure 10 shows four samples that were subjected to 250 h in a salt fog chamber (15).

Figure 10a shows the kind of damage incurred by the rust-susceptible areas of an automobile having the average protection available before the early 1960s. During the late 1950s and early 1960s, galvanized steel began to be substituted in those portions of the body to which it could be adapted. Its use increased until the

Figure 10. Samples of steel after 240 h in salt spray chamber: (a) unprotected cold-rolled, (b) galvanized, (c) zinc-rich primed, and (d) coil coated.

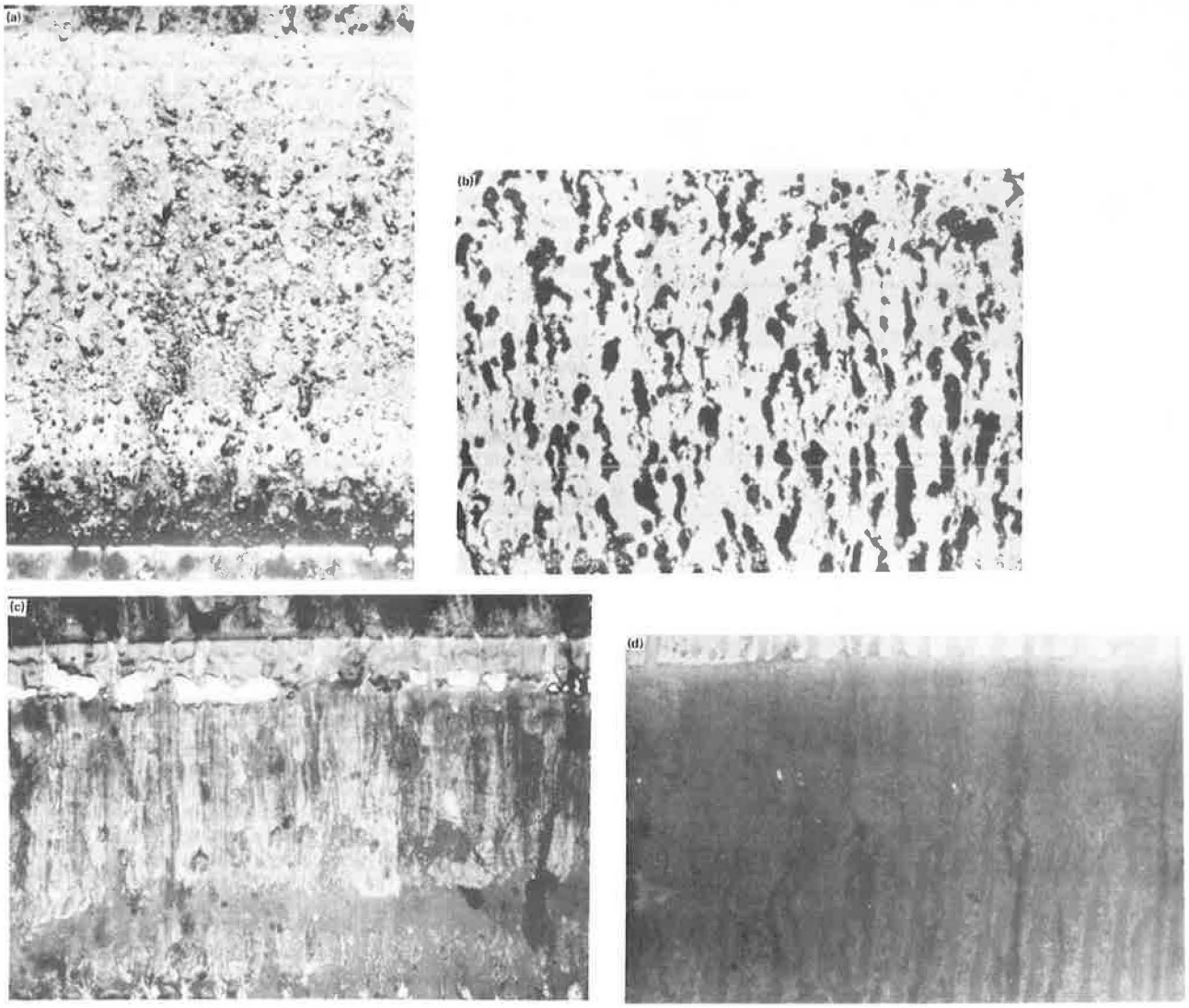

late 1960s and has held fairly constant since then. Figure 10b shows the damage incurred by this type of material.

Zinc-rich primers were first sprayed on some interior components, such as the interiors of doors, at about the same time that galvanized steel began to be incorporated into the underbody members, and by the late 1960s, dip tanks using electrocoating procedures were installed, and the consistency of application of corrosion-resistant coatings improved. Figure 10c shows the damage incurred by this type of material.

The next major step in improving corrosion resistance was introduced in 1975. The process, referred to as coil coating, is being incorporated on an increased scale in 1977 models. Figure 10d show the damage incurred by these materials. The improved corrosion resistance shown in Figure 5 for the late-1970s and 1980s is based on the eventual adoption of this type of product or its equivalent.

ANSWERS TO QUESTION TWO

Let us now return to the second half of the original question: How much damage can be assessed against deicing chlorides?

Proposition One

It can be argued (in brief) that the maximum cost of damage assessed cannot be greater than the capitalized investment paid out to protect against the damage.

One company has had available a process with a 5-year guarantee against perforation corrosion since the mid-1960s. The cost of this process in the 1960s was approximately $100, and at present, it is about $150.

Ackerman and others have shown that vehicle depreciation follows an approximately exponential decay curve (16). By the end of the fifth year of the lifetime of an automobile, its resale value is approaching the low end of its economic value. It is doubtful that corrosion perforation after that time could decrease its resale value very much. Even if all of the increased depreciation in the period following the fifth year were assigned to the corrosive environment, the maximum amount assignable to deicing salts could not exceed 50 percent of the increased depreciation because no more

TRANSPORTATION RESEARCH BOARD
National Research Council
ERRATA 1978

Transportation Research Record 589
page ii
Under Library of Congress Cataloging in Publication Data, change card number from **76-456671** to **76-45671**

Transportation Research Record 617
page 7, column 1, line 3 after Abstract
Change **effect** to **affect**
page 71, column 2, line 39
Insert **from** after **eliminating**
page 71, column 2, line 41
Change : after **1970** to ,

Transportation Research Record 630
page iii, line 5
page 7, title of Abridgment
Change **County** to **Countywide**
page 7, authorship of Abridgment
Change **Florida** to **Detroit**

Transportation Research Record 635
page 39, column 2, line 7
Change **$1.32 to $2.46/liter** to **9 cents to 17 cents/L**

Transportation Research Record 644
page 107, column 1, last line of Abstract
Change **load factor** to **average individual delay**

Transportation Research Record 651
page 39, column 2, lines 50-51
Change **Committee on Coatings, Signing, and Marking Materials** to **Committee on Mineral Aggregates**
page 42, column 2, line 12
Change **Committee on Mineral Aggregates** to **Committee on Coatings, Signing, and Marking Materials**

Transportation Research Record 654
page 30, column 2, lines 24-25
Change **Committee on Transportation Programming, Planning, and Evaluation** to **Committee on Bus Transit Systems**

Transportation Research Record 658
page iii, third paper listed
After authors, add
Discussions
Anthony James Catanese 15
Anthony R. Tomazinis 15

Transportation Research Record 660
page iii, line 18
Change **Francis X. McKelvey and William C. Taylor** to **Francis X. McKelvey, William C. Taylor, and Kunwar Rajendra**
page iii, line 26
Change **Robert E. Paaswell** to **Robert E. Paaswell, J. Falcocchio, R. Knighton, D. Hartgen, D. Teixeria, R. Stevens, J. Burkhardt, and A. Lago**
page 30, authors of Abridgment
Add **Kunwar Rajendra, Planning Department, City of Lansing, Michigan**
page 38, authors of paper
Add
J. Falcocchio, Department of Transportation Engineering, Polytechnic Institute of New York
R. Knighton and D. Hartgen, Planning and Research Bureau, New York State Department of Transportation
D. Teixeria and R. Stevens, A.R.I., Inc., Boston
J. Burkhardt and A. Lago, Ecosometrics, Inc., Bethesda, Maryland

Transportation Research Record 664
page ii
Change Library of Congress data given to
Library of Congress Cataloging in Publication Data
Bridge Engineering Conference, St. Louis, 1978
Bridge engineering.
(Transportation research record; 664-665)

1. Bridges—Congresses. I. National Research Council. Transportation Research Board. II. Title. III. Series.
TE7.H5 no. 664-665 [TG5] 380.5'08s [624.2]
78-71939
ISBN 0-309-02696-2 (v. 1)
ISBN 0-309-02697-0 (v. 2)

Transportation Research Record 665
page ii
Change Library of Congress data given to
Library of Congress Cataloging in Publication Data
Bridge Engineering Conference, St. Louis, 1978
Bridge engineering.
(Transportation research record; 664-665)

1. Bridges—Congresses. I. National Research Council. Transportation Research Board. II. Title. III. Series.
TE7.H5 no. 664-665 [TG5] 380.5'08s [624.2]
78-71939
ISBN 0-309-02696-2 (v. 1)
ISBN 0-309-02697-0 (v. 2)

NCHRP Report 188
page 39, first figure
Add caption: **Figure A-9. Fillet-weld end details of specimen.**

NCHRP Synthesis of Highway Practice 42
page 65, Equation A-1
Change $(+ \sin\phi)$ to $(1 + \sin\phi)$
page 67, footnote to table
Change $\underline{N}_\sigma{}^*$ to $\underline{N}_c{}^*$ and $\underline{N}_c$ to $\underline{N}_\sigma$

NCHRP Synthesis of Highway Practice 53
pages 47 and 48
Figure shown as B-3 is B-4; figure shown as B-4 is B-3.

than 50 percent of the increased corrosion damage can be assigned to deicing salts (17). The assessed portion of costs against deicing salts of a postconstruction corrosion-proofed vehicle, therefore, will have to be small.

Also, since consumers have not taken advantage of the available postconstruction rust-proofing process, the apparent costs of corrosion to them must be less than the additional costs of postconstruction protection and increased depreciation. Therefore, the costs assessed against deicing salts cannot be greater than the costs assignable to rust proofing a vehicle.

Proposition Two

The corrosion resistance of the average automobile is significantly better now than it was in 1955. So much so that one motor company is offering a 36-month warranty against perforation corrosion on all of its passenger automobile lines in Canada. On the basis of this warranty offering and the general improvement in technology, as shown by the metal coupons in Figure 10, it can be assumed that the average well-manufactured automobile today should be able to withstand at least 2 years in a severely corrosive area without perforating, and in the near future, 3 years.

The differences between this proposition and proposition one are these: (a) the depreciation assignable to corrosion would at present begin in the third year of the lifetime of the automobile and in the near future in the fourth year, and (b) there would be no charges assignable to postconstruction rust proofing.

SUMMARY

It is reasonable to assume that changes in manufacturing practices were more responsible than deicing salts for the high rust susceptibility of automobiles manufactured after 1955. However, in the last 20 years, the corrosion resistance of the average automobile has been improved substantially. And, if the manufacturers continue their present trend in adopting new corrosion technology, the automobile should continue to improve in corrosion resistance for some time to come. As the population of vehicles with improved corrosion resistance increases, the costs assignable to the corrosive environment, with or without deicing salts, will be reduced, eventually to the capitalized investment of manufacturer-installed corrosion protection.

In the spring of 1976, the cost to coil coat all the nongalvanized body parts of an automobile [approximately 270 kg (600 lb) of sheet steel] would have been approximately $35 dollars.

REFERENCES

1. B. H. Welch. Economic Impact of Highway Snow and Ice Control, State of the Art. National Pooled-Fund Study, Utah Department of Transportation, Rept. MR-76-7, Sept. 1976.
2. M. C. Belangie. Vehicle Corrosion, a Synthesis. Utah Department of Transportation, Rept. MR-76-9, 1976.
3. Automobile Facts and Figures. Motor Vehicle Manufacturers Association, 1975.
4. W. G. Patton. Iron Age, April 1971, p. 53.
5. R. L. Chance. Corrosion, Deicing Salts, and the Environment. Materials Protection and Performance, Oct. 1974.
6. R. F. Waindel. Automotive Body Rusting: Causes and Cures. SAE, Rept. 680145, Jan. 1968.
7. Motor-Vehicle Corrosion and the Influence of Deicing Chemicals. Road Research, Organization for Economic Cooperation and Development, 1969.
8. H. J. Fromm. Corrosion of Automobile-Body Steel and the Effects of Inhibited Deicing Salts. HRB, Highway Research Record 227, 1968, pp. 1-47.
9. Corrosion Inhibitors. National Association of Corrosion Engineers, 1973.
10. H. H. Uhlig. Corrosion and Corrosion Control. Wiley, New York, 1963.
11. N. D. Tomoshov. Theory of Corrosion and Protection of Metals. Macmillan, New York, 1966.
12. Corrosion Inhibitors Investigation. Univ. of Manitoba, 1966.
13. G. F. Bush. Corrosion of Automobile Bodies. SAF, Rept. 650494, May 1965.
14. Survey of Salt, Calcium Chloride, and Abrasive Use in the United States and Canada for 1969-70. Salt Institute, Alexandria, Va.
15. Cry for Zincrometal—Car Rust Hurts. Diamond Shamrock Corp., April 5, 1975.
16. S. R. Ackerman. Used Cars as a Depreciating Asset. Western Economic Journal, Vol. 2, 1973.
17. Vehicle Corrosion Caused by Deicing Salts. APWA, Rept. APWA-SR-34, Sept. 1970.

Publication of this paper sponsored by Committee on Corrosion.

Preformed Elastomeric Joint Sealers for Bridges

George S. Kozlov and Bruce Cosaboom, Division of Research and Development, New Jersey Department of Transportation

A proven effective solution to the problem of sealing joints in bridge decks is described. The basis of the solution is the use of specially designed joint armor in combination with currently available, preformed elastomeric sealers. The approach is adequate for simple-span, composite, concrete, or steel structures having span lengths up to 52 m (170 ft). The special armored-joint system was field tested on three structures. Two of these were monitored both manually and with automatic instrumentation to determine the causes and range of magnitudes of bridge-end movements; they were also tested for leakage with dyes at periodic intervals over a 5-year time span. The third structure was used to conduct load tests on the joint armor and armor anchorage components. Application of the results led to the development of practical

procedures for the design and construction of armored bridge joints and the selection of an appropriate size of elastomeric sealer.

In 1965, the New Jersey Highway Department, now the New Jersey State Department of Transportation (NJDOT), began a study of the behavior of preformed, elastomeric bridge-joint sealers, which had by that time become a common means of sealing bridge joints. The preliminary results showed a lack of adequate knowledge of the characteristics of sealer materials and the behavior of bridge joints, and in response, a formal research project was launched. The first phase of the project, the subject of this report, concentrated on testing and improving the suggested methods of design and construction of joint systems and establishing relations among deck temperatures, air temperatures, and joint movements. The second phase will concentrate on the development of realistic acceptance specifications for preformed sealers.

In phase 1, methods for the design and construction of an effective joint-sealing system for bridges have been developed and proved successful. Armored joints sealed with preformed sealers have been installed on two typical highway bridges and have functioned flawlessly for over 5 years. The relation between joint movements and air temperatures for simple-span bridges has been determined.

This summary of phase 1 of the joint-sealing project omits many details of how the research was conducted, which are available elsewhere (1, 2, 3, 4). It is expected that the reader here will be most interested in the project's accomplishments. Accordingly, this summary primarily presents the results, particularly those methods for design, construction, and sealing of bridge joints that have been found successful for New Jersey highway structures.

SCOPE OF PHASE 1

The scope of phase 1 of this project was to test suggested methods for the design and construction of joint systems, to establish the causes of joint movements, and to identify the relations of design and construction methods to such movements. For the most part, the study was limited to two simple-span, composite-design bridges that had significantly different joint skews and length-to-width ratios. Together, these bridges typify the great majority of highway bridges in New Jersey today. The study included the design, construction, and performance evaluation of the armored and sawed joints of the two bridges.

The performance evaluation consisted of frequent visual observations, measurement of movements and structure and air temperatures, and use of liquid dye tests to locate leakage through joints. Movement and temperature data were obtained by both manual and automated methods. The extensive data gathered by the automated method were used to establish the effective temperature of a bridge deck and its correlation to the air temperature and to the movements at the deck joints of the bridge. The long-term stability of these relations were verified by using the manually recorded information.

To further evaluate the movement and temperature data, the coefficient of thermal expansion of a concrete deck was determined, and the influence of moisture on it was isolated.

Although it was not originally considered within the scope of this project, a test program was included involving the load testing of an armored bridge joint. The full-scale field tests were designed to evaluate the load distributions and reinforcement stresses that must be accommodated in designing joint armor.

CONCLUSIONS OF PHASE 1

This phase of the project has resulted in the development of procedures for (a) the design of joint armor, (b) the construction of armored joints, and (c) the selection of sealers. Each of these has been successfully field tested for more than 5 years on two experimental bridges, and a third experimental installation of an armored joint that was completed in the fall of 1974 included the final modifications of all of the procedures. The conclusions of phase 1 are summarized below:

1. The use of a combination of an armored joint and an appropriate preformed, elastomeric joint sealer is a practical and proven solution to the problem of bridge-joint leakage and intrusion.
2. It is essential to recognize the realities of joint design and construction. In the absence of adequate quality control in construction, no material and no method of its application will succeed. The procedures suggested here and given in detail elsewhere (1) require only a little care in manufacturing and construction and should lead to a totally satisfactory result.
3. The formed and sawed methods of joint construction evaluated were unsuccessful principally because they required an unattainable quality of workmanship from the contractor. In contrast, the success of the armored joint system can be attributed in part to the fact that it can be prefabricated and then installed within the constraints of normal construction practices.
4. For simple-span bridges, the movements of deck ends are affected predominately by temperature changes. The correlation between ambient air temperature and bridge expansion was shown to be linear. Other environmental parameters (such as insolation, precipitation, and moisture) and physical characteristics (such as creep) were found to have no significant influence on bridge-end movements; hence, the correlation between bridge expansion and air temperature changes is also unique (i.e., for practical purposes, it is the only correlation that need be considered).

   For design purposes then, it is the range of ambient air temperatures at the particular site that may be assumed to be the effective temperature for a bridge. This is, of course, consistent with normal design assumptions. For New Jersey, climatological records indicate that this temperature range should be taken as -18 to 43° C (0 to 110° F).
5. The movements of fixed joints are insignificant, although somewhat erratic. This demonstrates the adequacy of the bridge-bearing design used in New Jersey and the validity of the basic design assumptions. The erratic features, of course, are due to the normal 1.5-mm ($\frac{1}{16}$-in) tolerances that are permitted for bolted connections of metal parts. In view of the critical need of attaining well-controlled movements, the bearing system used in New Jersey is compatible with the use of preformed elastomeric joint sealers; furthermore, only bearing systems that are known to similarly control the joint movements should be used in conjunction with these sealers.
6. The displacements at expansion joints that are predicted on the basis of the normal air temperature range will probably not be exceeded provided the thermal coefficient of expansion of the particular bridge is known fairly accurately. For composite bridges constructed of a steel superstructure and a reinforced concrete deck, this coefficient lies between the accepted coefficients of steel and concrete. Although the volume of the concrete in such a bridge is significantly greater than that of the

steel, the thermal coefficient of the total mass lies closer to that of steel and is probably 0.000 011 5 m/m/° C (0.000 006 3 in/in/° F). There seems to be no reason why the usual average values of the coefficient of expansion for all-concrete or all-steel structures should not be used, and the thermal coefficients should be taken as linear throughout the temperature range.

7. For bridges having skews of less than 15° (0.25 rad) and the kinds of bearing systems used by NJDOT, the overall joint movements may be accurately calculated by using the following general formula:

$$\Delta L = \alpha L \Delta t \quad (1)$$

where

L = length of bridge in direction of stringers,
t = temperature, and
α = coefficient of thermal expansion.

The effects of the skew can be neglected.

8. For bridges having skews approximately between 15 and 50° (0.25 and 0.9 rad), the joint movements that occur in the direction perpendicular to the joint can be assumed as uniform across the length of the joint. The magnitudes of these movements will be less than that predicted by use of the general formula. However, as the skew angle increases and the ratio of the length of the bridge to the length of the joint becomes less than 1, the joint movements in the direction parallel to the joint become substantially larger than those in the direction perpendicular to the joint. Thus, caution is necessary to ensure that these movements are accommodated or minimized, depending on the type of joint system in use.

9. In general, the bearing system that is in standard use by NJDOT for bridge construction is effective in controlling and directing bridge displacements.

10. In a 200 to 230-mm (8 to 9-in) thick concrete bridge deck, temperature gradients through the thickness of the deck exceed 11° C (20° F) at times throughout the year. These large gradients are of short duration and are primarily due to intense solar radiation. Most of the temperature differential at such times occurs in the top 25 or 50 mm (1 or 2 in) at the surface of the deck and has little immediate influence on the displacement response of the bridge.

11. A general, although guarded, conclusion can be made that—provided there is compatiblity of materials—many of the effects of temperature or the lack of effects of moisture, creep, and such are transferable; i.e., generally similar effects can be expected in other simple-span, composite bridges and also in all-steel and all-concrete simple-span structures. On the other hand, however, bridge-end displacements are also a function of the particular bridge design and are unique for each and every design system. For example, the bridge-ends in a cantilever design system behave differently from those in a simple beam or a continuous beam design. To attempt to combine the movement characteristics of all bridge designs or to extrapolate from one to another could lead to gross errors. Thus, the selection of the simple-span type of structure for instrumentation, because of its functional simplicity, served well to isolate the phenomena affecting bridge-end movements.

RECOMMENDATIONS OF PHASE 1

In addition to those that can be derived from the above conclusions, phase 1 led to the following recommendations:

1. The procedures for the selection of an elastomeric joint sealer, the sizing of the joint opening, and the design and construction of an armored bridge joint are given below. Strict adherence to these procedures will provide leak-proof and intrusion-proof joints for bridges up to 52 m (170 ft) in span length.

2. For bridges with spans exceeding 52 m in length, many deficient joint seals are being marketed. Recommendations on this subject have been given elsewhere (5).

3. Because of the unpredictable behavior of bridge approach slabs, under no circumstances should an armored, elastomeric sealer joint be placed directly between a bridge deck and its approach slab.

4. The use of preformed, elastomeric compression sealers in concrete pavement joints of the type [19-mm (¾-in) expansion joints] and spacing [24 m (78 ft)] used by NJDOT is unwarranted and is specifically not recommended.

5. The investigations performed in this study should be broadened to include varied locations, larger spans, and different types of bridges. The behavior of structures having skew angles larger than 50° (0.9 rad) and a ratio of bridge length to length of joint of less than 1 was not quantified, and further investigation is warranted.

6. The manner in which a bridge approach slab should tie into a structure and the performance characteristics of such slabs are in reality unsettled questions. A research study is suggested to identify the warrants for and structural behavior of these slabs.

PROCEDURES FOR DESIGN, CONSTRUCTION, AND SEALER SELECTION

General

The selection of one specific joint-armor design rests on the basis of rather extensive experimentation in construction. There is no such thing as a foolproof design, but there is also no reason why a complete and a satisfactory solution cannot or should not be expected; i.e., if at least a little care is exercised in the manufacture and construction of a joint and if the following basic design principles are adhered to:

1. The deck joints must be horizontally straight from outer edge to outer edge, and the sidewalk joints must be directly above in the same straight fashion.
2. The main sealers must be placed out to out, and the sidewalk sealers must also be placed out to out; i.e., bottom of curb to outside of structure with only one vertical shallow bend [60° (1 rad)] at the curb.

Joint-Armor Design Procedure

Basic Design Considerations

In the United States, there is no official specification that deals directly with the design of armored joints. Therefore, the AASHO specifications (6) were adopted for the purpose of establishing loads, load distributions, and impact factors for the design of armored joints, and an armored joint was then designed and constructed, instrumented, and tested for stress-strain determination under load. The information gained from those tests is reflected in the final armored-joint design presented here. However, the tests were limited, and deviation from the 230 by 50 by 13-mm (9 by 2 by 0.5-in) armor angle or the offered anchorage would require discretely exercised engineering judgment. Basically, the important features of the armored joint, shown in Figure 1, are as follows:

1. A small top flange to minimize incurred loads,
2. No bottom flange (as would occur with the use of a channel section),
3. Top and bottom anchors (as opposed to a single row of anchors),
4. Thirteen-mm (0.5-in) minimal thickness of armament to minimize localized deflections, and
5. Close anchor spacing (to ensure that more than one anchor takes the burden of incurred loads).

The problem of an actual stress analysis of this structurally indeterminate system was solved by the use of reasonably severe but safe assumptions based on engineering judgment. If the effectiveness of the concrete beneath the turned-down angle is neglected, a unit length of joint may be rendered statically determinate, which makes further stress analysis rather straightforward. The size and spacing of the anchorage reinforcement then follows directly from consideration of the assumed loads, which also reflect the field-test results. (In my engineering judgment, the joint armor should be designed to carry the full, dual-wheel load of the AASHO HS20-44 loading, which is sufficiently conservative to ensure a safe design.)

Because of the dynamic nature of a wheel load, the joint-armor design must also allow for the impact and frictional effects that increase the vertical load and create horizontal forces on the armor angle.

Regrettably, no dynamic load response could be ascertained in the joint-armor tests and therefore, the true impact and frictional effects, which must be considered, remained unknown. As a result, the degree of allowance for these effects is left to the designer's discretion. The design procedures reflect this; an impact factor of between 0 and 30 percent and a coefficient of friction of between 0 and 0.80 were permitted. However, in the follow-up example and in the standard drawings shown in Figures 2, 3, and 4, definite practical values for these two parameters are used. (The design procedure discussed in this paper was developed for U.S. customary units only; therefore, SI units are not given in the figures, tables, or remainder of the text.)

Figure 1. Features of joint-armor design.

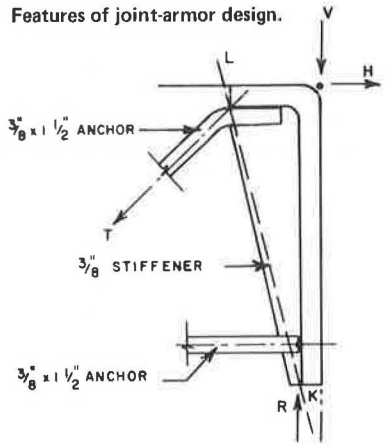

Design Loads and Allowable Stresses

Figure 1 also gives a schematic representation of how the wheel load and its horizontal frictional component is applied to the joint armor. The AASHO specifications (6) for the HS20-44 loading, which is considered applicable for this joint-armor design, are given below:

Figure 2. Deck-joint plan and sections.

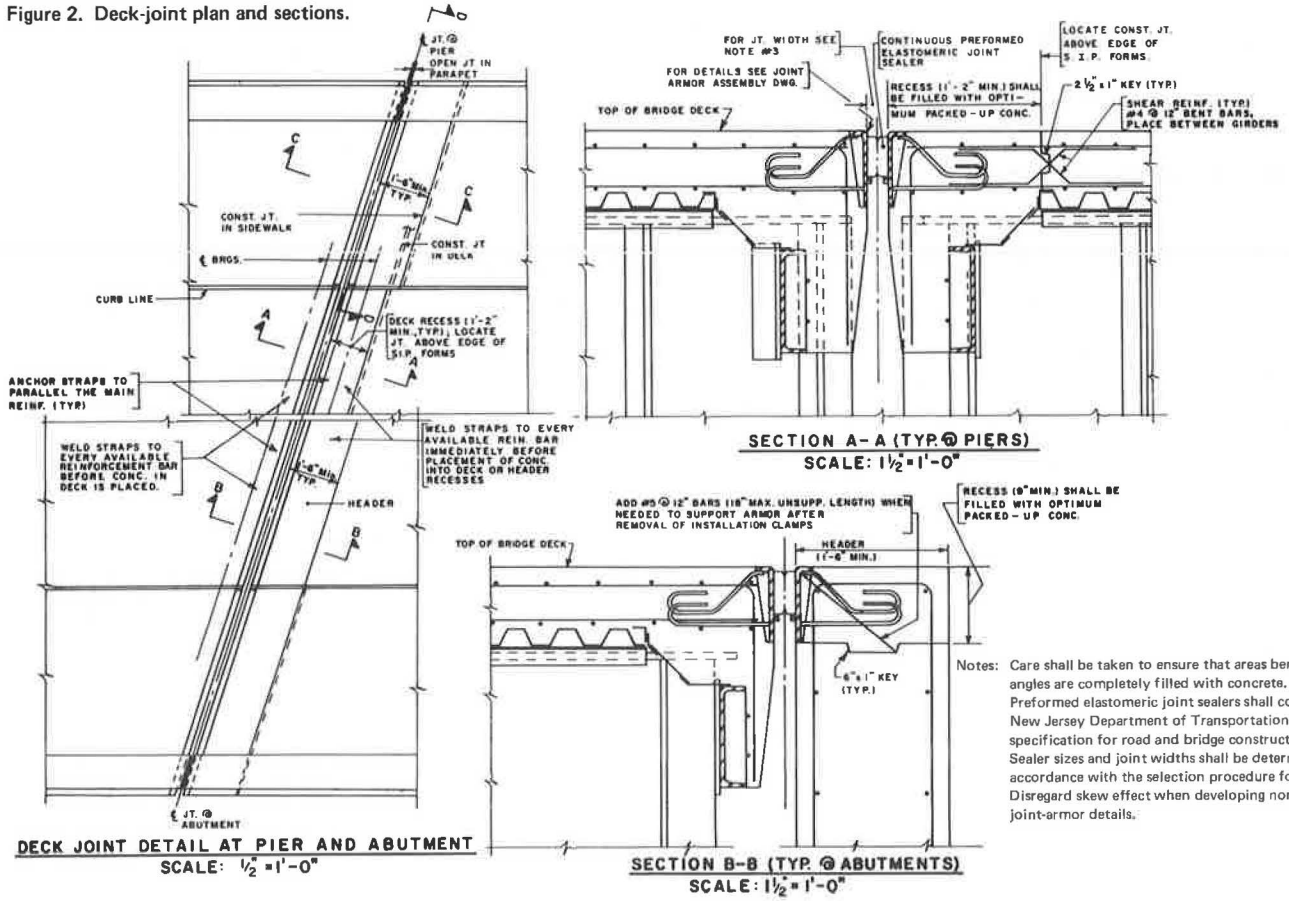

Notes: Care shall be taken to ensure that areas beneath the angles are completely filled with concrete. Preformed elastomeric joint sealers shall conform to New Jersey Department of Transportation standard specification for road and bridge construction. Sealer sizes and joint widths shall be determined in accordance with the selection procedure for sealers. Disregard skew effect when developing nonskew joint-armor details.

Figure 3. Sidewalk and curb elevations and sections.

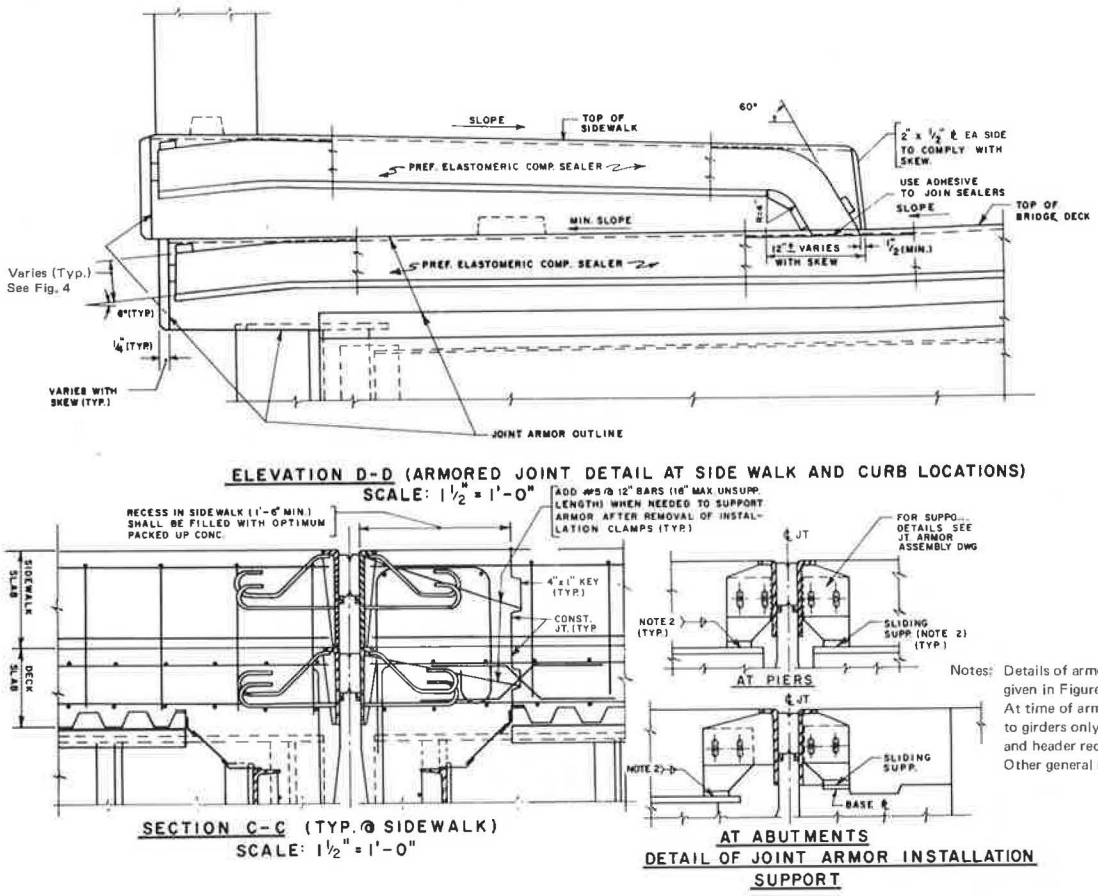

Notes: Details of armor assembly and its installation are given in Figure 4.
At time of armor installation, weld armor supports to girders only on no-recess side of joint. In deck and header recesses, provide sliding armor supports.
Other general notes are given in Figure 2.

Factor	Value
Wheel load, kips	16.0
Impact fraction, %	0 to 30
Friction factor, %	0 to 80

As shown by the load tests of the armored bridge joints, the load distribution can be assumed to be E = 4.0 ft. The applied loads will, of course, create stresses in the various armored-joint components and in the concrete surrounding the joint system. A safe armor design will be one that keeps these stresses below allowable limits. The applicable allowable stresses are given in sections 5 and 7 of the AASHO specifications (6).

Anchorage Reactions

In Figure 1, the concrete in contact with the steel angle is considered to be ineffective, with that portion above line LK giving no support to the angle. It is quite possible that poor construction practices could produce such a condition. If this concrete is omitted from consideration, the applied loads are transmitted into the deck only by the upper and lower anchor bars. The field investigations established that it is appropriate to assume the load reactions of these anchor bars to be as shown in Figure 1. The magnitudes of the reactions can be computed from straightforward analysis of the static equilibrium conditions.

In the diagrams and formulas and their derivations, the following notation is used:

V = vertical load (wheel load),
H = horizontal load,
T = top anchor reaction,
T_H = horizontal component of T,
T_V = vertical component of T,
R = bottom anchor reaction,
R_H = horizontal component of R,
R_V = vertical component of R,
I = impact fraction,
C = friction factor,
E = distribution factor (taken as 4 ft),
W_L = resultant of shearing stress in the weld,
W_R = resultant of bearing stress at end of anchor,
P_R = total allowable load to be carried by cross weld between top of anchor and angle,
D = leg size of fillet welds (in),
L = effective length of weld (in),
L_1 = effective length of cross weld (in),
n = number of anchors/ft of length,
a = thickness of anchor (in),
b = width of anchor (in),
A = area of anchor (in^2),
L_{bond} = effective bond length (in),
L_{bear} = effective bearing length (in),
f_{all} = allowable unit stresses of fillet welds,
f'_c = unit ultimate compression strength of concrete,
f_{sh} = allowable shearing unit stress of concrete,
f_{bond} = allowable bond unit stress of concrete,
f_{bear} = allowable bearing unit stress of concrete,
f_s = allowable tensile unit stress of steel,
f_{sv} = allowable shearing unit stress of steel,
f_r = combined unit stress due to shear and moment,
f_v = vertical component of combined unit stress, and
f_h = horizontal component of combined unit stress.

Figure 4. Joint-armor assembly—details, sections, and elevations.

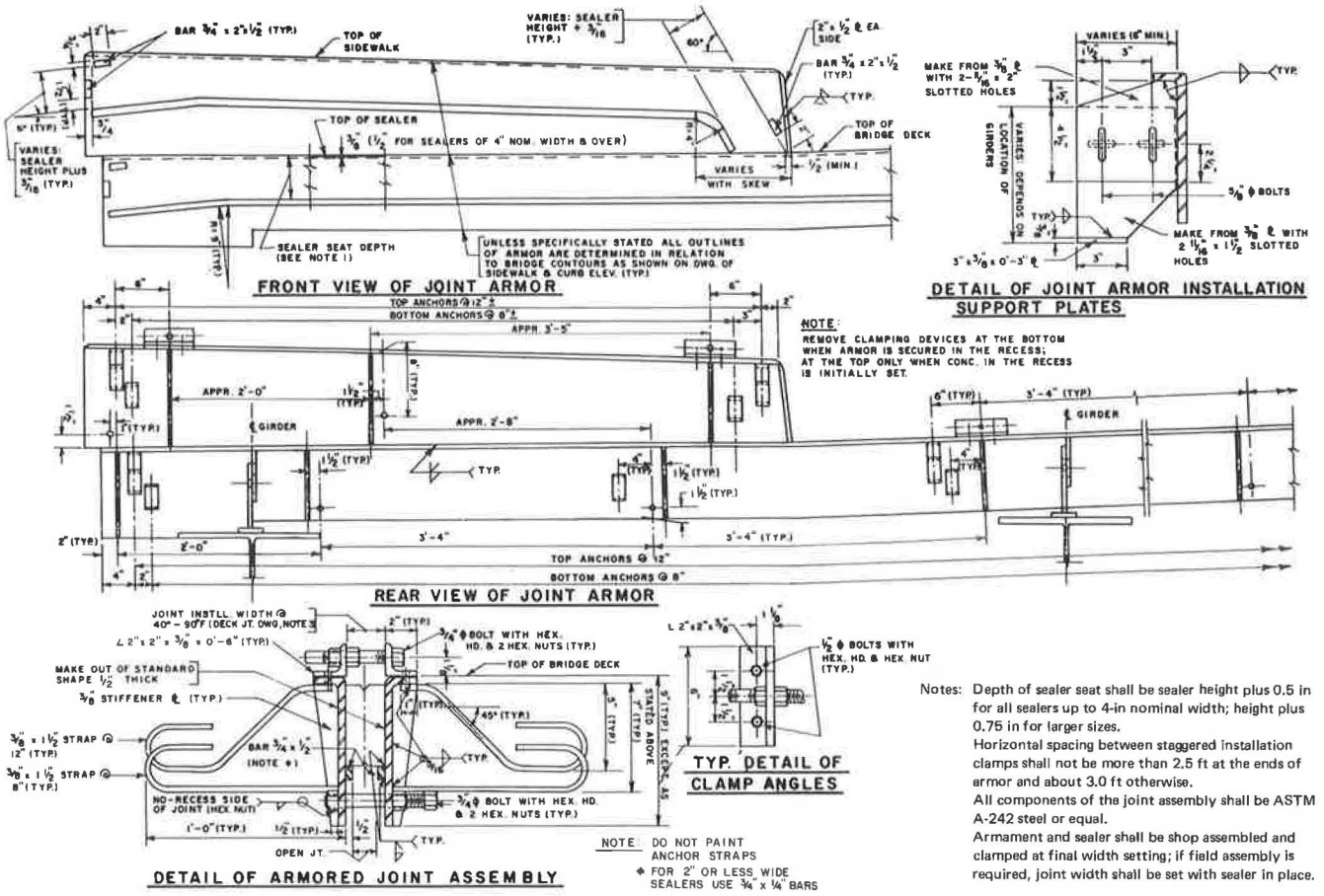

Notes: Depth of sealer seat shall be sealer height plus 0.5 in for all sealers up to 4-in nominal width; height plus 0.75 in for larger sizes.
Horizontal spacing between staggered installation clamps shall not be more than 2.5 ft at the ends of armor and about 3.0 ft otherwise.
All components of the joint assembly shall be ASTM A-242 steel or equal.
Armament and sealer shall be shop assembled and clamped at final width setting; if field assembly is required, joint width shall be set with sealer in place.

The applied loads are given by the following equations:

$$V = 16.0(1 + I) \quad (2)$$

$$H = 16.0 \times C \quad (3)$$

both in kips per E, and

$$V = (16/E)(1 + I) = 4.0(1 + I) \quad (4)$$

$$H = (16/E) \times C = 4.0 \times C \quad (5)$$

both in kips per feet.

The geometric relations between the loads and the anchor-ban reactions for the specific steel angle proposed and the suggested location and orientation of the anchor bars are shown in Figure 5 (the horizontal force can act in either direction). By using the laws of statics and taking Σ(moments about B), Σ(horizontal forces), and Σ(vertical forces), the following equations for the reaction components (T_H, T_V, R_H, and R_V) and the anchor reactions (T and R) are readily developed. (Selection of an armor and anchorage system having different geometry and dimensions from that shown in Figure 5 would result in different equations and reactions.)

$$T_H = T_V = (0.5/8.3)V \pm (7.3/8.3)H \quad (6)$$

$$R_H = (0.5/8.3)V \pm (7.3/8.3) \mp H \quad (7)$$

$$R_V = V + (0.5/8.3)V \pm (7.3/8.3)H \quad (8)$$

$$T = \sqrt{2}\, T_V \quad (9)$$

$$R = (R_V^2 + R_H^2)^{1/2} \quad (10)$$

The anchor reactions derived by inserting appropriate load values for V and H in the equations and considering the possible ranges of impact and friction factors are shown in Tables 1 and 2 and Figure 6. In Figure 6, for design purposes, the R_H and minimum R_V values are disregarded; R_H is negligibly small and minimum R_V values depend on the direction of traffic and, therefore, should be neglected because both joint-armor angles must be designed to carry maximum load reactions.

Application Example

Assume that an armament and anchors of the size and configuration shown in Figure 1 are selected for design, and select an impact factor of 30 percent and a maximum horizontal friction factor of 80 percent. The anchor reactions (per linear foot of joint)—R and T—can be found from Table 2 or Figure 6. The size, spacing, and welding requirements are determined as shown below, and the final, detailed joint design is that shown in Figures 2, 3, and 4 and requires the following: T = 4.42 kips and R_V = 8.327 kips.

1. The welding requirements can be determined from the procedures given in a standard design manual (7). (These procedures are described in the manual as following a middle course and yielding results that appear reasonable by test results.) From Figure 7, in the top anchors, $W_L = W_R = {}^{5}/_{12} f_v L$ and $P_R = 0.707 f_{all} DL_1$. The moment about W_R is $(T_V - P_R) \times {}^{17}/_{18} L = W_L \times {}^{2}/_{3} L \times 2$, and therefore, f_v =

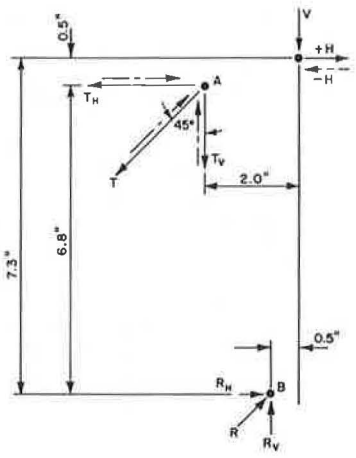

Figure 5. Geometric relations between loads and anchor-bar reactions.

$^{17}/_{10}(T_v - 0.707f_{all}DL_1)/L$; $f_h = T_H/(2L + L)$; and $f_r = (f_v^2 + f_h^2)^{1/2}$.

2. If the top anchor spacing is 12 in on center (OC) (determined by the field-load tests), $T_v = T_H$, $L_1 = 1.5$ in, $L = 1.0$ in, $D = {}^5/_{16}$ in, and $f_{all} = 12.4$ kips/in^2. Then, by using the formulas for f_v, f_h, and f_r, we can solve for: $T_H = 5.45$ kips and $T = T_H\sqrt{2} = 7.71$ kips > 4.42 kips (Figure 6).

In the bottom anchors (for a spacing of 8-in OC), $n = {}^{12}/_8 = 1.5$, and $a = 0.375$ in, $b = 1.5$ in, $f_{all} = 12.4$ kips/in^2, and $R_v = 0.707f_{all}D \times 2(a + b) \times n = 15.45$ kips > 8.327 kips (Figure 6).

3. The shearing stresses in the bottom anchors [for an 8-in OC spacing ($n = 1.5$) and $f_{sv} = 12.0$ kips/in^2] are $R_v = f_{sv} \times A \times n = 10.13$ kips > 8.327 kips.

4. The bearing stresses in the bottom anchors [assuming a triangular bearing distribution with available $L_{bear} = 10.5$ in, 8-in OC spacing ($n = 1.5$), and $f_{bear} = 0.7$

Table 1. Components of joint-armor design-load reactions.

			$T_v = T_H$ (kips)		R_H (kips)		R_v (kips)	
I(%)	V (kips)	H (kips)	+H	-H	+H	-H	+H	-H
0	4.00	0.0 to 3.20	0.241 to 3.055	0.241 to -2.573	0.241 to -0.145	0.241 to 0.627	4.241 to 7.055	4.241 to 1.427
5	4.20	0.0 to 3.20	0.253 to 3.067	0.253 to -2.561	0.253 to -0.133	0.253 to 0.639	4.453 to 7.267	4.453 to 1.639
10	4.40	0.0 to 3.20	0.265 to 3.079	0.265 to -2.549	0.265 to -0.121	0.265 to 0.651	4.665 to 7.479	4.665 to 1.851
15	4.60	0.0 to 3.20	0.277 to 3.091	0.277 to -2.537	0.277 to -0.109	0.277 to 0.663	4.877 to 7.691	4.877 to 2.063
20	4.80	0.0 to 3.20	0.289 to 3.103	0.289 to -2.525	0.289 to -0.097	0.289 to 0.675	5.089 to 7.903	5.089 to 2.275
25	5.00	0.0 to 3.20	0.301 to 3.115	0.301 to -2.513	0.301 to -0.085	0.301 to 0.687	5.301 to 8.115	5.301 to 2.487
30	5.20	0.0 to 3.20	0.313 to 3.127	0.313 to -2.501	0.313 to -0.073	0.313 to 0.699	5.513 to 8.327	5.513 to 2.699

Note: Applied vertical load = 4.0 kips/ft, applied horizontal load = (4.0 x C) kips/ft, and C = 0 to 80%.

Table 2. Joint-armor design-load reactions.

			T (kips)		R (kips)	
I (%)	V (kips)	H (kips)	+H	-H	+H	-H
0	4.00	0.0 to 3.20	0.341 to 4.320	0.341 to -3.639	4.248 to 7.056	4.248 to 1.559
5	4.20	0.0 to 3.20	0.358 to 4.337	0.358 to -3.622	4.460 to 7.268	4.460 to 1.759
10	4.40	0.0 to 3.20	0.375 to 4.354	0.375 to -3.605	4.673 to 7.480	4.673 to 1.962
15	4.60	0.0 to 3.20	0.392 to 4.371	0.392 to -3.588	4.885 to 7.692	4.885 to 2.167
20	4.80	0.0 to 3.20	0.409 to 4.388	0.409 to -3.511	5.097 to 7.904	5.097 to 2.373
25	5.00	0.0 to 3.20	0.426 to 4.405	0.426 to -3.554	5.310 to 8.115	5.310 to 2.580
30	5.20	0.0 to 3.20	0.443 to 4.422	0.443 to -3.537	5.522 to 8.327	5.522 to 2.788

Note: Applied vertical load = 4.0 kips/ft, applied horizontal load = (4.0 x C) kips/ft, and C = 0 to 80%.

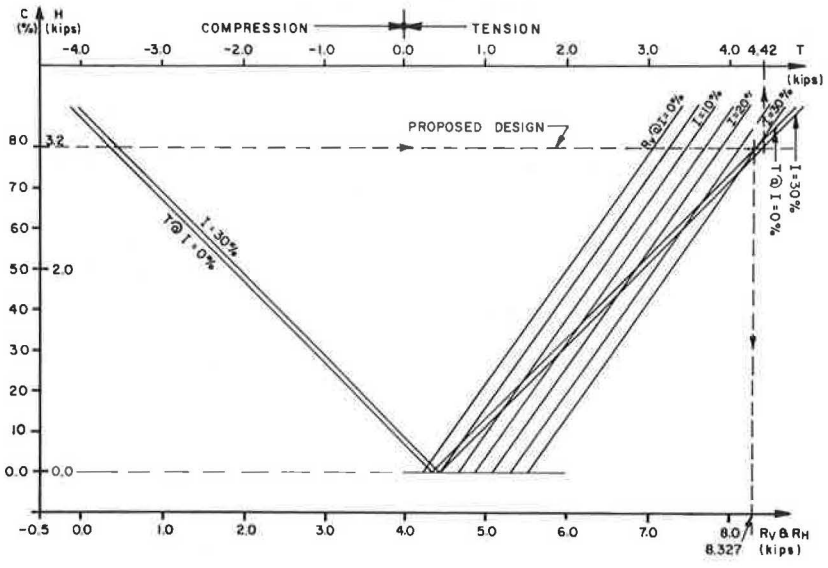

Figure 6. Joint-armor design-load reactions.

Figure 7. Welding stresses.

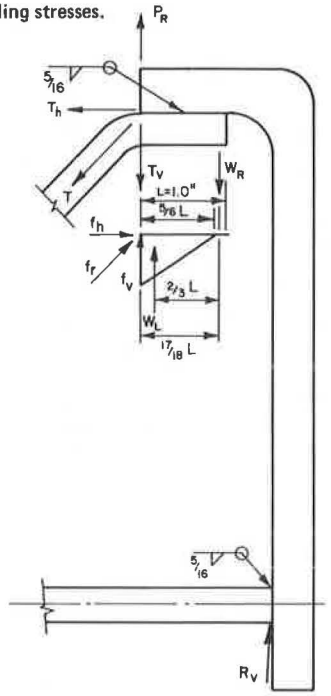

kips/in^2], will be $R_v = f_{bear} \times b \times (L_{bear}/2) \times n = 8.265$ kips, which is sufficiently close to 8.327 kips.

5. The tension stresses in the top anchors (for 12-in OC spacing and $f_s = 20$ kips/in^2) will be $T = f_s \times A = 11.25$ kips > 4.42 kips (Figure 6).

6. The bond stresses (neglecting the bottom anchors because R_H is negligible) in the top anchors (assuming that hook develops 50 percent of allowable stress) will be $T = f_{bond} \times [2(a + b) \times L_{bond} \times 2] = 1.20\ L_{bond}$, and if $L_{bond} = 7$ in, T = 8.4 kips > 4.42 kips.

DISCUSSION OF DESIGN

This design is for maximum impact and close to maximum friction factors; however, the selection of these factors is left to the discretion of the engineer. The impact factor should not be less than 30 percent, but because the wheel load of 16.0 kips has been conservatively chosen, the friction factor of 40 to 50 percent should be more reasonable.

As shown in Figure 6 and described in Tables 1 and 2 and the preceding design analysis, it is the bearing in the bottom anchors that controls their spacing. The proposed standard drawing shown in Figures 2, 3, and 4 shows that the only practical bottom anchor spacing that will prevent interference with other elements would be 4, 6, 8, or 12 in because the spacing of the top anchors cannot exceed 12 in and the approximate spacing of clamping devices should be 3.0 ft to control armor-angle deflections before installation.

The design discussed above uses an 8-in bottom-anchor spacing. For a 12-in spacing and I = 30 and C = 40 percent respectively, Figure 6 gives $R_v = 6.92$ kips required.

The bearing analysis for 12-in spacing gives $R_v = 5.51$ kips < 6.92 kips. A similar calculation with 8-in bottom spacing gives $R_v = 8.265$ kips > 6.92 kips. Therefore, 8-in bottom-anchor spacing is shown in Figures 2, 3, and 4.

Finally, the basic design requirements must include the following considerations:

1. Armored deck joints should be continuous throughout the full width of the deck, and termination should be accomplished as shown in Figures 2, 3, and 4 to armor the joints where necessary and to form the best sealed joint possible.

2. The seal groove in the sidewalk should be armored in the same manner as the curb and the outside ends should be installed as shown in Figures 3 and 4, but a stay-in-place anchor seat could be added to the curb end at the bottom outside face of the armor shapes.

3. All the steel at the armor network except for the parts in contact with concrete should be shop painted and touched up in the field after removal of the armor-holding elements. ASTM A 242 or A 588 steel is recommended for the armor because its stable rust characteristics will be advantageous in those areas where paint is likely to deteriorate.

Procedure for Header Design

Failure of headers is not uncommon. The probable causes are as follows: (a) loading, such as indicated in armor design; (b) inadequate preparation of the backfill; and (c) concrete approach slabs directly supported by headers. Only one remedy can be suggested—improvement of quality control in construction—for problem (b). In view of these causes, the severity of the assumptions made below is well justified. Also, the stresses produced on the commonly used section discussed below are well within the practical range.

Design Loads

Many of the load conditions considered in the joint-armor design are also applicable to bridge headers. For design purposes, the header loading is given by the following: wheel loads = 16.0 kips, I = 30 percent, C = 1.0, and E = 3.0 ft; thus, $V = (16.0/E)(1 + I)$ kips/ft, and $H = (16.0/E) \times C$ kips/ft.

Analyses of Applied Loads

To determine the reinforcement sizes and spacing and the basic header dimensions, an analysis (8) of the applied loads is necessary. This analysis (Figure 8) uses the following additional notation:

- P_s = reasonable estimate of sealer load (1.0 kip/ft when compressed to 50 percent,
- w = unit weight of concrete,
- N = total vertical load (axial load),
- M = moment,
- p = load on reinforcement,
- b′ = header width,
- h = header height,
- d = effective depth of flexural member,
- d″ = distance from centerline of concrete section to tensile reinforcement,
- e = eccentricity measured from tensile steel axis, and
- j = ratio of distance (jd) between resultants of compressive and tensile stresses to effective depth.

The moment about plane AB, the total vertical load, and the reinforcement design (8) are given by Equations 11, 12, and 13 and 14 respectively.

$$M = V \times (b'/2) + (H + P_S) \times h \quad (11)$$

$$N = V + (w \times b' \times h) \quad (12)$$

$$e = (12M/N) + d'' \quad (13)$$

Figure 8. Header loading.

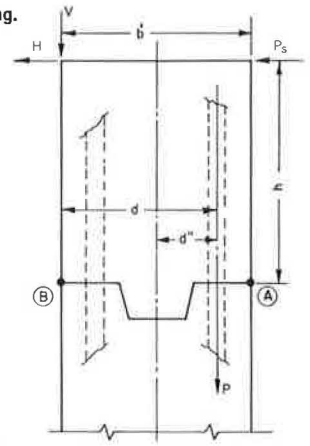

where e is in inches

$$p = N(e - jd)/jd \quad (14)$$

where p is in kips per foot of width.

Although the stresses in the region of B due to moving loads are somewhat smaller, the use of the same reinforcement on both sides of a header is suggested.

The headers used with joints sealed by preformed elastomeric sealers must be designed as absolutely stationary for the sealers to function properly. There can be no horizontal movement and no rotation of the header because the sealer and the joint width are selected on the basis of predictable movements; i.e., on the basis of bridge-deck expansion only.

Because of this, approach slabs, which are supported on one end elastically and on the other by a vertically rigid member, present a complex problem. This is especially so if the rigid slabs have an eccentrically located, static, vertical load and possibly a substantial horizontal static force, as well as other dynamic reactions to a horizontally flimsy header. Even a perfect solution of the joint-sealing problem will be useless if a header failure disallows proper functioning of the joint. In the experimental bridges studied, the backfill was adequately compacted, and bituminous pavement was substituted for approach slabs.

Construction Procedure for Armored Joints

The concept on which this method is based is that the entire system (armor angles with straps and seats welded to them and sealer properly precompressed between the angles and the supporting elements such as clamps and attached bolts) is assembled and then placed in the joint before the concrete is poured. The best approach is to have the elements of the system fully assembled, delivered to the construction site, and placed true to its elevations, joint widths, and proper position in the bridge deck. (The width of the joint between armors, adjusted according to the design requirement, and all other pertinent information is shown in Figures 2, 3, and 4.) If complete factory assembly is not feasible, the joint should be factory preassembled to the fullest practicable degree and the assembly completed on the construction site. Standard lubricant should be applied on each joint-armor face when the sealer is located in the armor. Before the assembly is lifted into place on the bridge, the joint opening should be checked at each clamp and reset if necessary.

As shown in Figures 2 and 3, the deck should be poured without a recess on only one side of the joint. The necessary recess should be left on the abutment (or header) side of the joint, or in a movable deck end when the joint is between spans, with the deck (or header) reinforcement properly extended into the recess. The recess area should be the last concrete poured.

On the side of the joint on which the deck is poured without a recess, the armor-installation supporting plates should be welded to the main bridge girders at the time of installation of the joint assembly; this fixes the assembly at its proper elevations and positions it in the bridge deck. The anchorage straps are welded to all the available deck reinforcement bars only after those bars are checked for proper placement; this ensures stress-transfer continuity into the concrete deck, which can be poured any time thereafter.

From the initial setting of the assembly to the final pouring of concrete into the recess, the armor supporting plates on the recess side must slide freely on top of the stringers (or header recess). This allows the joint assembly to maintain its proper joint width during construction of the bridge decks. After the deck concrete has stabilized by curing, shrinking, and camber settlement (about 1 week after pouring), the recess may be poured.

On the day when concrete is poured into the recess, there are three steps that should be performed during the 2 h immediately preceding the actual pour.

1. Make a final check of the joint opening at each top clamp and adjust it if necessary.
2. Weld the anchorage straps to every available reinforcement bar and to the auxiliary no. 5 by 12-in support bars. This is done to ensure stress-transfer continuity and also to prevent the joint from opening before interaction between the armor and the concrete is ensured. Curb and gutter areas present the greatest problem in this regard.

Because the two sides of the armored joint are fastened to each other, as well as to their respective deck spans, the importance of pouring the concrete immediately is obvious.

3. Remove the bolts from the bottom clamping devices of the joint assembly.

The entire pour requires about 1 h. Immediately after the initial set of the concrete, the top clamps of the assembly should be removed, and the concrete in these areas should be refinished if necessary. This procedure will provide a satisfactorily sealed joint with a minimal amount of care.

In summary, the successful construction of this type of bridge joint has the following basic requirements:

1. The structural integrity of the armor must be preserved; i.e., it must be fabricated and constructed exactly in accordance with the drawings and specifications.
2. Once the joint armor is fabricated and assembled with a sealer in place, there should be no tampering with its integrity until completion of construction.
3. Precise placement of the armor is absolutely essential; i.e., before the concrete is poured, the armor must be located true to the bridge-deck surface. The installation should be performed so that until the concrete is set, no bridge-end movements are transferred into the joint armor.

Selection Procedure for Sealers

The procedure for the selection of sealers is an em-

Figure 9. Δ-movement for L = 0 to 180 ft.

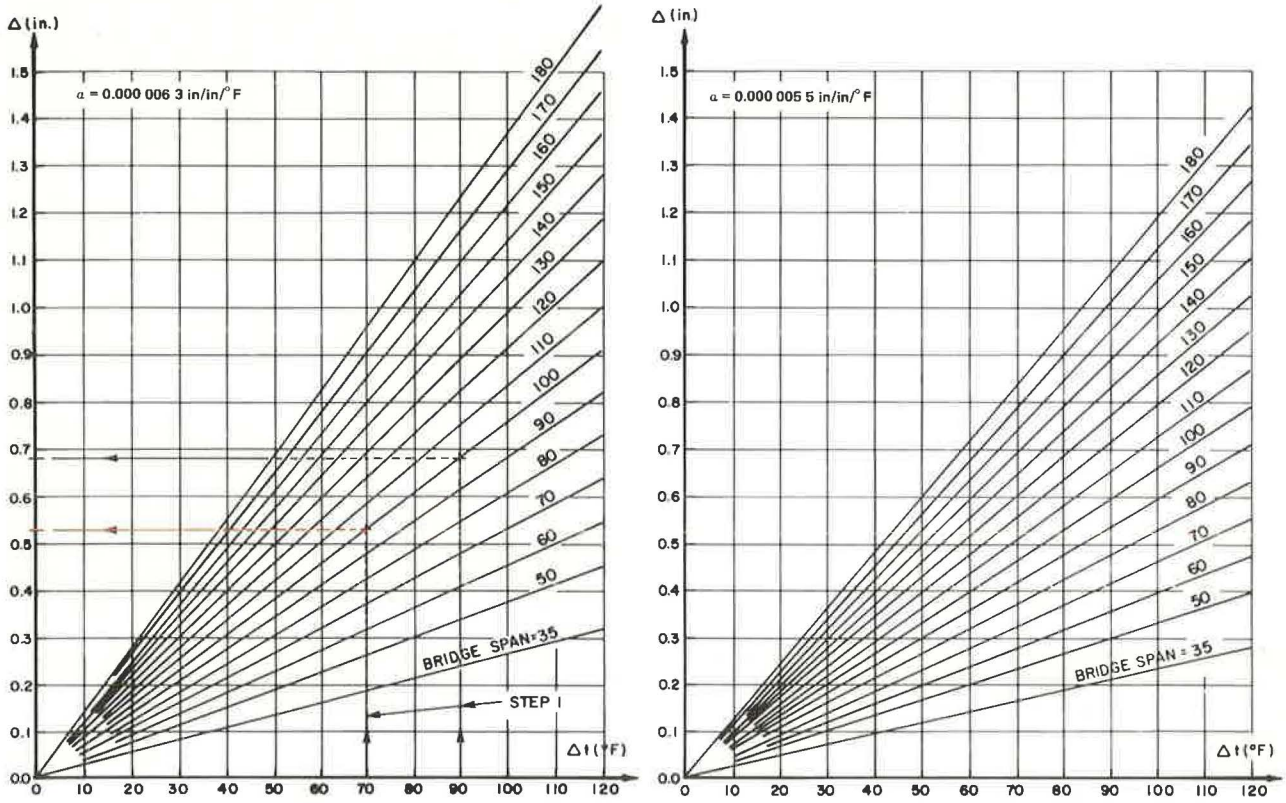

Figure 10. Joint-sealer efficiency chart.

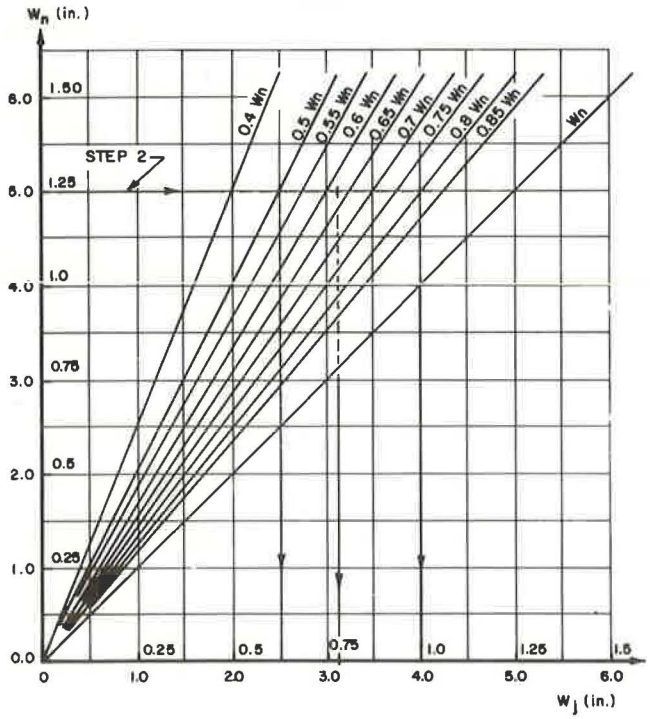

pirical method that establishes the size of sealer to be used in a joint and determines the width at which the joint must be constructed to ensure the effectiveness of the sealer. The capabilities of the sealer are determined in terms of three empirical efficiency coefficients. Each of these parameters is the ratio of the width of the sealer at a certain level of compression to its nominal width (W_n), multiplied by 100. Z is the ratio at the maximum permitted compression of the sealer; Y is the desired ratio at the time of sealer installation; and X is the ratio at the minimum permitted compression of the sealer (enough compression to prevent leakage between sealer and joint face). In New Jersey, X cannot be greater than 80 percent. Z should be not more than 50 percent and, therefore, Y should be approximately 60 to 65 percent.

Any bridge joint will be constructed at a width that is preset at the factory assembly of the armored joint. The bridge temperature at the time when the joint will become an integral part of the deck cannot be known, but it is known that all subsequent bridge movements will occur from that preset width. Therefore, the design consists of establishing the maximum magnitude of these movements (Figure 9) and selecting a sealer and construction joint width on the basis of the values of X and Z.

The following calculation illustrates the use of Figures 9 and 10 by a solution for a composite bridge design with a span of 100 ft.

1. Assume (a) an ambient temperature range of 0 to 110° F and a construction ambient temperature range during installation of the joint armor of 40 to 90° F (the use of a construction air temperature range, rather than a particular value, is the only realistic approach to existing construction practices), (b) Z = approximately 50 percent at the minimum width of joint (W_{jmin}) and 110° F, (c) Y = approximately 60 percent at the installation width of joint (W_{jinst}) and a construction air temperature range of 40 to 90° F, and (d) X = approximately 80 percent at the maximum width of joint (W_{jmax}) and 0° F.

2. For a joint installation temperature of 40° F and a subsequent maximum bridge temperature of 110° F,

Table 3. Guide to design of sealers in composite and steel bridges.

Limit of Span (ft)	W_n (in)	At 110°F		Δ At Δt = 70°F	At 40 to 90°F			At 0°F	
		W_{jmin} (in)	Z		$W_J \pm 1/16$ in Tolerance (in)	Y	Δ At Δt = 90°F	W_{jmax} (in)	X
≤30	1½	0.875 to 0.715	0.58 to 0.48	0.00 to 0.16	15/16	0.625	0.00 to 0.20	1.00 to 1.20	0.67 to 0.80
30 to 35	1¾	0.90 to 0.87	0.515 to 0.50	0.16 to 0.19	1⅛	0.64	0.20 to 0.24	1.39 to 1.43	0.79 to 0.82
35 to 45	2	1.00 to 0.95	0.50 to 0.47	0.19 to 0.24	1¼	0.625	0.24 to 0.31	1.55 to 1.62	0.78 to 0.81
45 to 55	2½	1.26 to 1.21	0.50 to 0.48	0.24 to 0.29	1 9/16	0.625	0.31 to 0.37	1.94 to 2.00	0.77 to 0.80
55 to 70	3	1.52 to 1.44	0.51 to 0.48	0.29 to 0.37	1⅞	0.625	0.37 to 0.48	2.31 to 2.42	0.77 to 0.81
70 to 95	4	2.07 to 1.94	0.52 to 0.49	0.37 to 0.50	2½	0.625	0.48 to 0.65	3.04 to 3.21	0.76 to 0.80
95 to 120	5	2.56 to 2.42	0.51 to 0.48	0.50 to 0.64	3⅛	0.625	0.65 to 0.82	3.84 to 4.01	0.77 to 0.80
120 to 150	6	3.05 to 2.90	0.51 to 0.48	0.64 to 0.79	3¾	0.625	0.82 to 1.02	4.63 to 4.83	0.77 to 0.80

Notes: $\alpha = 0.000\,006\,3$ in/in/°F.
Controlling temperature range = 0 to 110°F and construction temperature range = 40 to 90°F (these are the actual ambient temperatures at a bridge site studied).
Z = approximately 0.50 W_n, Y = approximately 0.60 to 0.65 W_n, and X = approximately 0.80 W_n.

Table 4. Guide to design of sealers in concrete bridges.

Limit of Span (ft)	W_n (in)	At 110°F		Δ At Δt = 70°F	At 40 to 90°F			At 0°F	
		W_{jmin} (in)	Z		$W_J \pm 1/16$ in Tolerance (in)	Y	Δ At Δt = 90°F	W_{jmax} (in)	X
≤35	1½	0.875 to 0.715	0.58 to 0.48	0.00 to 0.16	15/16	0.625	0.00 to 0.21	1.00 to 1.21	0.67 to 0.81
35 to 40	1¾	0.90 to 0.88	0.515 to 0.50	0.16 to 0.18	1⅛	0.64	0.21 to 0.24	1.40 to 1.43	0.80 to 0.82
40 to 50	2	1.01 to 0.96	0.51 to 0.48	0.18 to 0.23	1¼	0.625	0.24 to 0.30	1.56 to 1.61	0.78 to 0.81
50 to 65	2½	1.27 to 1.20	0.51 to 0.48	0.23 to 0.30	1 9/16	0.625	0.30 to 0.39	1.93 to 2.02	0.77 to 0.81
65 to 80	3	1.51 to 1.44	0.50 to 0.48	0.30 to 0.37	1⅞	0.625	0.39 to 0.48	2.33 to 2.43	0.78 to 0.81
80 to 110	4	2.07 to 1.93	0.52 to 0.48	0.37 to 0.51	2½	0.625	0.48 to 0.65	3.04 to 3.21	0.76 to 0.80
110 to 140	5	2.55 to 2.41	0.51 to 0.48	0.51 to 0.65	3⅛	0.625	0.65 to 0.83	3.84 to 4.02	0.77 to 0.80
140 to 170	6	3.04 to 2.90	0.51 to 0.48	0.65 to 0.79	3¾	0.625	0.83 to 1.01	4.64 to 4.82	0.77 to 0.80

Notes: $\alpha = 0.000\,005\,5$ in/in/°F.
Controlling temperature range = 0 to 110°F and construction temperature range = 40 to 90°F (these are the actual ambient temperatures at a bridge site studied).
Z = approximately 0.50 W_n, Y = approximately 0.60 to 0.65 W_n, and X = approximately 0.80 W_n.

$\Delta t = 70°$ F. From Figure 9a, if $\Delta t = 70°$ F and L = 100 ft, $\Delta_1 = 0.52$ in. However, if the installation temperature is 90° F, the bridge may subsequently cool to 0° F and $\Delta t = 90°$ F, and from Figure 9a, if $\Delta t = 90°$ F and L = 100 ft, $\Delta_2 = 0.68$ in. Although the bridge will only incur a temperature range of 110° F, because of the wide range of possible installation temperatures, the sealer must actually be designed for a total range of 160° F.

3. Estimate a sealer size for $W_n = 5.0$ in, $Z = 0.5W_n$, and $X = 0.8W_n$. Figure 10 gives $W_{jmax} - W_{jmin} = 4.00 - 2.50 = 1.50$ in. The preset width of the joint has a tolerance of $\pm 1/16$ in, which effectively increases the required sealer movement range at each end by 1/16 in, and therefore, the required $\Delta = (\Delta_1 + 1/16) + (\Delta_2 + 1/16) = 1.32$ in < 1.50 in.

4. The joint installation width would be between 3.26 (4.00 - 0.74) and 3.08 (2.50 + 0.58) in, and $3\frac{1}{8} \pm 1/16$ in is an appropriate choice of $W_{jconstr}$.

The preceding steps illustrate the principles underlying sealer selection. Each designer can choose particular values of α, ambient air temperatures, and limits for X and Z with which to construct tables (such as Tables 3 and 4), from which the required sealer and armored-joint installation widths can be easily obtained for various bridge-deck lengths.

Considerations for Replacement of Sealers

Replacement of sealers is ill-advised unless it is performed with great care; it involves considerable expense and inconveniences the riding public. Thus, if a sealer needs replacement, the cause of its demise should first be determined. But generally, if the joint is not a proper, intact armored joint, then achieving the best results will require the use of the armored-joint construction method described above as the replacement procedure. This could be performed by removing concrete at the joint to provide a sufficient recess for the armored joint assembly and then following the normal armored-joint construction procedure.

The replacement of a sealer in a properly constructed armored joint could be due to failure of the sealer itself or to the addition of an overlay on the bridge deck. In the first case, the sidewalk concrete at the joint would be removed and the armament spread to facilitate the removal of the old and the installation of the new deck sealer. In the latter case, it would be necessary to build up the top lateral surface of the existing deck armament and to add higher sealer seats.

ACKNOWLEDGMENT

In presenting this report, an expression of appreciation goes to the organizations and individuals who have given assistance and advice. The Federal Highway Administration has provided the financial support and patiently awaited the results. Its continued cooperation is gratefully acknowledged. Special thanks go to the members of the research team and others in this organization, past and present, without whose help success would not have been possible.

The contents of this report reflect our views; we are responsible for the facts and the accuracy of the data presented here. The contents do not necessarily reflect the official views or policies of the state of New Jersey or the Federal Highway Administration. This report does not constitute a standard, specification, or regulation.

REFERENCES

1. G. S. Kozlov and B. Cosaboom. Preformed Elastomeric Joint Sealers for Bridges: Phase 1—Sealed Bridge Joints, Design, Construction, and Evaluation. Division of Research and Development, New Jersey Department of Transportation, Trenton, Rept. 75-009-7731, 1975.
2. B. Cosaboom, T. Fuca, and G. S. Kozlov. Preformed Elastomeric Joint Sealers for Bridges: Phase 1—Remote Electronic Data Gathering and Storage Systems. Division of Research and Development, New Jersey Department of Transportation, Rept. 75-009A-7731, 1975.
3. B. Cosaboom and G. S. Kozlov. Preformed Elastomeric Joint Sealers for Bridges: Phase 1—Relationship of Environmental Parameters to Displacement Responses of Highway Bridges. Division of Research and Development, New Jersey Department of Transportation, Rept. 75-009B-7731, 1975.
4. B. Cosaboom and G. S. Kozlov. Preformed Elastomeric Joint Sealers for Bridges: Phase 1—Load Tests of Armored Bridge Joints. Division of Research and Development, New Jersey Department of Transportation, Rept. 75-009C-7731, 1975.
5. G. J. Mehalchick and G. S. Kozlov. Field Evaluation of Various Bridge-Deck Joint-Sealing Systems. Division of Research and Development, New Jersey Department of Transportation, Trenton, Interim Rept., March 1976.
6. Standard Specifications for Highway Bridges. AASHO, 1973, paragraphs 1.2.5, 1.2.12(C), and 1.3.2(H).
7. G. LaMottee. Manual of Design for Arc Welded Steel Structures. Air Reduction Co., New York, 1946.
8. Reinforced Concrete Design Handbook. ACI, Detroit, 1955.

Publication of this paper sponsored by Committee on Sealants and Fillers for Joints and Cracks.